INSTITUTE OF NATURAL AND APPLIED SCIENCES

DEPARTMENT OF ELECTRICAL AND ELECTRONICS ENGINEERING

LOAD SHARING STRATEGY USING INTELLIGENT CONTROLLER OF HYBRID VEHICLE WITH FUEL CELL, BATTERY AND ULTRA-CAPACITOR ENERGY STORAGE

A THESIS

submitted by

MUSTAFA ASSIM MOHAMMED KAMOONA

in partial fulfillment of the requirements for the degree of

MASTER OF SCIENCE

October 2022

Program: Power Electronics and Clean Energy System

LOAD SHARING STRATEGY USING INTELLIGENT CONTROLLER OF HYBRID VEHICLE WITH FUEL CELL, BATTERY AND ULTRA-CAPACITOR ENERGY STORAGE

A THESIS

by

MUSTAFA ASSIM MOHAMMED KAMOONA

submitted to the Institute of Natural and Applied Sciences of

ISTANBUL OKAN UNIVERSITY

in partial fulfillment of the requirements for the degree of

MASTER OF SCIENCE

Approved by:

Assoc. Prof. Dr. Omer Cihan Kivanc
Supervisor

Asst. Prof. Dr. Oday Ali Ahmed
Co-supervisor

Prof. Dr. Ramazan Nejat Tuncay
Member

Assoc. Prof. Dr. Salih Barış Öztürk
Member

Assoc. Prof. Dr. Shirin Koc
Member

October 2022

Program: Power Electronics and Clean Energy System

ABSTRACT

LOAD SHARING STRATEGY USING INTELLIGENT CONTROLLER OF HYBRID VEHICLE WITH FUEL CELL, BATTERY AND ULTRA-CAPACITOR ENERGY STORAGE

An intelligent controller is proposed in this work for hydrogen fuel cell hybrid electric vehicles that integrated battery, fuel cell, and ultracapacitor to reach a high dynamic response and keep high efficiency of energy storage resources. The developed controller manages the power flow of the proposed system in an intelligent tracking to be optimal for hydrogen fuel cell hybrid electric vehicles. An effective management system has been developed and put into use to ensure that three power sources are functioning with high efficiency and optimum mechanism performance since the success of this project depends on an energy management system (EMS).

In this work controlling the distribution between those three power sources and feeding into the load as efficiently, reliability and satisfaction, while, keeping fast dynamic response of each power source. The Fuzzy Logic Controller (FLC) and the Artificial Neural Networks (ANNs) are employed to meet the EMS requirements and efficiently meet the load power demands as well as use less hydrogen consumption. Moreover, the control strategies of the proposed Wavelet Neural Network and Recurrent Wavelet Neural Network are linked with the PI controller, where called as WNN-PI and RWNN-PI respectively; whereby their parameters are tuned by using the Particle Swarm Optimization (PSO) algorithm. The control strategies are employed for

considering the battery and ultra-capacitor state-of-charge (SOC) with power conditioning unit converters that control the output of fuel cell and battery and provide the desired voltage level of the DC bus as well as keep the voltage stable at
300 volts. Analysis and evaluations of the system have been done by MATLAB/Simulink environment while various vehicle driving cycles have been applied to test the proposed system by using ADVISOR Simulator.)

Keywords: Intelligent Controller, FLC, ANNs, Wavelet Neural Network, Recurrent Wavelet Neural Network, EMS, PSO Algorithm, FCHEV.

KISA ÖZET

LOAD SHARING STRATEGY USING INTELLIGENT CONTROLLER OF HYBRID VEHICLE WITH FUEL CELL, BATTERY AND ULTRA-CAPACITOR ENERGY STORAGE

Bu çalışmada, yakıt hücresi, pil ve ultra kapasitör entegreli hidrojen yakıt hücreli hibrit elektrikli araçlar için yüksek dinamik yanıta ulaşmak ve enerji depolama kaynaklarının yüksek verimliliğini korumak için akıllı bir kontrolör önerilmiştir. Geliştirilen kontrolör, önerilen sistemin güç akışını, hidrojen yakıt hücreli hibrit elektrikli araçlar için optimal olacak şekilde akıllı bir izlemede yönetir. Bu çalışmanın başarısı bir Enerji yönetim sistemi (EMS) ile ilgilidir; bu sayede üç güç kaynağının mekanizma performansları ile yüksek verimde çalışmasını sağlamak için verimli yönetim geliştirilmiş ve kullanılmıştır.

Bu çalışmada, her bir güç kaynağının hızlı dinamik tepkisini korurken, bu üç güç kaynağı arasındaki dağılımın kontrol edilmesi ve yüke verimli, güvenilirlik ve memnuniyet olarak beslenmesi sağlanmıştır. Bulanık Mantık Denetleyicisi (FLC) ve Yapay Sinir Ağları (YSA), EMS gereksinimlerini karşılamak ve yük güç taleplerini verimli bir şekilde karşılamak ve daha az hidrojen tüketimi kullanmak için kullanılır. Ayrıca, önerilen Dalgacık Sinir Ağı ve Tekrarlayan Dalgacık Sinir Ağı'nın kontrol stratejileri, sırasıyla WNN-PI ve RWNN-PI olarak adlandırılan PI denetleyicisi ile bağlantılıdır; bu sayede parametreleri Parçacık Sürü Optimizasyonu (PSO) algoritması kullanılarak ayarlanır. Kontrol stratejileri, yakıt hücresinin ve pilin çıkışını kontrol eden ve DC barasının istenen voltaj seviyesini sağlayan ve aynı zamanda enerjiyi muhafaza

eden güç koşullandırma birimi dönüştürücüleri ile pil ve ultra kapasitör şarj durumunu (SOC) dikkate almak için kullanılır. 300 voltta kararlı voltaj. Önerilen sistemin ADVISOR Simülatörü kullanılarak test edilmesi için çeşitli araç sürüş çevrimleri uygulanırken, sistemin analiz ve değerlendirmeleri
MATLAB/Simulink ortamında yapılmıştır.

Anahtar Kelimeler: Akıllı Kontrolör, FLC, YSA, Dalgacık Sinir Ağı, Tekrarlayan Dalgacık Sinir Ağı, EMS, PSO Algoritması, FCHEV.

ACKNOWLEDGMENT

First of all, I will give my thanks forever to my God who makes me able to complete this project.

Words cannot express my gratitude and appreciation to my supervisors "**Assoc. Prof. Dr. Ömer Cihan Kıvanç**" and "**Asst. Prof. Dr. Oday Ali Ahmed**" for their great help, suggestion, invaluable patience and feedback till the completion of this work. I also could not have undertaken this journey without, their encouragement and support.

I would like to thank the staff of the Department of Electrical Engineering and International Office at the Istanbul Okan University for their useful assistance and support.

I would like to thank my family and especially my parents for their great and continuous support, patience and contribution during the years of my study. Also, their belief in me has kept my spirits and motivation high during this process. Finally, special words of thanks to all my classmates and friends who provided me with any kind of help during the period of my study.

Mustafa Assim Mohammed Kamoona

TABLE OF CONTENTS

3

LIST OF TABLES

LIST OF FIGURES

SYMBOLS

A Exponential voltage (V)

$AAii$ Interfacial area between electrons and electrolyte (mm2)

$AAmm$ The effective area of membrane B Firing

threshold c Molar concentration (mol/m3) equal to c =

1/(8NAr3) c1 Self-recognition PSO coefficient c2

Social PSO coefficient $\psi(t)$ Mother wavelet $\psi_{a,b}(x)$

The daughter wavelet

$CCTT$ Total capacitance (F)

D Duty cycle *D* Diode d1

Duty cycle for boost switch d2

Duty cycle for buck switch E

Energy stored

E_{Batt} Nonlinear voltage (V)

E0 Constant voltage (V) e(t)

Error signal

Exp(s) Exponential zone dynamics (V)

F Activation function F Faraday

constant 96485 A s/mo fs

Switching frequency

h Planck's constant = 6.626×10^{-34} J s i

Extracted capacity (Ah) i* Low

frequency current dynamics (A)

$IIHH$ The current at the high voltage side

$IILL$ The current at the low voltage side

IL Inductor current Is

Switching current it

Extracted capacity (Ah)

$iiuuuu$ Ultra-capacitor current (A)

K Polarization constant (Ah^{-1}) or Polarization resistance (Ohms) k

Boltzmann's constant = 1.38×10^{-23} J/K

$LLmm$ Membrane thickness

N Number of cells

$NNAA$ Avogadro constant

$NNPP$ Number of parallel Ultra-capacitors

$NNee$ Number of layers of electrodes

ABBREVIATIONS

ANNs Artificial Neural Networks

FLC Fuzzy Logic Controller

ISE Integrated of Square Error

NN_{ss} Number of series ultra-capacitors

PSO Particle Swarm Optimization

P_{air} Absolute supply pressure of air (atm)

P_{fc_max} Maximum Fuel Cell Power

P_{fc_min} Minimum Fuel Cell Power

P_{fc_opt} Optimal Fuel Cell Power

P_{fuel} Absolute supply pressure of fuel (atm)

P_{H2} Partial pressure of hydrogen inside the stack (atm)

P_{O2} Partial pressure of oxygen inside the stack (atm)

Q Maximum battery capacity (Ah)

QQ_{TT} Electric charge (C)

r Molecular radius (m)

R Ideal gas constant 8.3145 J/(mol K)

RR_{ffuu} Ohmic resistance of the fuel cell

R_L Load resistance (Ω) **R_{UC}**

Total resistance of UC (Ω)

RR_{uuuu} Total resistance (ohms)

RWNN Recurrent Wavelet Neural Network

Sel(s) Represents the battery mode. Sel(s) = 0 during battery discharge, Sel(s) = 1 during battery charging

WNN Wavelet Neural Network

T Time in second

T Operating temperature (Kelvin)

$VV_{aauuaaiiaa}$ Voltage drop caused by activation losses

$VV_{uuccccuu}$ Voltage drop caused by concentration losses

$\mathbf{V_D}$ Diode voltage

VV_{HH} The voltage the high voltage side

$\mathbf{V_I}$ Input voltage

VV_{LL} The voltage at the low voltage side

$\mathbf{V_L}$ Inductor voltage

$\mathbf{V_{lpm(air)}}$ Air flow rate (l/min)

$\mathbf{V_{lpm(fuel)}}$ Fuel flow rate (l/min)

$\mathbf{V_o}$ Output voltage

$\mathbf{V_s}$ Switching voltage

VV_{ffuu} Fuel cell voltage

$VV_{cchmmiiuu}$ Voltage drop caused by ohmic losses

VV_{uuuu} Ultra-capacitor voltage (V)

x Percentage of hydrogen in the fuel (%) **y** Percentage of oxygen in the oxidant (%) **z** Number of moving electrons **γ** The conductivity of the membrane at the operation of temperature

I. CHAPTER ONE INTRODUCTION AND LITERATURE SURVEY

1.1. Vehicular Emission CO_2 Effectuation

Nowadays, demand for electric vehicles (EV) as well as the hybrid electric vehicles (HEVs) have increased, regarding the reasons for being environmentally friendly. Moreover, there are also several other benefits, such a decrease in pollution also a cessation of dangerous gas emissions.

The Internal Combustion Engine (ICE) is considered one of the most used in transportation services as the main power to drive vehicles also ICE is a great achievement in modern technology which provides a high power and can drive the vehicle for long distances. Whereby, ICE uses gasoline fuel then resulting in pollution emission of CO_2 also many else disadvantages such as a high degree of complexity, high noise level, also totally dependent on a single fuel source only. Although environmental pollution because of the CO_2 emission has a significant negative effect in terms of human life, global warming and the environment, the emission of CO_2 does not reach the required level and still increasing as shown in Figure I-1 [1] the

CO_2 emission by different sectors.

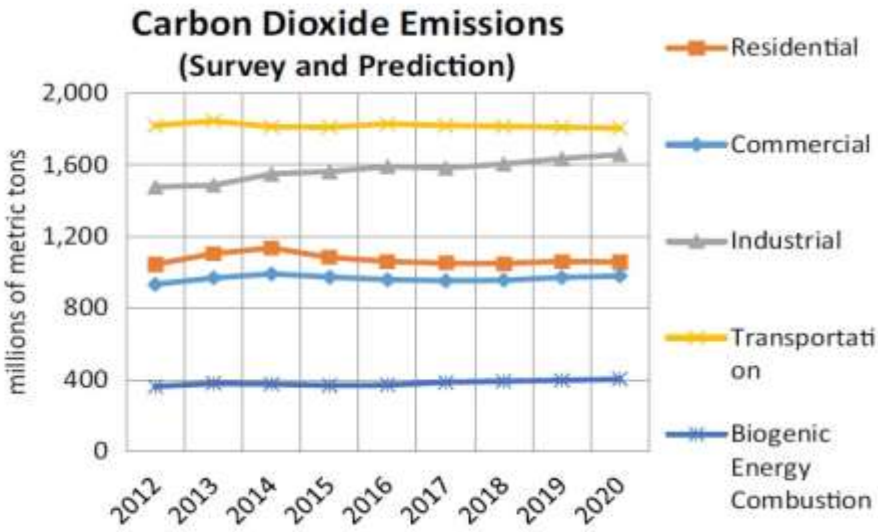

Figure I-1 Emissions of carbon dioxide by various sectors.

The compare between the EV with normal diesel vehicles in terms of several factors still complicated topic. Therefore, this topic has been one of the most important topics; recently researchers and developers focused on improving the performance of EV [2], [3]. Further, the determinations and figure out the motor and battery characteristics are significant for EV's [4], [5].

Particularly, Hybrid Electric Vehicles (HEVs) are more functional and cleaner for the environment than the usual vehicles [6], [7]. Hybrid electric vehicle no need to plug-in from an external source due to its ability to charge the battery by itself. However, there is Plug-in Hybrid Electric Vehicle (PHEV); which has one thing different from the HEVs which is it has the extra plug-in connection to charge from an external source at home or public charge stations.

Moreover, HEVs feed by two power sources within the vehicle. Different hybrid-electric vehicle system designs are utilizing either an internal combustion engine (ICE), clean diesel engines, alternative fuel cell (FC), gas turbines, or fuel cells in combination with batteries. Therefore, the HEV uses much less fuel, also have much lesser emissions of gases than conventional vehicles. The ICE burns gasoline, which releases CO2 into the atmosphere. It also has numerous additional drawbacks, including a high degree of complexity, a loud operating environment, as well as entire reliance on a single fuel source [11].

1.2. Propose the Fuel Cell Technology into Hybrid Electric Vehicle

As mentioned earlier in terms of the disadvantages of ICE then attract attention to invent a new technology solution for replacing the conventional ICE in the vehicular applications. The gasoline-hybrid-electric vehicle in all its classifications (Series, Parallel and Series-Parallel) that uses the batteries as energy storage and ICE together, it is doesn't meet the required power demand also it has a CO_2 emission. Same as well the Electric Vehicle (EV) that uses just batteries as main power, is cannot meet a high power to the vehicle, and cannot drive the vehicle for long distances, battery charging period requires hours to fully charge [8].

While, refueling time hydrogen tank of Fuel Cell (FC) vehicles is a few minutes [24]. For example, time to refueling tank storage pressure 70Mpa is about 3 minutes. Therefore, FC cars are able to address and solve all of the issues that ICE, gasolinehybrid, and EV vehicles face. Also, FC vehicles, have an economic advantage since using hydrogen as power, could lead to a new energy sector in terms of producing hydrogen economy, thereby a chance to be both a product creator and an energy user.

For automotive businesses engaging in the commercialization of FC cars, there are significant obstacles overall [9] such as using hydrogen efficiently and managements of power flow. The Full Cell Electric Vehicle (FCEV) utilizes only water as exhaust; hence it does not contribute to air pollution. In the meanwhile, the FC generator has limitations such as a poor dynamic reaction, a high cost of hydrogen, and the inability to take the vehicle's regenerative braking power. To accomplish Fuel Cell Hybrid Electric Vehicle (FCHEV), needs to add extra power sources with the fuel cell generator such as ultracapacitors (UC) and batteries (BAT).

The ultracapacitor (UC) has a very rapid dynamic reaction in order to adapt to the vehicle's unexpected load fluctuations. Therefore, the FC's output power must be regulated. In addition, throughout the charging and discharging phases, the power flow between the battery, UC, and the load also must be efficiently managed. In order to actively optimize the control system, an Energy Management System (EMS) is necessary; power electronics converters are required as well to interface the power sources with the load in conjunction with the central control system for each converter. The following section provides an overview of the fundamentals,
properties, and applications of fuel cells.

1.3. Fuel Cell Overview

1.3.1. Fuel cell work principle technology and characteristics

Fuel cells produce clean and efficient electricity, which works like batteries as the advantage of do not run down or need recharging. Although, fuel cell has a complex design, but operation principle is simple [48]. Hydrogen and other fuels are essentially used as chemical energy sources in fuel cells; if employees the hydrogen is the fuel, then output products are electricity, water, and heat only. The potential voltage of the fuel cell is reached through the process of flowing a chemical reaction between cathode and anode sandwiched around an electrolyte (an electrolyte membrane). fuel cell, in other terms, is a device used to convert energy electrochemically. For example, a fuel cell that used hydrogen as fuel, which connects hydrogen to the anode, while the air (oxygen) connects to the cathode. A catalyst at the anode site works for separating the hydrogen molecules into protons and electrons. The protons migrate through the porous electrolyte membrane and go through it, while the electrons are forced through an external wire circuit for generating an electric current then resulting in excess heat. On the cathode side, the protons, electrons, and oxygen are united to produce pure water molecules [12]. Since there are no moving parts in the operation of a fuel cell, so it operates silently and with extremely high reliability. There are many types and categorizing of fuel cell but the most widely used regarding the quick response of starting time and shutdown time and its simplicity is Polymer Electrolyte Membrane Fuel Cell (PEMFC) type. Figure I-2 shows diagram of the Proton-exchange membrane fuel cells (PEMFC) operation [10], the efficiency is between 40 and 60%; two categories of PEMFC in terms of temperature range which are high temperature and low temperature thereby 100 to 200 °C and 50 to 100 °C respectively.

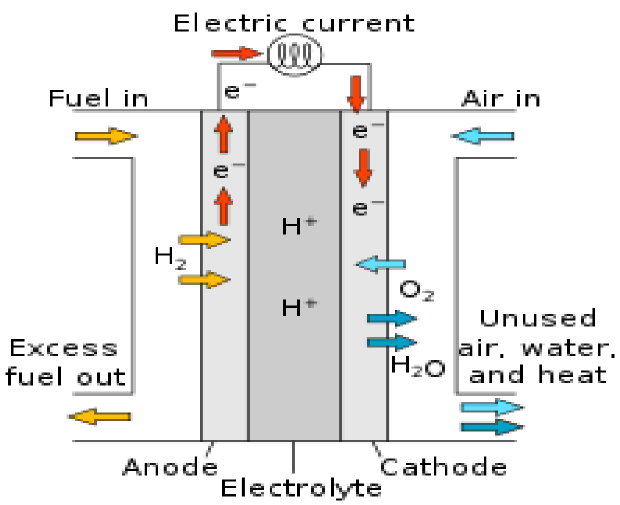

Figure I-2 Diagram of the PEMFC.

The following equations describe the chemical reactions occurring in a fuel cell [11]:

The reaction in anode: $H2 \rightarrow 2H^+ + 2e^-$ (1.1)

The reaction in cathode: $\frac{1}{2} O_2 + 2H^+ + 2e^- \rightarrow H_2O$ (1.2)

Total reaction is: $\frac{1}{2} O_2 + 2H^+ + 2e^- \rightarrow H_2O$ + electricity + Heat (1.3)

In terms of characteristics of fuel cell Figure I-3 shows the polarization curve of a typical fuel cell [13].

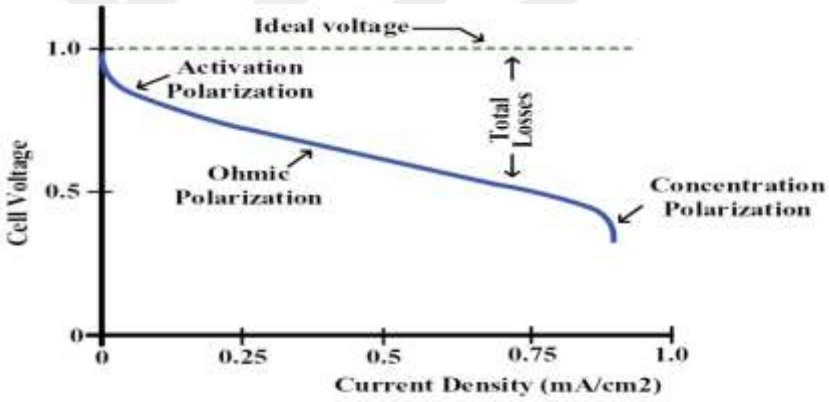

Figure I-3 polarization curve of typical fuel cell.

1.3.2. Fuel Cell Types and Applications

Using one single cell can produce a low voltage around 1 volt; so, a series of cells connect to each other for producing a high voltage this call the "FC stack" and accepts to use of a fuel reformer (additional power) to be integrated if required [14]. Moreover, providing backup power in FC stack is higher than batteries in terms of duration; may kw for more than 30 min [15], [16].

Fuel cells can be used for wide range of application regarding its benefits such as reliability, fuel flexibility, low-to-zero emissions, durability, high efficiency, scalability, quiet operation and energy security. Fuel cells system for transportation is a hot topic and interesting for transportation applications since emits zero emissions and filled up the hydrogen tank in three-five minutes [17]. Fuel cells applications in transportation as following [17]:

- Cares suck as Hyundai Nexo and Toyota Mirai.
- Fuel Cell Buses.
- Heavy-Duty Trucks.
- Medium-Duty Trucks.
- Material Handling such as Forklifts.
- Unmanned Aerial and Underwater Vehicles such as “drones”.
- Rail Transportation: “Fuel cell trains are now operational in Germany.”
- Marine Transportation.

Types of fuel cell	Electrolyte	Operating Temperatur e	Efficiency	Output Power	Application	Advantages	Disadvantages
Phosphoricacid fuel cell [18]	Liquid phosphoric acid soaked in a matrix	150-200_C	40%	400 kW (100 kW module)	Distributed generation	-Increase endurance to fuel impurities -Enables to combined high temperature and power (CHP[1] system)	-Low power and current -Pt catalyst -Long time for start-up

[1] The combined heat and power (CHP) is a system that has a highly efficient process; enables to reach and utilizes the heat to produce the generation process of electricity. In addition, since this method reduces energy usage and expenditures, it is deemed economically feasible [23].

Moltencarbonate fuel cell [19]	Liquid solution of lithium, sodium, and/or sodium carbonates soaked in a matrix	600-700_C	50%	300 kW- 3 MW (300 kW module)	-Distributed generation -Electric utility	-Fuel flexibility -Ability use as variety of catalyst -High efficiency	-Long time for start-up -Low power density -Cell components breakdown and corrosion of the materials due to hightemperature
Alkaline fuel cell [20]	Aqueous solution of KOH soaked in a matrix	90-100 _C	60%	10e100 kW	-Space Application -Military installations	-Ability use as variety of catalyst -Higherperformance due to negative electrode reaction in alkaline media	-Electrolyte Management -Sensitive to CO_2 in fuel and air
Solid oxide fuel cell [21]	Yttriastabilized zirconia	700-1000_C	60%	1 kW-2 MW	-Auxiliary Power	-High efficiency -Ability use as variety of catalyst -Fuel elasticity	-Long time for start-up and restrictions due to High temperature -Cell components breakdown and corrosion of the materials due to hightemperature
Proton exchange membrane fuel cell [22]	Perfluoro sulfonic acid	60-80_C	60:35% for transportation and stationary	Less than 1kW to 100kW	-Handy power tools -Back-up power Transportation	-Operates silently 2-Low temperature -high response for start-up time	-High cost -Heat squander due to low temperature -Receive and accept the fuel impurities

Table I-1 fuel cells type and their specifications.

1.4. Literature Survey

Many researchers have been proposed papers, projects, experiments study, explanations and simulations which addressed to evaluate and improve the performance of FCHEV; while the majority of the papers are focused on power management systems with high response of controlling for the power flow and energy storage as well as calculation of fuel usage and emissions.

Therefore, in order to complete this thesis, several related research papers have been evaluated and followed. The related research as following below:

N. Sulaiman, et al., 2018 [25]: With regards to the importance of transport systems, fuel consumption, CO_2 emissions as well as energy management system (EMS). Hybrid electric vehicle technologies have been presented. Especially, fuel-cell hybrid electric vehicles (FCHEVs) as one of the hottest topics. This paper presented FCEVs issues and challenges with recommendations for enhancing the performance of FCHEVs in the future under a critical review for developing the control strategies of EMSs. Moreover, optimization techniques control like Particle Swarm Optimization (PSO), etc. and the EMS control strategies which employed operational or state mode, rule-based or fuzzy logic (FL), proportional–integral–derivative (PID) controller and equivalent consumption minimization strategies (ECMS) have been explained and described their algorithms with refers to literature. Meanwhile, this study covered the economical and societal concerns. Also, this paper concluded that the results of optimization control of FCHEV EMS should be crucial with high accuracy, also stated on importance of implementation as simulation validation and experimental setup validation into the real-time application.

Manoharan, et al., 2019 [26]: This paper presented a review of developing hydrogen fuel cell engines to investigate the quality of FC engines in transportation systems; with FCs classification and the principle work of fuel cells. Also, described the mathematical equations of FCs reaction, hydrogen storage system in FCEVs, characteristics & specifications of pressurized tank storage as well as explained the efficient control strategies of FCEV.

Zhou, Bin, et al., 2020 [27]: One of many methods in control and calculations strategies for controlling the energy management of hybrid electric vehicles (HEVs), is the equivalent consumption minimization strategy (ECMS). This control minimizes energy consumption with consideration of the battery state of charge (SOC), through the process of optimizing the torque split between the motor and engine. Moreover, ECMS can be implemented in adaptive or non-adaptive applications. Since this method works in high-speed response, therefore, the battery may damage. In this paper, a novel optimal control in terms of the cost function, for both battery aging as well as fuel consumption; by Ah-throughput method that used to quantify battery aging. Also, present the battery aging model and vehicle of parallel HEV calculation as well as ECMS aging equation. Simulation has been done with different drive cycles (UDDS, HWFET, US06 and SC03) under the scope of the investigation for state of charge, battery remaining state of health vs equivalence factors and battery temperature with three battery packs (1st is 1 kW, 2nd is 2 kW and 3th is 4 kW). Resulted, the ECMS minimizes the cost function regarding battery life progression. Furthermore, compared to ordinary ECMS, this study showed that battery aging life has been improved meanwhile minimizing the cost.

Bendjedia, Bachir, et al., 2018 [28]: There are many limitations of FCHEV like energy storage problematic issues in terms of FC and BAT sizing, range, the cost, etc. This research provides an ideal way for sizing the energy needed of a lightweight car with 700 km driving range, by calculation composed of a fuel cell and an assistant source by the progress of methodology Energy Storage System (ESS). Also, shows up the benefits of a hybridization system of fuel consumption, weight, and cost; the hybrid sources have been compared. The hybridization system purposed has been chosen after testing with three secondary sources for improving the characteristics. In this work, the PEM fuel cell has been chosen, the one that is used in Toyota Mirai 2016. In addition, included estimates of hydrogen consumption based on the driving range of the vehicle and determined the power load, battery power, and FC power under simulation using three energy management strategies: Optimal, Maximum, and Frequency Separation. On the basis of the comparison between the New European Driving Cycle (NEDC) and the Assessment and Reliability of Transport Emission Models Inventory Systems (ARTEMIS), it is confirmed that the driving cycle has a slow influence on the ESS sizes. The ESS design compared the power and energy of the FC mission profile and the three secondary source profiles.

Tao, Fazhan, et al., 2020 [29]: Artificial Intelligent (AI) is used as advanced and accurate techniques in EMS over all kinds of EVs, including wavelet strategies. Whereby, [29] presents a frequency decoupling-based energy management strategy (EMS) for electrical hybrid vehicles with fuel cells, batteries, and ultracapacitors (FCHEV) by employing fuzzy control approach. This method decomposes the frequency into three ranges by using Harr wavelet transform and an adaptive-fuzzy filter. Resulting in, increase fuel efficiency, prolonged fuel cell lifespan as well a 7.94% decrease in fuel consumption over the ECMS.

Hu, Xiao, et al., 2021 [30]: This paper used an online data-driven constructed as a speculation model of fuel cell health and controlled by a rule-based fuzzy as control method that optimized by a genetic algorithm under consider both the economy and durability for this fuzzy controller "to achieve the optimal state of health and equivalent hydrogen consumption of the fuel cell". Moreover, an artificial neural network (ANN) has been used for predictive control purposes. Then, for the validation side, the results have been compared which were carried out by MAPE and RMSE which overall results prediction accuracy is very similar. Therefore, the design is capable to use for different driving cycles; whereby the ANN meets optimal control under all driving conditions. Model runed by three driving cycles start with command widely used which is "Urban Dynamometer Driving Schedule" (UDDS), "New Europe Driving Cycle" (NEDC) and "Highway Fuel Economy Test Cycle" (HWFET). This study showed the future work for improving the SOH for FCHEV.

Veerendra, Arigela Satya, et al., 2021 [31]: This paper used the hybrid power management (HPM) method to improve the fuel usage and performance of a fuel-cell series hybrid electric vehicle (FCHEV) and compared the results with the FCEV version 2017 Toyota. While the vehicle model has two sources FC and supercapacitor (SC) type is proton exchange membrane fuel cell (PEMFC), whose vehicle weight is 2180 kg. In order to evaluate the SC state of charge, the extended Kalman filter (EKF) and traditional coulomb counting (CC) have been combined and used. Moreover, the drive cycle is combined Environmental Protection Agency (EPA) used for the simulation by MATLAB/Simulink computer software.

Gharibeh, Hamed Farhadi, et al., 2021 [32]: In this study, the hybrid FCEV has four sources which are “fuel cell” type is Proton exchange membrane fuel cell (PEMFC), battery, ultracapacitor UC, as well as photovoltaic array (PV); these sources have been controlled by a new energy management strategy (EMS) under multi controllers: operational mode control, equivalent consumption minimization and online multi-mode EMS via fuzzy logic control. Moreover, considering the various movement conditions of the vehicle, so the control for the maximum power point tracking (MPPT) has presented as fast-tracking. Furthermore, run the operational mode control strategy that depends on classifying the efficiency of fuel cell power. Overall, simulation has been with two different structures (1st without PV and 2sd with PV) and three driving cycles (UDDS, NEDC, and JP 10 Mode). Resulting, increasing the range, reduces fuel consumption as well as reducing fluctuations of the battery power.

Barelli, L., et al., 2020 [33]: This paper uses the hybrid energy storage system of FCEV for a heavy-duty vehicle, as a fuel cell which is Solid Oxide Fuel Cell (SOFC) and a Lead-Acid battery pack in order to the efficient operation of auxiliary power unit (APU). Also, the Simultaneous Perturbation Stochastic Approximation (SPSA) based algorithm strategy has been used to manage the power flow. The dynamic model simulation of the SPSA strategy for controlling the APU behavior has been carried out by MATLAB/Simulink.

Zhang, Hongtao, e al., 2019 [34]: This study aimed to extend the range of fuel cell plug-in hybrid electric vehicles (FC-PHEVs) by creating a new configuration of FC-PHEVs that new configuration has three fuel cell stacks, and one battery pack. Whereby, power management method is hysteresis control strategy which is switching (ON-OFF) these three fuel cells stacks to ensure the working time is even into the three stacks, as well as reduce the number times of switching (on-off). Simulation has been done with three drive cycles which are urban, highway and a combined urban-highway. Resulting in that, "the fuel cell durability can be enhanced 11.8 times for the urban driving cycle (LA92×2+UDDS×2), 4.8 times for the highway driving cycle (US06×4+HWFET×4), and 6.9 times for the combined urban highway driving cycle (LA92×1+US06×2+HWFET×2+ UDDS×1), respectively."

Numerous research papers and studies for energy management of FCHEVs [3538], even for hybrid electric aircraft application [39], as well as, a number of brief/comprehensive review papers [40-43].

Our work differs from the foregoing survey. Hence, the system has been tested by different driving cycles standards. Compared and analyzed three different powertrain configurations with different ESR as well as different control methods. Increasing the BAT lifecycle within keeping at minimizing the fuel consumption, by proposing a developed control system. achieved outstanding results in terms of effectiveness and fuel economy, with less complexity than other EMS controllers.

1.5. The Thesis Aim

The thesis proposes an intelligent controller-based optimum power flow management for a hydrogen Fuel Cell Hybrid Electric Vehicle (FCHEV) in order to improve transportation system and reduce fuel usage and CO_2 emissions. The proposed hybrid system has been combined with a lithium-ion battery that has high energy density and ultracapacitor that has high power density both are sources to increase the dynamic responsiveness of the fuel cell generator and minimize fuel consumption. An energy management system is designed to make sure the three power sources are running as efficiently as possible with respect to their mechanism performance.

An optimal power flow management based on an intelligent controller for the hybrid power system will be proposed in this work. The energy stored in the battery is utilized to compensate for part of the transient peak power demand, that the fuel cell is unable to fulfill; since the fuel cell is used to supplement the intermittent production. Consequently, prevent the fuel cell from getting too large. A system for energy management will be designed in order to guarantee that the used power sources operate at a high level of mechanism efficiency. An intelligent controller will be utilized to distribute load power amongst power sources effectively and fulfill the dynamic response of each power source. Different energy management system strategies will be compared to select an optimal power flow management.

The suggested energy management system will be able to monitor the output fuel cell power as well as retain the DC-bus voltage close to its reference level when combined with the converters' controller. By supplying propulsion power and recapturing braking energy, this is possible. In order to demonstrate the effectiveness of the suggested energy management system, MATLAB and Simulink will be utilized.

1.6. Outline of the Thesis

This thesis contents of five chapters whereas each chapter description as below:

Chapter One: Presents an overview of the fuel cell vehicle topologies in terms of issues and challenges as well as provide recommendations with a literature survey.

Chapter Two: Introduces an overview of the fuel cell vehicle configurations and details the operational principle of the energy storage resources. Also, this chapter selects the proper power electronic converters for the power sources used in the proposed system.

Chapter Three: Introduces a detailed modeling analysis of the proposed energy management system. Moreover, described the controller: Fuzzy, ANN, Wavelet Neural Network parallel with PI controller (WNN-PI and RWNN-PI) and Particle Swarm Optimization (PSO).

Chapter Four: Presents the verification and validation of the proposed approach through different analysis results. The developed EMS system has been performed and validated over different drive cycles.

Chapter Five: presents the study's results conclusions and recommendations for further research.

II. CHAPTER TWO OVERVIEW OF THE FUEL CELL HYBRID ELECTRIC VEHICLE CONFIGURATIONS

2.1. Introduction

Developing the EVs has many factors, the most important one is the energy source cost factor that represents in its optimal control as well as the hybridization system. Therefore, researchers are being conducted using different designs of storage the energy as well as a control system which aimed to reduce the cost of energy storage with consideration of keeping a high level of improving efficiency. Thus, different configurations of EVs have been introduced [44], for example, some classifications of

Hybrid Electric Vehicle (HEV) such as Series, Parallel and Series-Parallel. Meanwhile, the Plug-in Hybrid Electric Vehicle (PHEV) has the same configuration as HEV but with an extra Plug-in port connection to charge from an external source at home or public charge stations. As shown in Figure II-1 the PHEV block diagram.

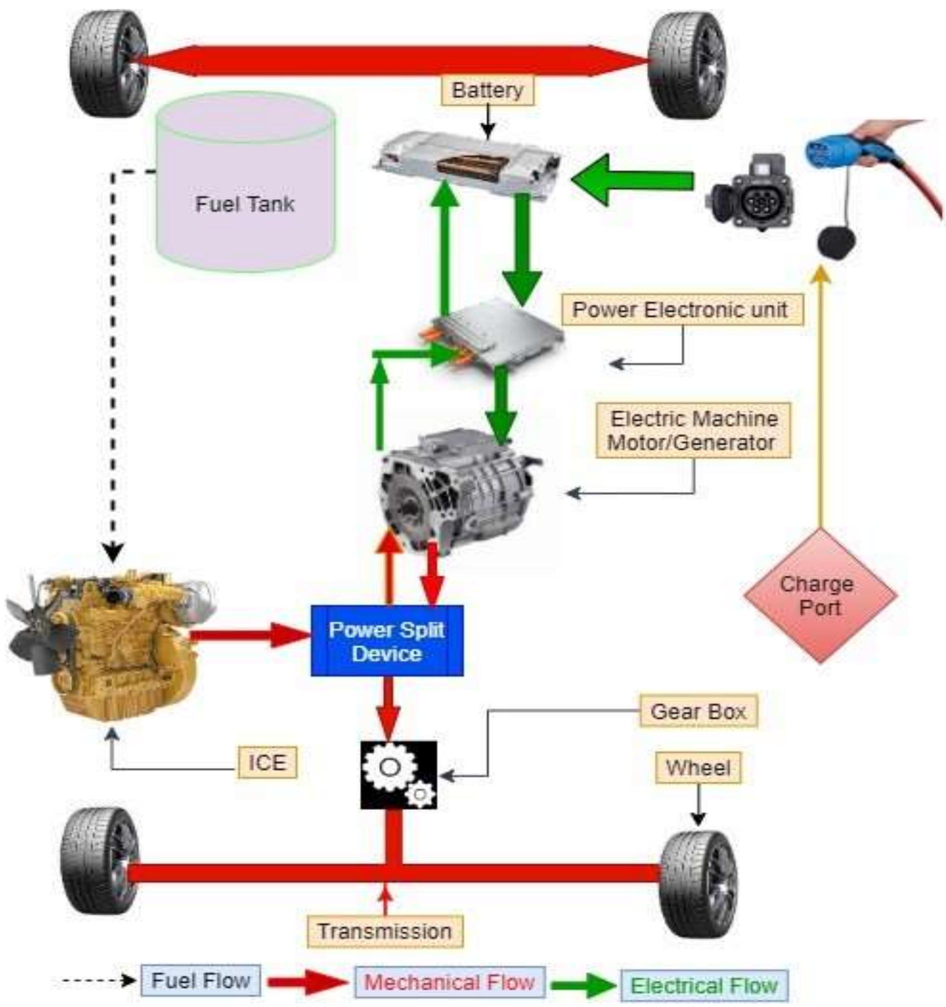

Figure II-1 PHEV block diagram.

Overall, the electric vehicles driven by electrical power can be classification into six topologies types as shown in Figure II-2 [45], however, we summarized the EVs into three basic kinds which are Battery Electric Vehicles (BEVs) which used only batteries, Fuel Cell Electric Vehicles (FCEVs) which use only fuel cells stack, and Hybrid electric vehicles (HEVs) which used a hybrid system like batteries and other energies (BHEVs) or fuel cells stack and other energies (FCHEVs). Moreover, all

HEVs types can be Plug-in or not.

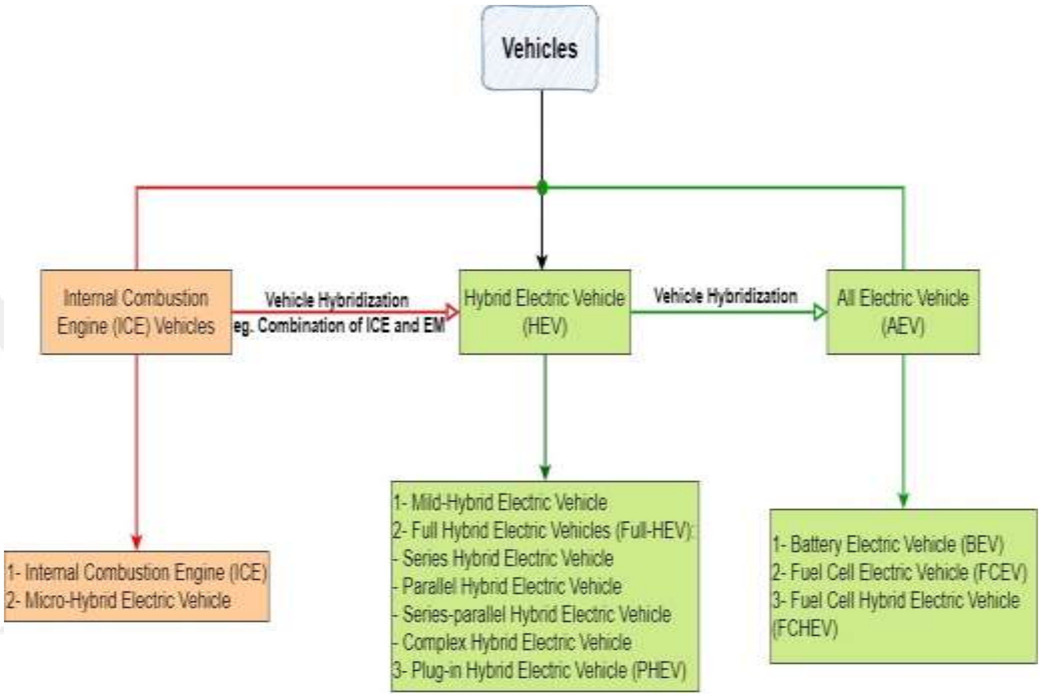

Figure II-2 The classification of vehicle.

The FCEV and BEV are similar in terms of powertrain configuration. Moreover, FCHEV and BEHV are similar as well; one main difference is that the FCHEV uses the fuel cell stack instead of ICE, and battery/ultracapacitor as storage system. The work principle of FCHEV can be summarized and simplified in three steps:

A. Two or three powers in FCHEV which are a fuel cell, Battery and/or ultracapacitor combined; and controlled by an (ex: intelligent control method) for the energy management system (EMS). First starting and at very low load driving (very low speed) of the FCHEV by one of power source ultracapacitor or battery if the vehicle. That is when the ultracapacitor/battery has sufficient energy.

B. The FCHEV is run by fuel cells stack individually that by chemical reaction of oxygen (from the front of the vehicle and by air filter) and hydrogen (from hydrogen in the fuel tank) at normal load driving (normal speed) to drive the vehicle and charge ultracapacitor/battery; but at accelerating (high speed), the fuel cells stack and ultracapacitor/battery are combined together to get powerfully driving.

C. When deceleration (Brake) the vehicle recovering the kinetic energy of tires friction and convert it into electricity, in order to charge the ultracapacitor/battery.

This chapter presenting an overview on various of FCHEV configuration topologies to illustrate the connection of the BAT/UC with the FC generator. Moreover, the simplified work principle of FCHEV is introduced. Also, this chapter contains an explanation of using the Energy Storage Resources (ESR) in terms of hybridization systems and the importance of the EMS role. The and basic operational principles of the BAT and UC and output characteristics are presented as well. Finally, the selected power conditioning unit for the FCEV system, additionally the operation principle of this unit.

2.2. Configurations Structure of the FC Hybrid Vehicle

Generally, there are three main classification topologies of FCHEVs configuration which are as follows below [45]:

1. Passive Connection.
2. Full Active Connection.
3. Semi-Active Connection.

2.2.1. Passive Connection Structure of FCHEV

In the passive configuration, where is directly connecting the fuel cells stack FC, battery BAT, and ultracapacitor UC to the DC bus, without employing any electrical power converters, as seen in Figure II-3.

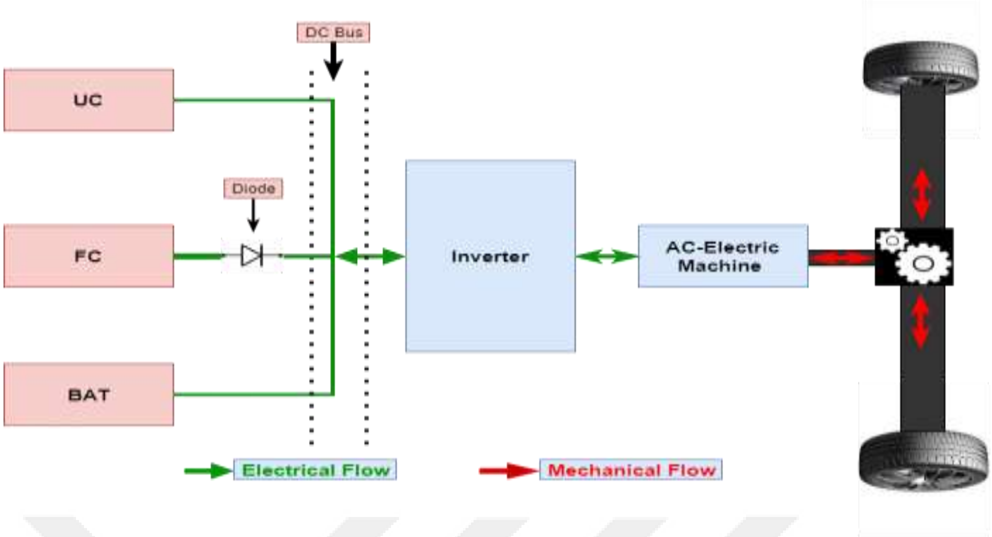

Figure II-3 The fundamental block diagram of the passive connection topology.

The system design of the passive connection structure is flexibility and simplifies construction, since no power electronic converters are needed; then, this is the main advantage of this topology as well as other features such as a higher efficiency with lower power losses and fewer costs [45]. Meanwhile, this topology structure has disadvantages [45], [46] as follows below the disadvantages:

1. Since there are no power electronic converters, then the output voltage of three power sources (FC, BAT and UC) must be the same. Therefore, independent control for the power source is impossible. Hence, this structure should have a control regulation of these three power sources.
2. The main problem of the passive structure system is that the power between the FC and the BAT is unable to be controlled under the control energy management system.
3. The power control in this system is dependent on calculating the respective internal resistance of power sources. Therefore, there is no form of control for the power flow of each energy storage source. Resulting, the current always flows from both Energy Storage Resources (ESR).
4. There is an extra diode for preventing the back-reverse current into the FC stack. So, it is causing extra power losses.
5. The mass (weight) of this construction is high since also requires a large FC generator to meet the DC bus voltage requirements of the EV. Resulting, higher cost.

2.2.2. Fully Active Connection Structure of FCHEV

The fully active configuration uses three DC-DC converters for all power sources (FC, BAT and UC) where each one is connected to the DC bus via independent power electronic converters as shown in Figure II-4.

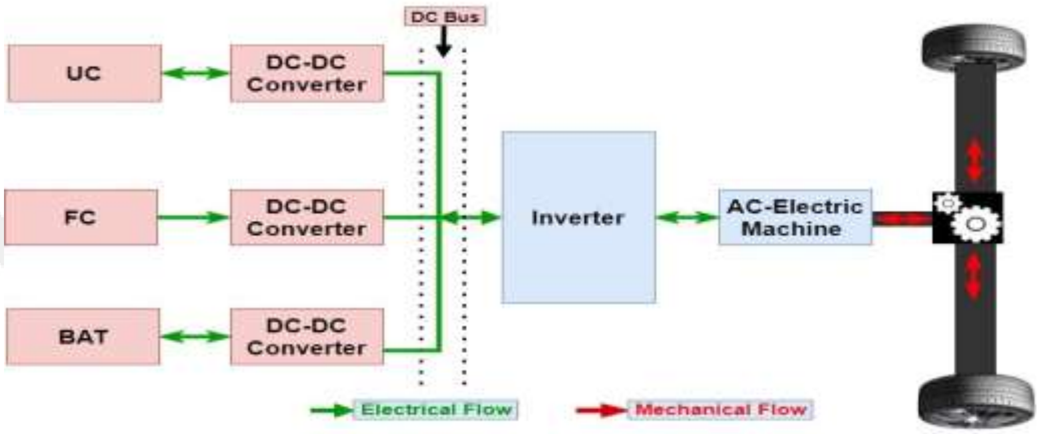

Figure II-4 The fundamental block diagram of the fully active connection topology.

The system design of the fully active configuration structure can use the FC generator with a voltage much less than the DC voltage bus if it is combined together with the boost DC-DC converter configuration; then, this is the main advantage of this topology. Hence, this topology structure has more advantages [62], which are listed below:

1. Whatever, the output voltages of the FC and ESR are different, the DC-bus voltage can be regulated since there are three DC-DC converters.
2. Ability to keep the terminal voltage of the power sources nearly as constant, whereas smaller variation than the passive connection.
3. The weight of the vehicle in terms of the power sources (FC, BAT and UC) for supplying peak power can be smaller than the passive connection if compared with the same load.
4. The optimal control for power-sharing among the power sources can be obtained and regulated.

The fully active configuration has some drawbacks such as adding extra mass of three converters, high cost, and power losses to the FCHEV system. Moreover, in order to provide a free ripple DC-bus voltage, it is required a capacitor to be install in DC-bus voltage. Resulting, this configuration is usually undesirable, since using three converters with no considerable benefit [46].

2.2.3. Semi-Active Connection Structure of FCHEV

In order to find the most efficient configuration, the semi-active topology is proposed which combines and uses the features of the active and the passive connections. Moreover, there are two types of semi-active topology. The first one is the fuel cell is link to the DC-bus voltage through a unidirectional DC-DC converter, while the BAT is link tied directly to the DC-bus voltage and UC is connected to the DC-bus through a bidirectional DC-DC converter as illustrated in Figure II-5. The second type is the FC is connected to the DC-bus through a unidirectional DC-DC converter, while the UC is tied connected directly to the DC-bus and BAT is link to the DC-bus voltage via a bidirectional DC-DC converter as illustrated in Figure II-6. In the connection topology illustrated in Figure II-6, which used the bidirectional converter with its controller system then the BAT power flow can be controlled independently in terms of charging and discharge. While the UC power can be controlled indirectly, because the UC power is the difference between load power demand and the summation power delivered by FC and BAT.

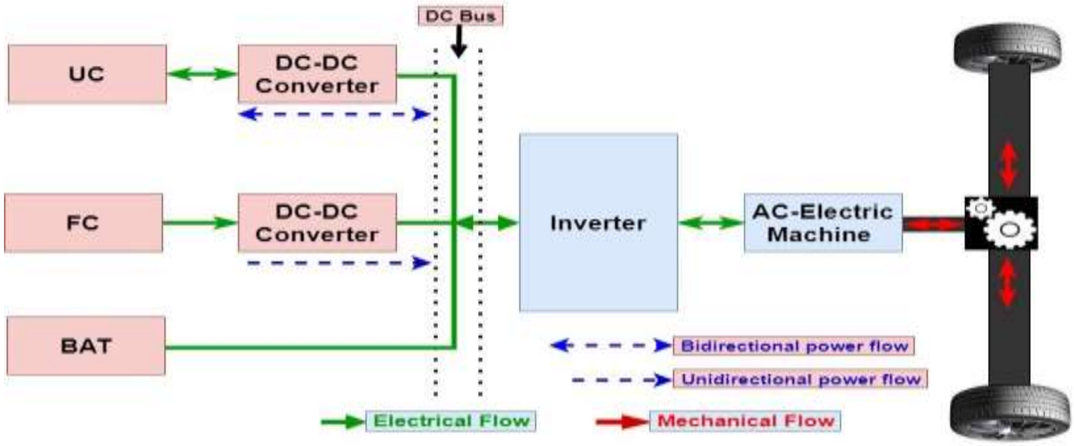

Figure II-5 Semi-Active Connection topology: BAT link directly to the DC-bus.

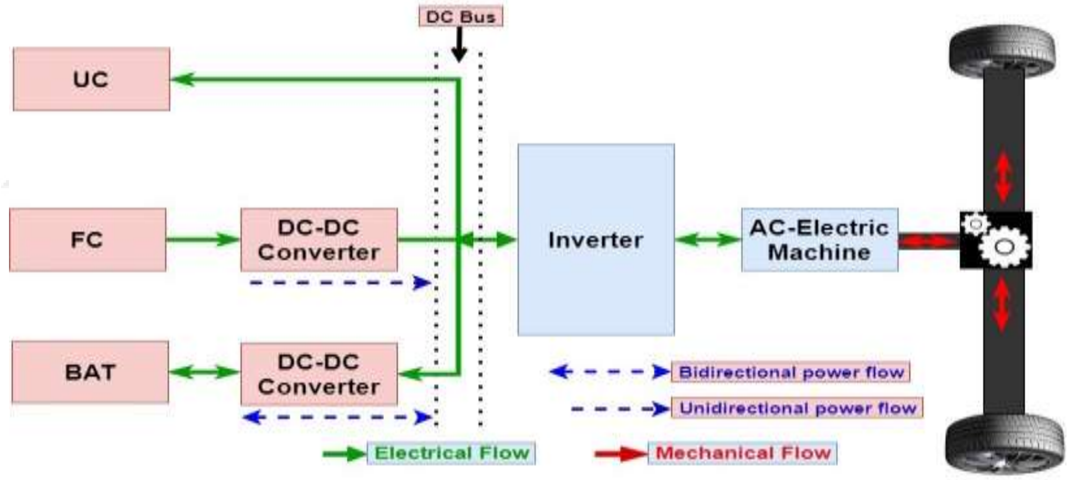

Figure II-6 Semi-Active Connection topology: UC link directly to the DC-bus.

Although, this topology is the most efficient one, but it has some drawbacks in terms of extra weight since there are two DC-DC converters then high cost, as well as power losses due to two converters are used. Moreover, the architecture of the reversible DC-DC converter is typical for active BAT charging of high power. Because of switching and conduction losses, high-power converters are impractical at low loads.

Furthermore, may increase the BAT’s losses in charging mode that happen at the high current, due to the internal series resistance of the BAT. In addition to charging the BAT via the FC, then the FC and BAT converters work at the same time which results in increase the losses.

Overall, these drawbacks have been overcome by this work. In this thesis, the EMS has been designed so that the BAT responds to load power that has the lowfrequency orders. The UC will directly respond to power demand that has the highfrequency orders. And the FC provides steady-state power. Therefore, the efficiency has been increased.

2.3. Energy Storage Resources for the FCHEV

As mentioned previously in chapter one, the strategy to produce the electricity by fuel cell generator has some disadvantages such as the main problem that is the slow dynamic response, hence slacking the response to the transient load. Moreover, the cost of pure hydrogen fuel is relatively high as well as the fuel cell generator unable to recharge using the energy conversion by the concept of the regenerative braking, so there is losing the energy of braking. In order to overcome these problems of the fuel cell generator that can solve by hybridizing the FC vehicles with Energy Storage Resources (ESR), combining FC with ultracapacitors, and the batteries. Resulting improves greatly the slow dynamic response of the FC, then a quick response to sudden load is achievable. In addition to the ESR's ability to help the FC meet the load requirement, as they have high energy and power densities; also reduces the high fuel cost, fuel consumption as well as resulting the stack fuel cell will be small meanwhile provides a high efficiency [47], [48]. The energy produced by the braking state can store in UC and BAT. The power of a sharp slowdown is returned to the generator to first charge the ultracapacitor, while the leftover power is used to charge the battery. Only steady-state power should be supplied to the load in order to operate the fuel cell at a high efficiency. That is why required to manage the output power of the fuel cell. Additionally, throughout the charging and discharging phases, it is necessary to control the power flow between the BAT, UC, and the load as efficiently as possible. The EMS, which has power electronic converters to give control between the power sources and the load together with a central control system for each converter, is ultimately needed to actively achieve. However, the EMS with the controllers should be in charge of regulating the state of charge for the ultracapacitor and battery while also maintaining the DC-bus voltage and monitoring the power flow between the FCHEV sources. Whereas the flowchart shown in Figure II-7 [47] is used to describe the primary function of the EMS of the FCHEV system.

Figure II-7 The main role of the EMS and converters controllers in FCEV.

In energy storage systems, ultracapacitors and batteries are ESR which is the most commonly used in FCHEV. Moreover, the BATs differ from the UCs where batteries have higher energy and lower power density, while the UCs have lower energy and higher power density as well as higher efficiency and longer lifecycles as shown in Figure II-8 different types of energy sources in terms of the specific energy and specific power [49]. Hence, fuel cell and battery have a higher energy density, but with low power density, in contrast, UCs has higher power density. Further Figure II8 shows that BATs and UCs are much higher specific power than FC generators; the specific power of the lithium-ion BATs is close to the UCs.

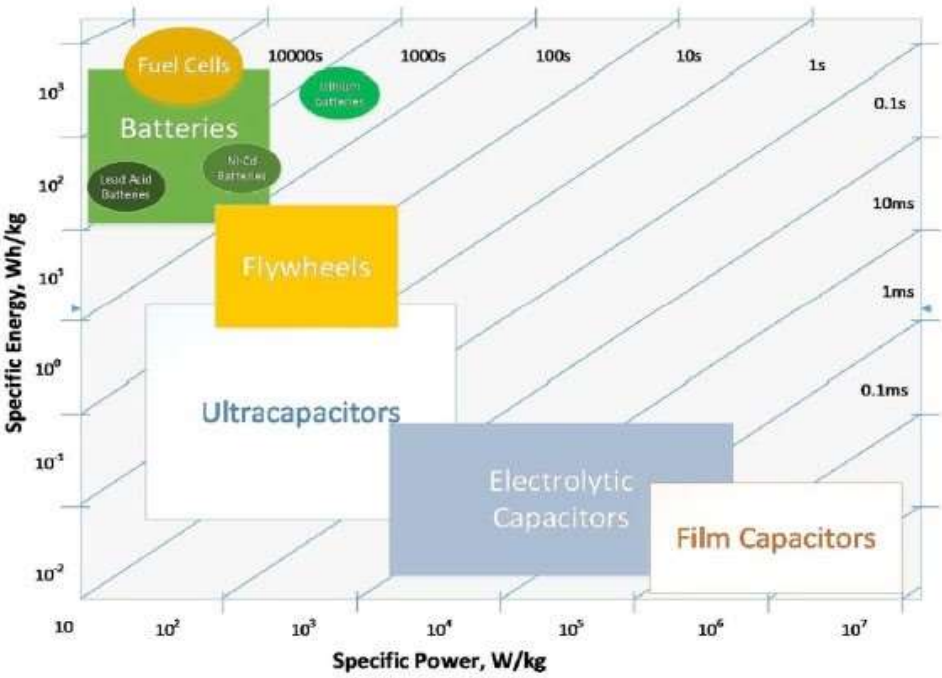

Figure II-8 Energy storage system in terms specific energy and specific power.

The considerations that should be followed when choosing the ESR for FCHEV are the energy storage ability, durability, mass, efficiency, positive and negative power capability, cost, and easiness of interface connections. The description of BATs and UCs characteristics and a brief explanation for their operation are present in the sections below.

2.3.1. Battery Energy Storage Resource

The battery produces electricity by chemical reaction. The battery consists of cathode, anode and electrolyte. The cell is the smallest element component of a battery, and when connect a several of cells will make a module. Therefore, several modules connected in series or parallel will make a complete battery pack as shown in Figure II-9. While some HEVs are starting to use lithium-ion batteries, many HEVs that were previously available on the market used NiMH batteries to store energy. Compared to NiMH batteries, lithium-ion (Li-ion) batteries offer a similar amount of energy in a more compact and lightweight form factor. Li-ion batteries are chosen in high-tech cars due to their performance in cold climates, reduced self-discharge, and capacity for rapid recharging.

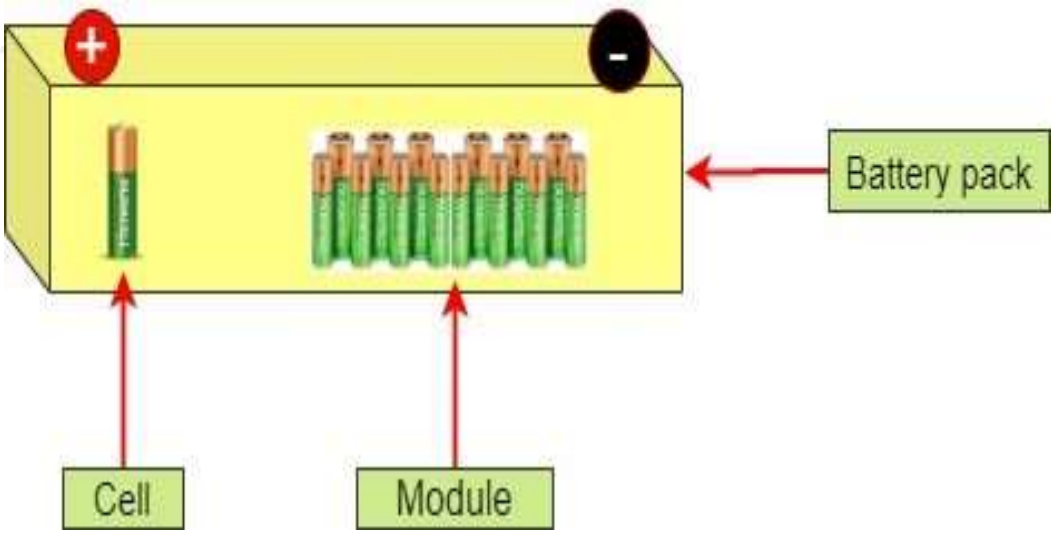

Figure II-9 relationship between cell, module, and battery pack.

Numerous battery kinds such as lead-acid batteries, nickel-metal-hydride, lithium-ion batteries, nickel cadmium … etc. [50]. While lithium-ion BAT is commonly used for HEV, regarding the many advantages that the lithium-ion BAT has such as has a long lifecycle, small volume, repeated charge and discharge, no maintenance required to ensure their performance, self-discharge is less rapid than with other BAT cells such as Ni-Cad and NiMH and no need for priming as in other BATs [50], [51]. Moreover, Li-ion BAT has a shorter lifecycle (2000-3000) cycle compared to the UCs. Furthermore, the lithium-ion batteries have disadvantages as well such as high cost and suffer from ageing and they need protection from being over discharged and charged [52].

Three main parts of lithium-ion BATs are two electrodes (the anode and the cathode), which are separated from one another by a polymer layer to prevent contact that may cause a short circuit. As shown in Figure II-10, an ion-rich fluid (the electrolyte) surrounds the anode and the cathode. Although the cathode composition varies greatly, the anode is formed of graphite. When an external circuit (load) is connected to the electrodes, as is seen in Figure II-10, the electric potential inherent across the cell pulls the ionized lithium elements from the anode through the electrolyte and polymer layer towards the cathode. Ions release their electrons when they reach the cathode, which then cross the external circuit and produce a current flowing backwards [53].

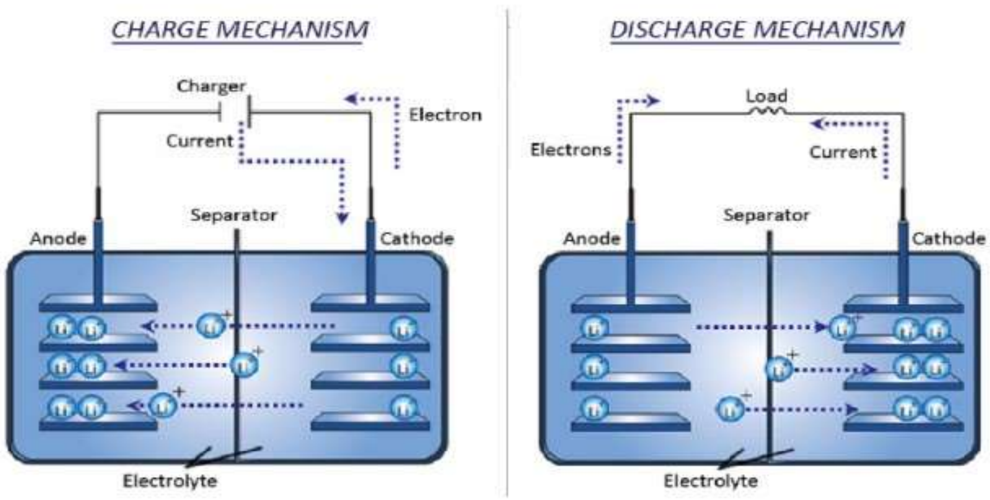

Figure II-10 Lithium-Ion battery discharge and charge procedures [55].

2.3.2. Ultracapacitor Energy Buffer

Ultracapacitors (UCs) and also called “electric double layer” capacitors, is an energy storage system that is commonly built up from an electrolyte, a separator, and two carbon-based electrodes; feature that has a high energy density also capacitance more than the traditional capacitors as well as energy higher than the conventional capacitors and are available in sizes up to 4000F [46]. The ultracapacitor, as opposed to batteries, physically holds segregated positive and negative charges to store electricity directly. Ultracapacitors are fundamentally different from normal capacitors in that they employ an electrical double layer to provide a massive surface area, enabling them to hold more charges. When compared with batteries, ultracapacitors' superior power density, excellent life cycle, higher efficiency, and other advantages make them a more attractive option for HEV applications. Moreover, since the UC has a very fast discharge, then provides a very high power within a short period of time, when compared with the BATs or the FC, an UC has a very high specific power reach up to 3kW/kg. Also, the UC has low maintenance and low internal resistance [9]. UC has disadvantages as well such as fast-self-discharge characteristics and the energy density is lower than a BAT (as much as twenty times) [54]. Resulting, increase in the vehicle weight because required a large number of cells to possess a specific energy capacity.

2.3.2.1. Principle of Operation

The capacitor stores electrical energy in an electric field, capacitor consists of two plates conductor separated by a dielectric. While the ultracapacitors have electrolyte positive and negative plates between the plates instate of a dielectric. It stores energy using charged carbon electrodes by separating the positive and negative charges at the electrolyte interface. Due to the impact of applying a voltage to the electrodes, electrons are therefore taken from the positive plate and deposited on the negative plate, creating an electric field between the plates. Moreover, the supercapacitor has only electrons movement from and to the (between) electrodes without chemical reaction that is why it has a very high response in terms of charging and discharging. in order to make the surface area larger than a traditional capacitor, the electrodes have a porous nanostructure made from carbon, where called this is called capacitor phenomenon as shown in Figure II-11 [47]. However, there are three types of UCs such as Double Layered Capacitors, Pseudocapacitors and Hybrid Capacitors. Singlecell provides around 1-3 volts then several cells could linked in series to have the UC module that has a high voltage.

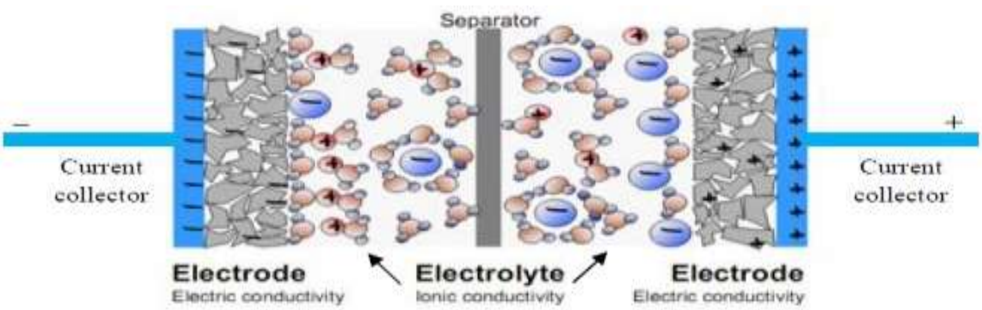

Figure II-11 Principle of operation of Ultra-capacitor.

2.3.2.2. Electrical Characteristic of UC

In terms of performance, a UC is characterized by its terminal voltage during the charging and discharging periods at various current levels. Hence, the parameters of the UC module are dependent on the voltage not the current, since the storage of charge in the UC relies on the capacitance and voltage. In addition, the voltage profile of UCs includes capacitive and resistive components. The capacitive component, on the other hand, represents the energy that is either discharged or charged inside the UC. While the resistive component represents the voltage drop caused by the ESR of the UC module [47], this voltage loss was caused by the UC module itself. Figure II-12 [47] depicts the voltage profile of the UC under continuous discharge current.

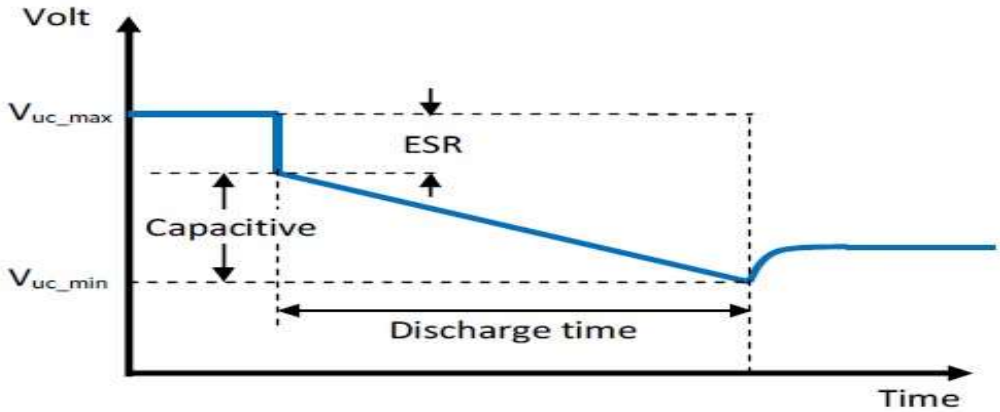

Figure II-12 Characteristic of discharge mode of the UC.

2.4. Power Conditioning Unit in FCEV

Regulation of the DC-bus voltage required DC-DC converters to regulate the voltage as well as adjusting the power flow between all power sources of the developed FCHEV system. In this work, using two topologies DC-DC converters as shown in Figure II-13 (a) the Unidirectional boost converter that is used to FC generator and Figure II-13 (b) shows converter of the BAT which is Bidirectional buck-boost type. Moreover, employing the DC-DC converter of fuel cell generator and finding the size of the FC generator based on the required average load power; not depend on that FC voltage that should match the high voltage of the DC link; because boost converters are able to rise the voltage independently of one another [54]. Moreover, DC-DC converters consider one of the main roles on the powertrain systems [55]. Switching models and average-value models are the two types of models most frequently used to illustrate

DC-DC converters. Since our work is focused on the validation of the proposed EMS. Therefore, the modelling of the converters been done by using an average-switch model to prevent excessive complexity since the converters' own nonlinearity operations as well as obtain a time-invariant circuit topology which results in removing the switching harmonics. The average-value models will be further

explained in section II-5 and II-6.

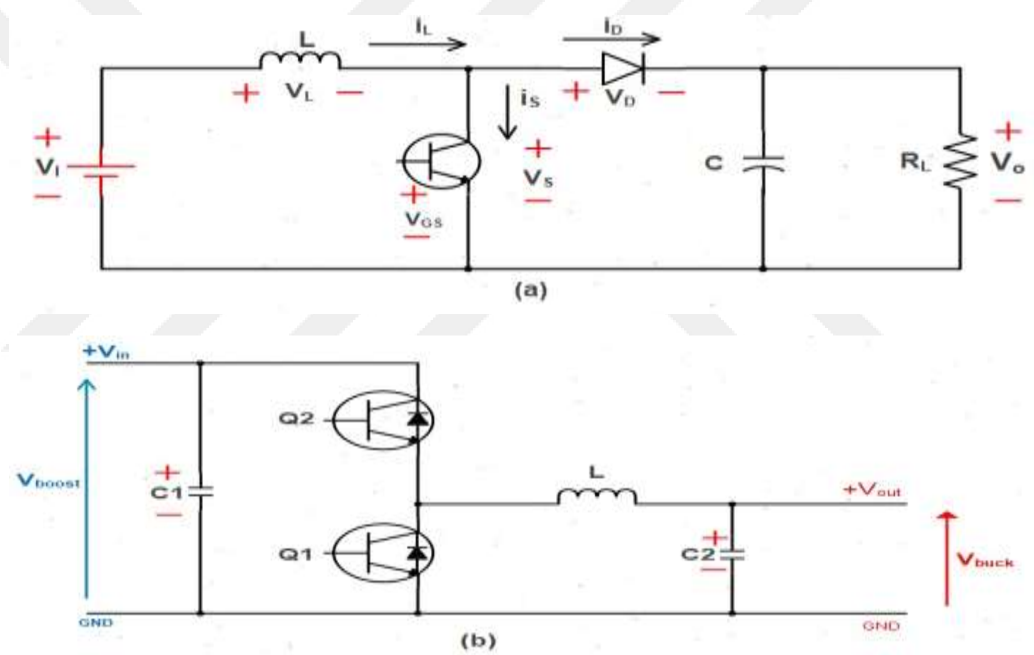

Figure II-13 Circuit diagrams of the converters (a) Unidirectional boost type and (b) Bidirectional buck-boost type.

2.4.1. Single Quadrature DC-DC Boost Converter

The proposed single quadrature DC-DC boost converter as shown in Figure II-13 (a) is intended to increase the output voltage so that it always exceeds the voltage input value in the steady-state operation [52]. The simple materials of the power electronics circuit have been used to implement this DC-DC converter by using a power switch (MOSFET or IGBT), an inductor (L), a filter capacitor (C) and a diode (D1) with a load resistor RL.

The operation of the DC-DC converter single quadrature type works in two modes, both works according to the following: Input inductance, the duty cycle (D), and the load, which are continuous conduction mode (CCM) and discontinuous conduction mode (DCM). Moreover, CCM mode can be achieved. by selecting the proper converters' parameters. Figure II-14 is illustrative for the operation of DC-DC in terms of the equivalent circuits for ON and OFF switch as well as shows the currents and the voltages waveforms.

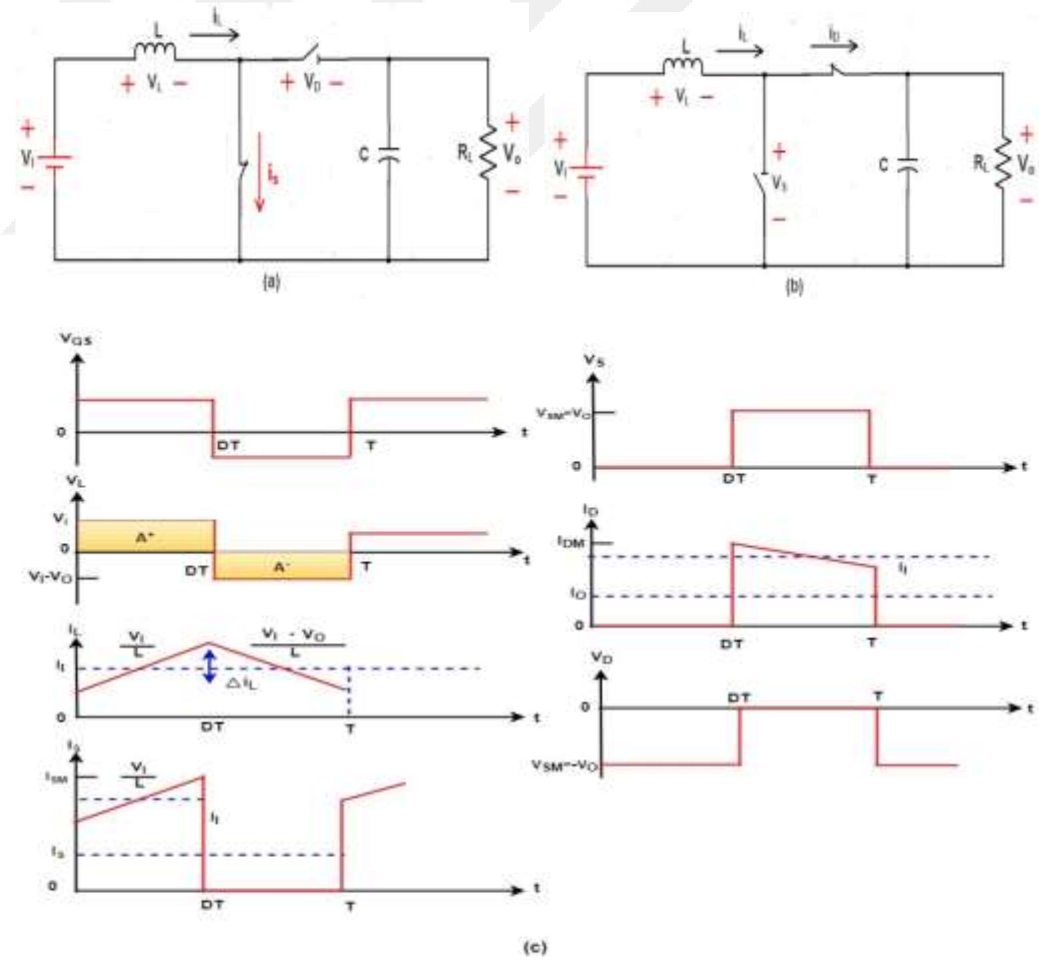

Figure II-14 Main waveforms and equivalent circuit diagrams for a single quadrature converter on and off states of operation (a) circuit diagram in the ON state, (b) circuit diagram in the OFF state, and (c) is the voltage and current waveforms in both cases.

As mentioned above, the DC-DC single quadrature converter works in two modes. The explanation of two states of operation as illustrated in Figure II-14 that simply summarized as below:

When 0 < t ≤ DT: switch ON and the diode is OFF consequently, the diode becomes reverse biased (VD=VO). Resulting in, the inductor current (IL) increasing linearly with a slope of (VI/L).

When DT < t ≤ T and **t = DT:** switch OFF and the diode is ON consequently, VL = VI − VO. As a result, the inductor current declines as a slope of (VI − VO)/L. And when time **t = T** consequently, the switch is reactivated (OFF/ON); the relationship between VI and VO can be calculated via the voltage second-balance across the inductor as shown in [52]:

$$V_O = \frac{V_i}{1-D} \tag{2.1}$$

The minimum inductance value needs to match these values in order to ensure that the converter functions in CCM mode:

$$L_{min} = \frac{V_i}{2I_{in} f_s} \tag{2.2}$$

The output capacitor should also be designed so that it has the following values in order to maintain the DC output voltage ripple at the acceptable limit (which is typically less than 20%):

$$C = \frac{I_{out}}{\Delta V f_s} \tag{2.3}$$

2.4.2. Two Quadrature DC Buck-Boost Converters

DC-DC converters typically are unidirectional which transfers the power in one direction, for both types buck and boost. However, the converter can work bidirectionally by replacing the freewheeling diode with an active switch that has an anti-parallel diode [56]. Figure II-13 (b) shows the two-quadrature bidirectional converter.

In this converter, there is two transistors switch (Q1 and Q2) which are working complementary as following the work of these switches: If the Q1 is conducting, then Q2 must be blocking and vice versa for both Q1 and Q2. Moreover, the converter behaves like a buck or a boost converter according to which of the voltages V-boost or V-buck is considered as input or output; Also depending on the direction of power flow. Furthermore, in this circuit topology, the polarity of the voltage is not reversible. Thus, this converter works in two of the four possible current-voltage quadrants. Therefore, this converter called two-quadrant converter [57], [58].

This converter is the two-quadrant converter, then the transistors Q1 and Q2 are switched, thereby that the converter operates in steady-state with four subintervals [57].

Overall, we can use the same equation for the boost type and buck type converters, since the relation range the V_o and V_i depends on the buck duty cycle switch as named d_1 and boost switch duty cycle as named d_2.

2.5. Average Modeling of the Single-Quadrature Converter

The waveforms can be averaged over a period of time that is brief in comparison to the system's inherent time constants without appreciably influencing the response [82].

When the basic condition is met, averaging the single-quadrature converter waveforms throughout the switching period is a good approximation. The converter's low-frequency behavior is predicted by the averaged model, which ignores the highfrequency switching harmonics. The single-quadrature converter in this section is modelled by using a conventional transformer-less single-quadrature architecture.

Figure II-15 [58] depicts the electronic circuit.

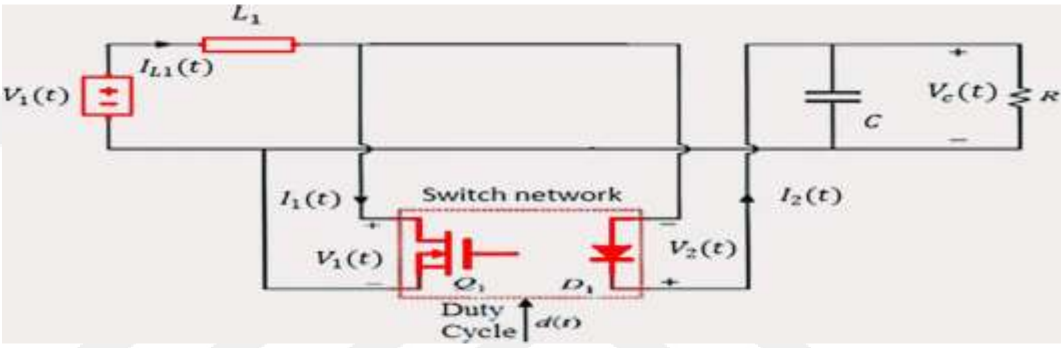

Figure II-15 Single-quadrature DC-DC converter equivalent circuit.

As illustrated in Figure II-16 below, the average model for the converter's switch can be derived in the form of a switch network, where the switches are substituted with dependent sources whose waveforms are conformity the waveforms of switch terminal dependent. From the two switch modes operation of the converter, and based on the current/voltage balance criteria [82], the relationships between the average of currents for the input and output converter are represented as:

$$I_o = \eta\,(1 - D)\,I_i \qquad (2.4)$$

Generally, the efficiency of the converter should be constant, however, we assumed to be 88% at full load.

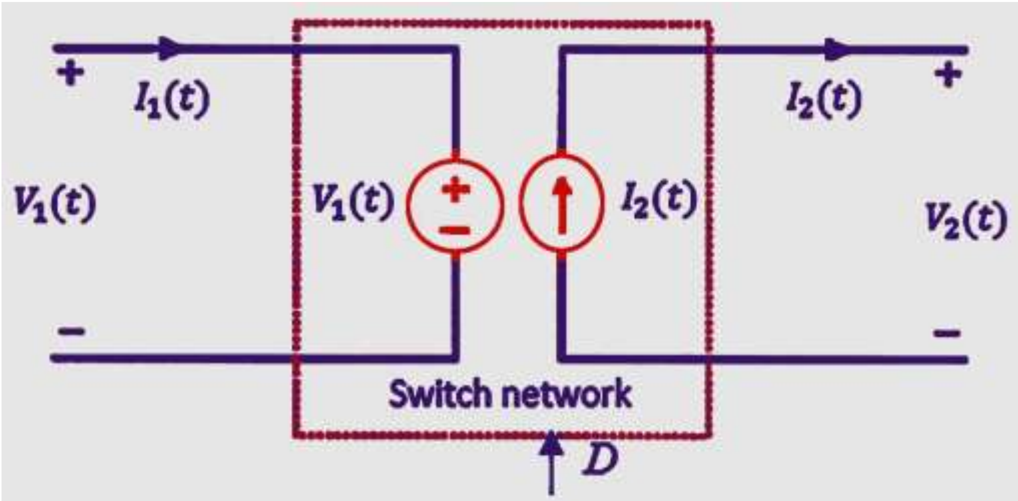

Figure II-16 Average Switch network model.

Figure II-17 depicts the model of the single-quadrature converter in its average steady-state form, which is derived from Figures II-15 and II-16 and based on the averaged steady-state equations in (2.1) and (2.4).

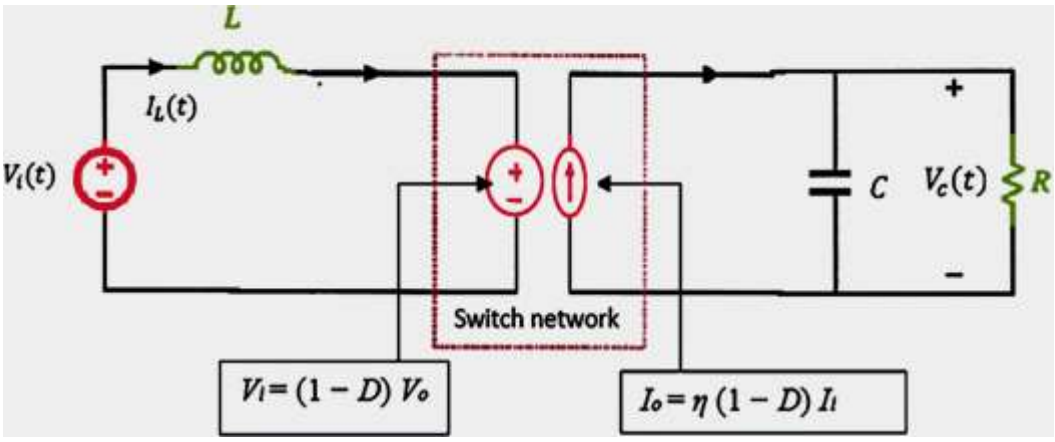

Figure II-17 Equivalent averaged model of single-quadrature DC-DC converter.

2.6. Average Modeling of Two-Quadrature Converter

The switching-function model is used to represent the two-quadrature converter that is directly controlled by the duty cycle signal. As previously mentioned, the twoquadrant bidirectional outputs can be utilized in either a buck or boost configuration. Two-quadrature DC-DC converter average switch model can be derived based on buck (Charging Mode) and boost (Discharging Mode) operations. As a result, the same average model of the boost converter can be employed in the discharging mode. While, the charging mode, a model for the buck converter should be developed on an average basis. Figure II-18 depicts the buck converter with a switch network.

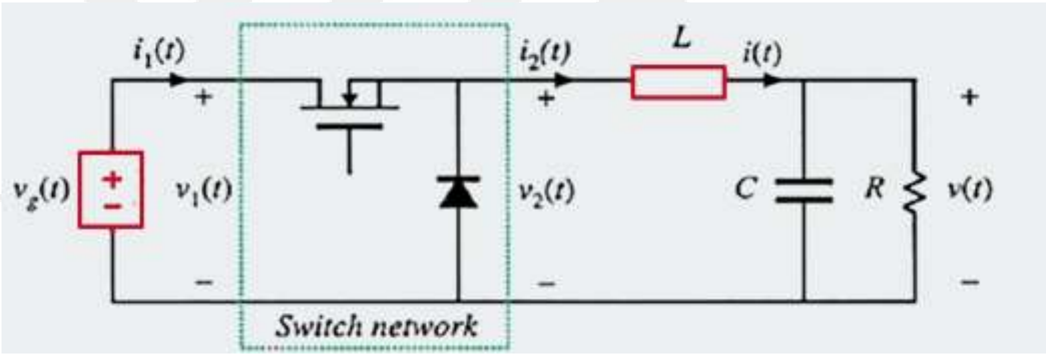

Figure II-18 DC-DC buck converter model.

The two-quadrature converter in the buck mode has been modelled based on using the average model method given in Figure II-15 and Figure II-19.

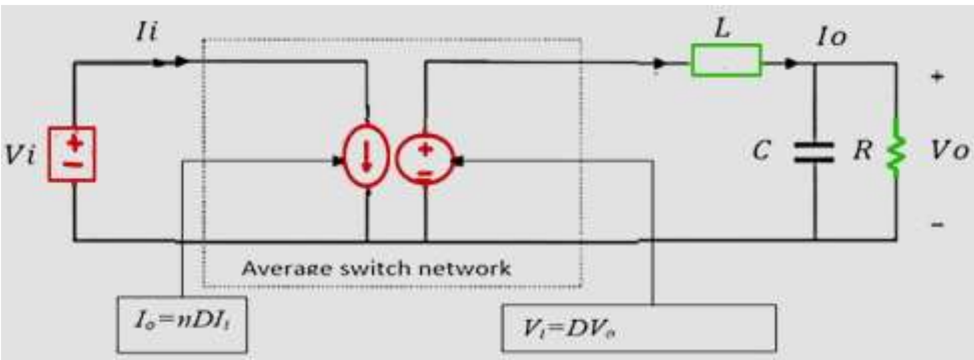

Figure II-19 Average model of two-quadrature converter in the buck mode.

The operation of buck mode, the relationships for V_i and I_o can be obtained as shown below:

$$V_i = DV_o \quad (2.5)$$

$$I_o = \eta D I_i \quad (2.6)$$

Where D consists of d1 for the boost switch and d2 for the buck switch.

III. CHAPTER THREE HYBRID MANAGEMENT SYSTEM DESCRIPTION AND METHODOLOGY

3.1. Overview of the Proposed intelligent EMS

Generally, approaches mathematical models and software computer applications (simulation) is developing the control methods as well as detailed study for vehicle models, prior to real applications. The most common control method used for flow power management of powertrain electric vehicles is optimal control, particularly the dynamic programming (DP) that is applied to different types of vehicles [59]. Optimal control works on the problem of defining a control law for a system such that a meet optimality criterion with the function of state and control variables which set as optimality for the control system. Introduced other controllers to control the power flow such as an Artificial Intelligent (AI) which are artificial neural network (ANN), neural fuzzy network [62-64], etc. Also, fuzzy wavelet neural network [60]. The wavelets control strategy is also employed to manage the power flow of the electric vehicle; while it is considered as a form of time-frequency representation for continuous-time signals. Therefore, it is suited for harmonic analysis [61]. Furthermore, the wavelet method optimizes the system and achieves great efficiency as well as extends the life of power supplies.

The objective of this work is to create an intelligent Energy Management System (EMS) for the FCHEV that meets efficiently the load power requirement and uses less hydrogen consumption. The main power source of our proposed model plug-in hybrid FCEV is FC that designed for delivering steady-state load power, while the UC is accountable for providing the transient load also controlling the DC bus voltage; additionally, the power of the BAT supports the power output of the fuel cell in feeding the load if needed. This can be achieved by supplying the switching converters of the FC and BAT with suitable signals to ensure the response of the hybrid fuel cell system is working properly to handle the load dynamics.

Two converters have been used to control the FC and BAT output and provide the desired voltage of the DC bus as well as keep the voltage stable at 300 volts. The FC is regulated and its voltage is increased by means of a single-quadrature boost converter, while the BAT is charged by means of a two-quadrature DC-DC buckboost converter. Meanwhile, the BAT converter also raises and controls the DC bus voltage at 300 volts as well as uses a cascade control structure that controlled by Wavelet Neural Network parallel with PI controller (WNN-PI) for the purpose of controlling the flow of electricity between the load and the DC-bus voltage by monitoring of the SOC for BAT’s. Then, the UC is linked to DC bus voltage directly without a converter which in turn has a high response to the change of power load within maintaining the DC voltage link at 300 volts promptly. In this work, intelligent control techniques and Particle Swarm Optimization (PSO) methods been used to manage the output power of both

BAT and FC for covering the desired power load of the vehicle efficiently and without power losses which result in the best control of hydrogen consumption. Overall, the controllers are used to inform converters for boosting or bucking output voltage within a closed control system. Figure III-1 shows the energy management system, WNN-PI based on PSO controllers' system and the developed hybrid plug-in FCEV configuration.

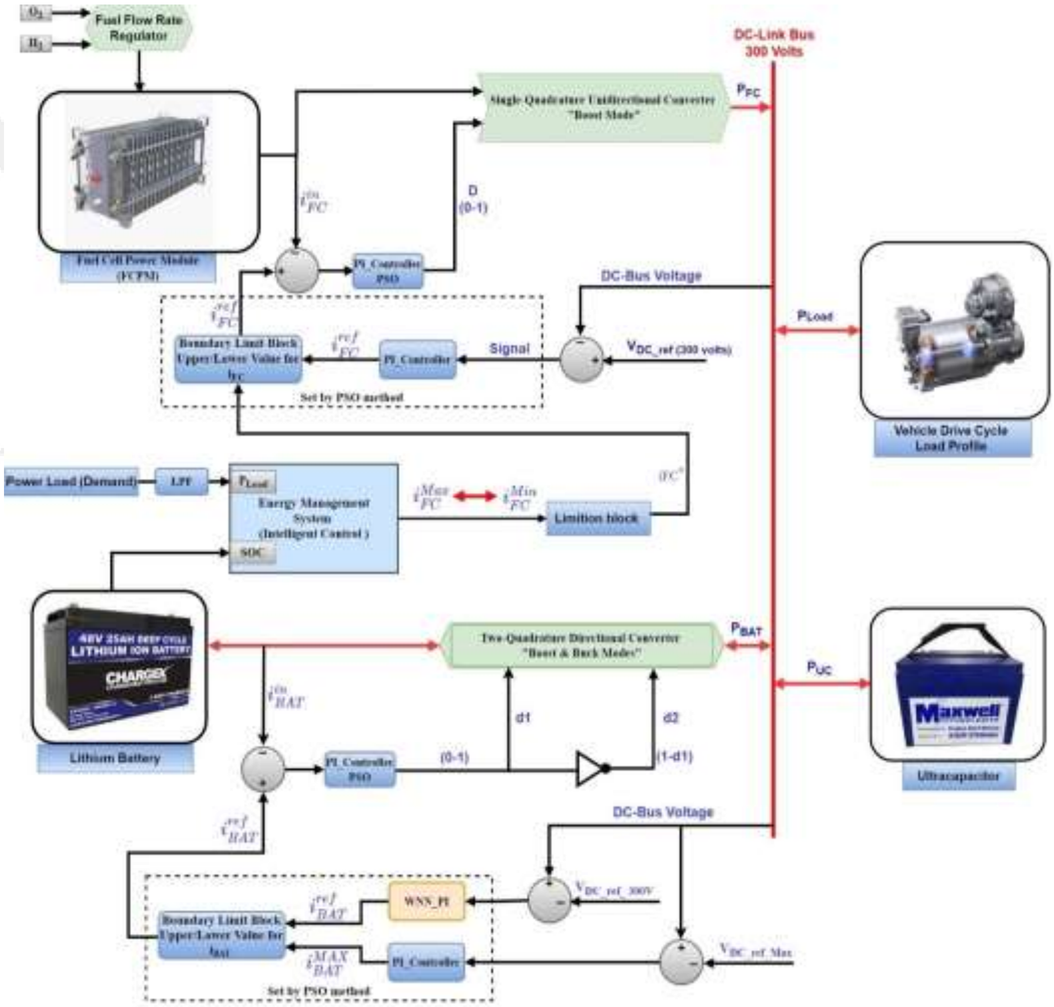

Figure III-1 The developed hybrid plug-in FCEV configuration of energy management system, WNN-PI based on PSO controllers.

Figure III-1 shows the development for the cascade control system of the converters that depends on the inner currents as a reference for being fast respond and for setting the stable signals for the duty cycle for these converters. Moreover, control the output voltage of the power sources (fuel cell and battery). To find the system's reference values, a DC voltage reference V_{DC_ref} is subtracted from the DC-bus voltage actual value to obtain the fuel cell reference current i_{FC}^{ref} then the outer voltage loop achieved of the converter that control fuel cell. Then, the i_{FC}^{ref} passed to the inner current control loop. The control method Particle Swarm Optimization (PSO) has been used to set the values of PI controller for i_{FC}^{ref}. Further, the EMS figure out the lowest and highest value of the i_{FC}^{*} for ensuring no negative power feed to the FC generator and respond only to the maximum positive power that is required for the vehicle since the FC does not accepted the regenerative braking power. The i_{FC}^{*} is depending on the load power and BAT status are taken into account by the EMS controller then set the rules; the controller will be further discussed in chapter-IV. Finally, the i_{FC}^{ref} and i_{FC}^{*} passed through the boundary limit block in order to find the final i_{FC}^{ref} then subtracted from the real output FC current (i_{FC}^{in}) which resulted in an error signal that processing by the PI controller to adjust the D (0-1) of the fuel cell converter; all PI controllers, boundary limit block and WNN values been set by PSO.

Due to the different speeds that may the vehicle go through such as a high speed at the beginning of the acceleration mode as well as suddenly braking at deceleration; all modes lead to high frequencies. Therefore, low pass filters (LPF) and Wavelet methodologies have been used to overcome these frequencies as well as to get a smooth response for the FC power. The LPF has been connected to the power load demand, while the Wavelet Neural Network (WNN) link with the PI controller and boundary limit block which all variables been set by PSO to generate a smooth current of the battery (I_{BAT}). Overall, the outer voltage loop has been built with a wider frequency range than the LPF's cut frequency for ensuring the following:

- No high frequencies.
- Remove the interaction between BAT and FC.
- Allows the UC to deal with load fluctuations when the FC power is insufficient.

As mentioned in chapter-II that the UC has many advantages; consequently, the UC has been used more often than BAT in this design due to its advantages of UC such as a longer lifespan than the BAT also greater efficiency. Hence, the UC straight connect to the DC bus without using any kind of converters. Resulting the UC is the first response to transit load demands as well as charging and discharging of UC are the first response for suddenly acceleration and deceleration periods mode. Moreover, if the load power demands of the vehicle are higher than the FC power and less than the maximum transit load demands then the BAT will respond to handle the load power demands by rising the DC voltage link to the reference value (300 volts) via the BAT boost converter that controlled by WNN-PI based on PSO method controllers to generate the correct duty cycles for the BAT converter. Furthermore, the system also responds to braking periods which transfer the energy of the braking to charge the UC and then BAT through the DC voltage link.

Instead of using conventional sigmoid functions in artificial neural networks, wavelet functions are employed in the hidden layer as sigmoid functions. The WNN inherits has many advantages in terms of both wavelet analysis and neural network which are the nonlinear function imitation, time-frequency location, self-learning, self-adapting as well as robustness. Furthermore, the wavelet analysis theory ensures that the WNN can accurately and quickly imitate the nonlinear system [74]. Overall, the wavelet neural network and the PI controller are coupled to produce the WNN-PI controller, which is an improved controller. Moreover, the WNN-PI controller's parameters are learned by using the Particle Swarm Optimization (PSO) algorithm. Section 3.3 contains modifications for feed-forward WNN methods as well as recurrent wavelet neural networks. Furthermore, the next section explained the algorithm of the particle swarm optimization (PSO).

3.2. Particle Swarm Optimization

The term "Particle Swarm Optimization" (PSO) refers to a population produced by computer approaches influenced by the imitation of social behavior (socialpsychological theory); then been resulting called a swarm theory. Moreover, Eberhart was one of the original designers and developers of PSO [67]. Further, a newer version has been introduced in 1998 by incorporating the inertia weights idea. It has been discovered that using this approach to resolve non-linear, non-differentiable issues is a trustworthy methodology.

Overall, this method can be simplified by considering that each companion, is called a particle, in the population, which is called swarm intelligence. Additionally, should fly in various directions over the search area, the process will then meet the need for the fitness function. [68].

3.2.1. Algorithm of Particle Swarm Optimization

As mentioned earlier, the PSO method uses to solve problems with high optimization. Then, a PSO algorithm depicts a number of people flying through the search space (referred to as particles) [69]. These particles represent a candidate solution every try then reach out to the optimization problem. Generally, the best position visited by a particle, i.e., their own experience in a swarm trip (under several trips), as well as the position of the best particle in its neighborhood, impacts the particle's position (experience of neighboring particles). In this context, the optimal location for a particle within its neighborhood, the entire swarm, is described as the particle's global best position, and the resultant technique is called the global best position particle swarm optimization (PSO). To put it simply, the best previous location of a particle with the smallest fitness value is the local best position (lbest). The best particle in the population is given an algorithm named the global best position (gbest). When using condensed neighborhoods, this technique is sometimes referred to as the optimal PSO. The fitness function used to evaluate the effectiveness of each particle is different for each optimization problem. The fundamental PSO method is shown as a flowchart in Figure III-2 [70], [71].

According to Figure III-2 the following processes show the procedure of how PSO implement as summarized in five process:

Process No. 1 Generation of population particles

Set up a "population" of agents (particles) spread out evenly throughout x, then choose the number of particles and iterations as well as adjusting of accelerating coefficients c_1 and c_2, inertia first value called weight (w), and arbitrary numbers called R_1 and R_2 to begin searching for the best optimal solution.

Process No. 2 The initialization for each particle

For each particle, set the current position $x_i(t)$ and velocity $v_i(t)$ to the initialize position. The particles are generated at random between the parameter's minimum and maximum values. Then all the ith particle signified as x_i = ($x_{i1}, x_{i2}, \ldots, x_{iD}$). Moreover, particle i is the velocity that is represented as v_i = ($v_{i1}, v_{i2}, \ldots, v_{iD}$), resulting in the calculation to find the (lbest) also the (gbest).

Process No. 3 Calculation of fitness function

The goal (fitness) function monitors the optimization process and controls the PSO algorithm's overall performance (convergence speed, efficiency, and optimization accuracy). The domain constraints and the preference constraints are used to determine the optimal objective function. Only those objective functions that meet the required standard are considered. The most often used performance metrics based on the error criterion are the Integrated Absolute Error (IAE), the Integrated of Time Weight Square Error (ITSE), and the Integrated of Square Error (ISE), all of which can computed analytically in the frequency domain [73]. The system and controller are taken into account while selecting the criterion. The following multiobjective functions are used in this thesis, is the Integral of Squared Error (ISE) criterion and the overshoot (M_p) criterion:

$$\text{fitness function} = \min(ISE) + \min(M_p) \tag{3.1}$$

Where:

$$ISE = \int e^2(t)dt \tag{3.2}$$

$$M_p = \max(V) - (V_{ref}) \tag{3.3}$$

$$e(i) = D(i) - y(i) \tag{3.4}$$

Then, expressed that the output model is y(i), and expressed that the target is D(i). V is expressed the actual voltage, and V_{ref} is the reference voltage.

Process No. 4 Update the swarm

The equations (3.5) and (3.6) are used to update the velocity $v_i(t)$ and current position $x_i(t)$ for each particle in the swarm. The main loop starts as well as the objective function is calculated in order to update the particle positions. Resulting in, set the new value to lbest, if it is better than the previous best as a continuous loop. In the same way, the gbest value is updated as the best lbest. Finally, the following equation can be used to modify the velocity of each agent.

$$v_i^{k+1} = w * v_i^k + c_1 * R_1 * (lbest_i - x_i^k) + c_2 * R_2 * (gbest_i - x_i^k) \tag{3.5}$$

The below equation can be used to modify the current position:

$$x_i^{k+1} = x_i^k + v_i^{k+1} \tag{3.6}$$

Where the current position of particle i at iteration k represent as x_i^k, and the velocity of particle i at iteration k represent as v_i^k. Moreover, w is the inertia weight as shown in equation (3.7). Furthermore, positive acceleration constants are represented as c_1, c_2, while the random variables represent as R_1, R_2 which are uniformly distributed in the range between [0-1].

$$w = w_{max} - \frac{(w_{max} - w_{min})}{iter_{max}} \tag{3.7}$$

Where w_{min} represents the initial weight, w_{max} represents the final weight, and $iter_{max}$ represents the maximum number of iterations.

Process No. 5 Stopping criteria

In the event that the current iteration number is higher than the maximum number of iterations, the process will be terminated and the final data will be saved. If not, start again with a new value for every particle.

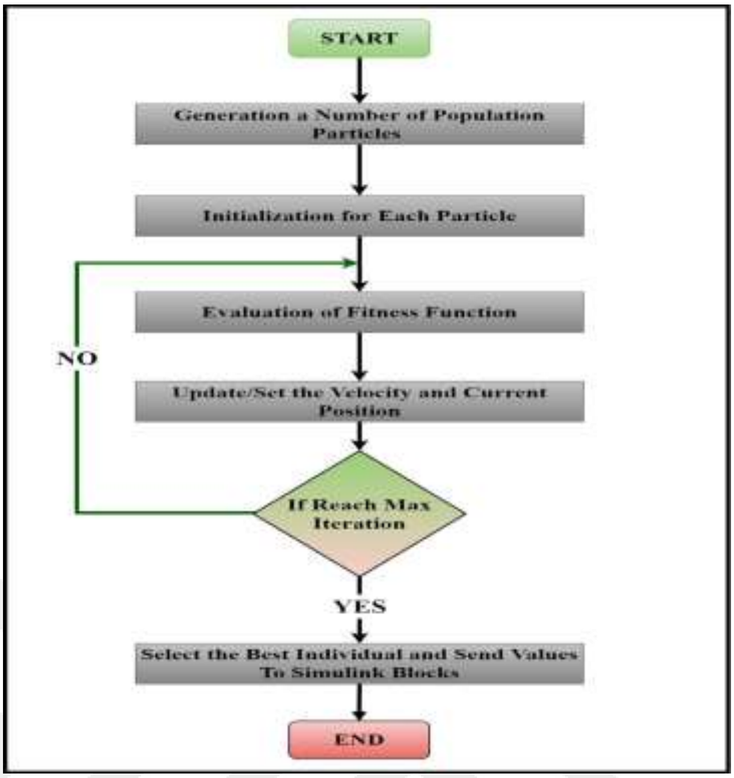

Figure III-2 The PSO process.

3.3. Wavelet Networks

The combination of wavelet theory and neural networks has resulted in the creation of a new mapping wavelet network of wavelet networks or wavelet neural network (WNN). Wavelet networks use wavelets as activation functions in feed-forward neural networks. Wavelet networks use the wavelets transform function to replace the global sigmoid activation units of traditional feed-forward artificial neural networks (ANNs). Moreover, weights aren't the only thing that's optimized, also dilation and the position (translation) are too. Wavelet nodes are used to create efficient networks that are best approximated for nonlinear and nonstationary functions [72]. The Wavenet (Fixed grid WNs) and the Wavelet Network (Adaptive WNs) are the two most common forms of Wavelet neural networks; this variant combines the two approaches. The wavelets' translation and dilation, as well as the summer weights, are modified according to a learning algorithm. Wavelet neural network modeling generally involves two steps: figuring out the network topology (number of layers, number of neurons in each layer, and kind of activation function, mother wavelet transform), and then adjusting the wavelet network parameters using any learning method [75].

3.4. Structure of Wavelet Neural Network (WNN)

The structure of a wavelet neural network (WNN) is similar to that of a neural network. In addition, a feed-forward neural network consists of one hidden layer and one output layer but accepts many inputs. The activation functions of neurons in the hidden layer are derived from a wavelet basis. These wavelet neurons, known as wavelons [76], receive as input parameters the wavelet dilation and translation coefficients. Wavelet neural networks are divided into two types: recurrent and nonrecurrent(feed-forward):

3.4.1. Structure of Feed Forward Wavelet Neural Network (FFWNN)

The FFWNN is a feed-forward artificial neural network with a hidden layer that uses the wavelet transform function. There is no feedback connection with the FFWNN. That is, through feed-forward connections, the output is calculated directly from the input. Feed-forward wavelet neural networks come in two forms which are:

3.4.1.1. Radial Basis wavelet neural network (RBWNN)

The simplest structure of the wavelet neural network, which is identical to the radial basis neural network (RBNN), is the Radial Basis Wavelet Neural Network (RBWNN) but uses the wavelet function instead of the radial basis function. The weights connections in this network are only between the hidden layer and the output layer [77].

Figure III-3 shows the structure of a radial basis wavelet neural network (RBWNN). Then by connect a number of daughter wavelets $\psi_{a,b}$, Where $\psi_{a,b}$ are formed by dilation (a) and translation (b) of the mother wavelet (ψ) [72].

$$\psi_{a,b} = \psi\left(\frac{x-b}{a}\right) \tag{3.8}$$

The output of this network is given as follows [80]:

$$y = \sum_{n=1}^{N} w_N \psi_{a_N,b_N} \tag{3.9}$$

Where the input signal is represented as x, whereas the number of neurons in the hidden layer is represented as N and the output weight is represented as w_N.

Generally, any optimization technique can be used to improve and set the network variables w_N, a_N and b_N. The particle swarm optimization (PSO) is used in this thesis to minimize the error based on the fitness function.

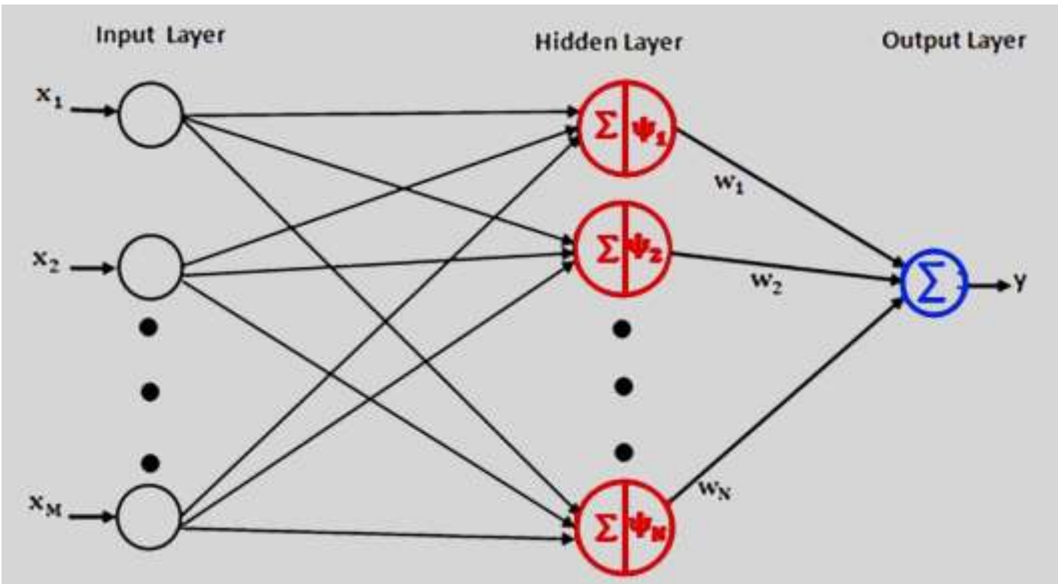

Figure III-3 The structure of a radial basis wavelet neural network (RBWNN).

3.4.1.2. Conventional Wavelet Neural Network

The radial basis wavelet neural network is simpler than the conventional WNN. The hidden layer of the conventional WNN is a multilayer feed-forward network with a wavelet activation function. This network also includes weights connections for each side in the hidden layer, as well as sigmoid function and bias in the output layer [78]. Figure III-4 depicts the structure of a conventional wavelet neural network. To build a suitable wavelet neural network, required to select the number of hidden layers and neurons, and algorithm to tuning the parameters we choose the PSO technique in this work. Input and output layers are represented as vectors, where input as x= $[x_1, x_2, \dots\dots, x_M$], and output as y= $[y_1, y_2 \dots\dots . y_K$] and the hidden layer's impulse function is wavelet basis function. The Y_j is the output where can express in the below equation [72], [78]:

$$Y_j = \sigma(u_j) = \sigma\left[\sum_{n=1}^{N} w_{j,n}\, \psi_{a_n b_n}\left(\sum_{m=1}^{M} v_{n,m}\, x_m\right) + g\right] \tag{3.10}$$

Where, j=1,etc,…,K, while the inputs umber is M, and the number of outputs layer represented as K, the number of hidden layer represented as N, the bias represented as g and activation function of the output layer is denoted by σ(u), activate by the sigmoid function, which is described as the function below [79]:

$$\sigma(u) = \frac{1}{1 + e^{-u}} \tag{3.11}$$

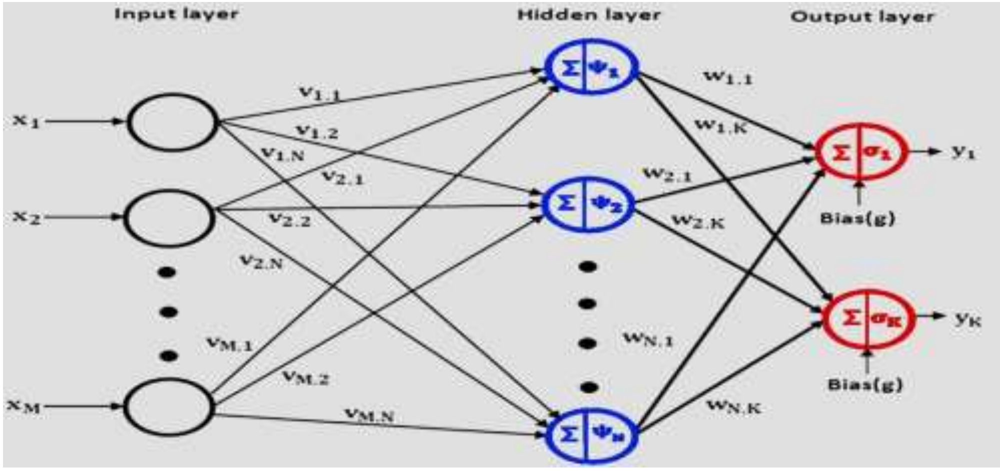

Figure III-4 The structure of a conventional wavelet neural network.

3.4.2. Recurrent Wavelet Neural Networks (RWNN)

In addition to the network's current inputs, a recurrent network's output also relies on its prior states and its outputs. Recurrent networks are thus more effective than nonrecurrent networks and helpful for system identification and nonlinear control [81]. feedback networks in recurrent networks. Recurrent networks come in a variety of shapes and sizes depending on the feedback link. There are two basic categories of feedback connections: partial feedback, where just one layer's output is connected to that layer's input, and state feedback, where all layers' outputs are linked to each other's inputs and output networks. In the recurrent wavelet network configurations, the wavelet network input consists of delayed samples of the system input x_M and the system output y(k). The number of inputs to the wavelet network increases with the order of the system being modeled. The architecture of RWNN is depicted in Figure III-5, and the output of each layer can find as the below [81]:

$$\psi_N = \psi\left(\frac{u_N - b_N}{a_N}\right) \tag{3.12}$$

Where, a_N and b_N are the dilation and the translation factors of the wavelets, respectively. Where layer inputs for time (n) represented as below:

$$u_N(n) = x_N(n) + \psi_N(n-1) * \emptyset_N \tag{3.13}$$

Where, denotes the weight of the self-feedback loop represented as $\emptyset_N$. Then, the output of the network is given as below:

$$y = \sum_{N=1}^{N} w_N \psi\left(\frac{u_N - b_N}{a_N}\right) \tag{3.14}$$

$$u(n) = x(n - D_i) + y(n - D_0) * r_N \tag{3.15}$$

The input signal is represented as X, the number of neurons in the hidden layer is represented as N, while the output weight is represented as w_N and D_i, D_0 is the number of delays for the input as well as the output network, r_n is the weight of the output feedback loop.

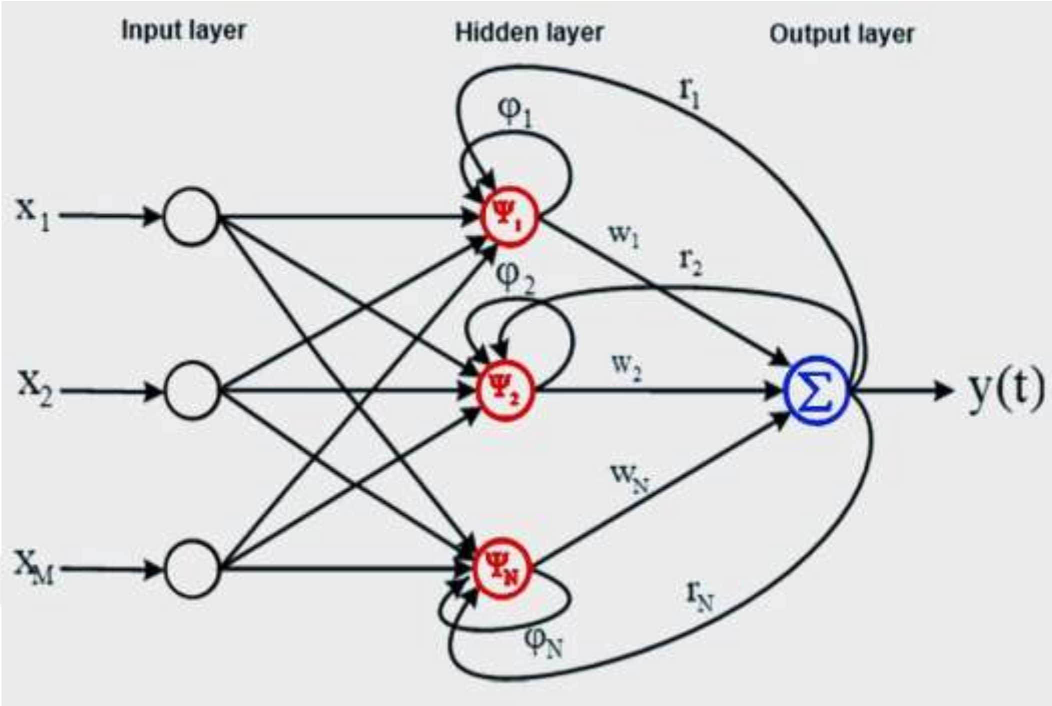

Figure III-5 The structure of recurrent wavelet neural network.

3.5. Control System Models for Single and Two Quadrature Converters

The power conditioning unit of FCEV is explained in the chapter-II sections 2.4 and 2.5 and 2.6 for both FC converter and BAT converter, in this section the control model for them will be explained in details. Moreover, the main block diagram of the proposed control architecture for the powertrain, hybrid FCEV and how to maintain the variations parameters into the vehicle driving cycles in terms of the produce and demand power also keeping the voltage link at the desired level of 300 volts by converters; all shown in Figure III-1 and explained in section 3.1.

Generally, the proposed controllers of PI-PSO and the developed EMS are used to determine and regulate the BAT and FC currents boundary to ensure the correct periods for charge and the discharge for BAT and discharging only for FC. Hence, the fuel cell

i^*_{FC}

is responding just for the load power that has steady-state condition, therefore, the is link to the single-quadrature converter; while, the output current of the battery is link to the two-quadrature converter. The main block modelling for FC and BAT in terms of current reference are illustrated in Figure III-6 (a) and (b) respectively. The setting parameters of both the single and two quadrature converters are aimed to regulated the DC-bus voltage which is based on output voltage signal then resulting in limiting the input current and controlling the output voltage for FC and BAT.

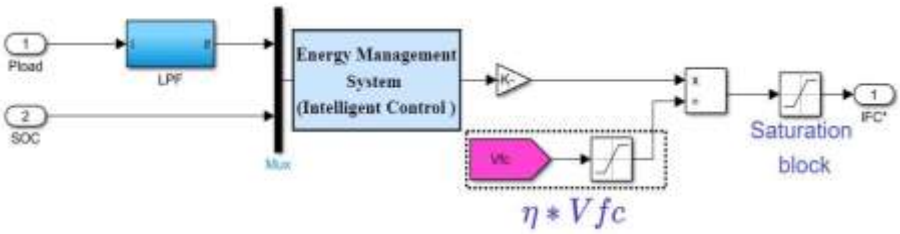

(a)

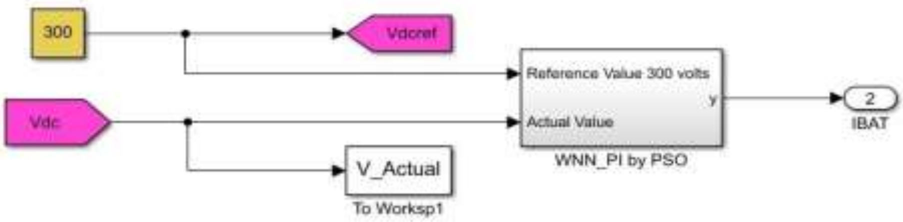

(b)

Figure III-6 The modelling controller for current reference into the converters (a) FC converter and (b) BAT converter.

There are many transfer functions of buck and boost converters which are mentioned in contexts [65], [66], and others. In this regard, the modeling for the present boost converter that controlled voltage loop only is based on the following transfer function:

$$\frac{V_o(s)}{D(s)} = \frac{\frac{V_i}{LC} - \frac{V_o^2}{RCV_i}s}{s^2 + \frac{1}{RC}s + \frac{1}{LC}\left(\frac{V_i}{V_o}\right)^2} \tag{3.16}$$

The boost converter used for FC in terms of controlling the flow power of the FCEV system; As shown in the numerator of equation (3.17) that converter owning a righthalf plane zero, which lead to phase-lag and acts as delay so there are problems in the stability as well as limits the available bandwidth of the converter controller. Nevertheless, these RHPZ effect can be overcome by using a cascade controller [48].

Overall, the control system of the converters is based on the cascade control as shown in Figure III-7 the structure basically depends on two PI controllers whereas mentioned earlier these PI controllers are set by PSO as well as the WNN to ensure the correct SOC of the battery and ultracapacitor and control the DC-bus voltage at reference volts.

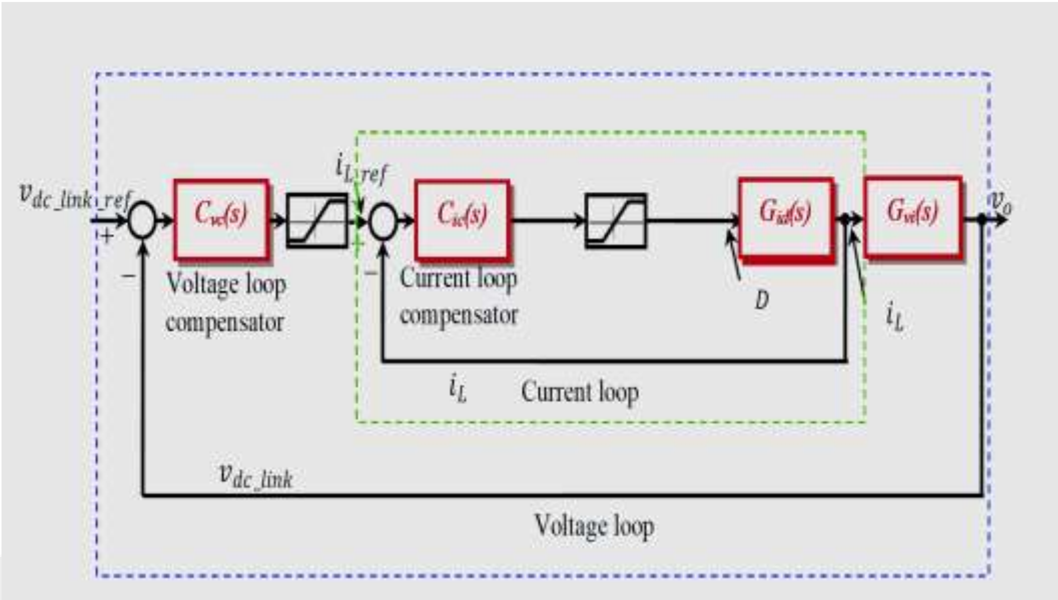

Figure III-7 The control system of the converters based on the cascade control.

The output voltage is regulated by the cascade controller system, as shown in Figure III-7, by means of the transfer function ($G_{vd}(s)$) of the converter, transfer functions of voltage ($G_{iv}(s)$) and current ($G_{id}(s)$). Parameters for entire system are ultimately selected using PSO, and the resulting PI controller equations for each are listed below.

$$C_{vc}(s) = K_{pv} + \frac{K_{iv}}{s} \tag{3.17}$$

$$C_{ic}(s) = K_{pc} + \frac{K_{ic}}{s} \tag{3.18}$$

The parameters of the voltage and current loops PI controller are defined as K_{pv}, K_{iv}, K_{pc} and K_{ic} respectively.

3.5.1. Design of the Single-Quadrature Converter Control Loops

In order to find the voltage across the input inductance port ($L \, {di_i}/{dt}$) and the current through the output capacitance ($C \, {dV_o}/{dt}$). KVL has been applied to the input port of the circuit shown in chapter-II (Figure II-18) then resulting as below:

$$L \, {di_i}/{dt} = V_i - (1-D)V_o \tag{3.19}$$

$$C \, {dV_o}/{dt} = \eta(1-D)I_i - I_o \tag{3.20}$$

Via the Laplace transform for (3.19) and (3.20), the inductor voltage and capacitor current in s-domain can be obtained as:

$$I(s) = \frac{V_i - (1-D)V_o}{Ls} \tag{3.21}$$

$$V_o(s) = \frac{\eta(1-D)I_i - I_o}{Cs} \tag{3.22}$$

Where Vo = Vc

Eventually, the last equations (3.21) and (3.22) resulting in the cascade controller of the boost converter is described as in Figure III-8.

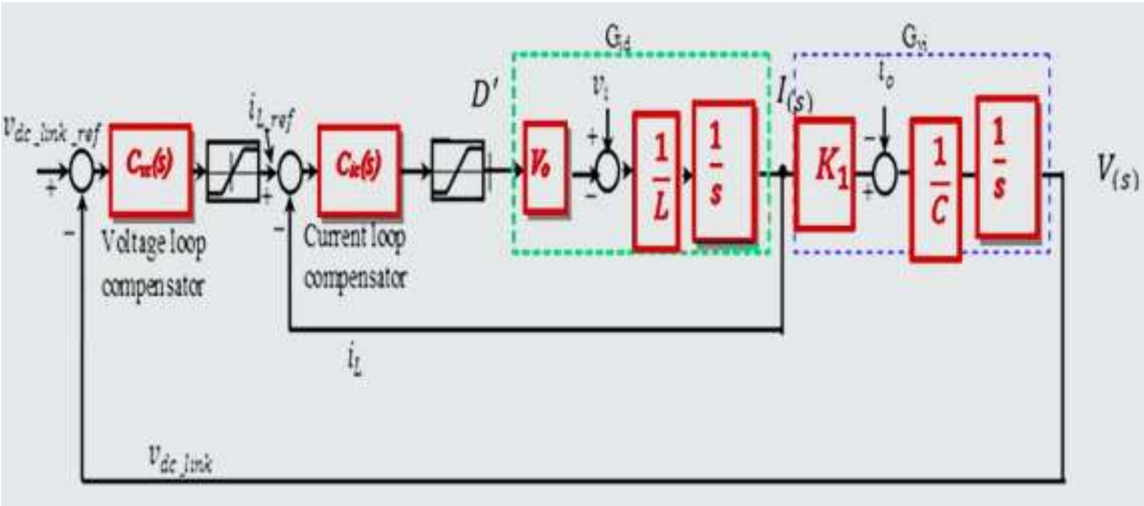

Figure III-8 The cascade controller of the boost converter.

Where, $K_1 = \eta \times (1\text{-}D)$ and $D' = (1\text{-}D)$

As shown in Figure III-8 we had to reduce the G_{id} and G_{vi} had to get first-order transfer functions, then the open-loop transfer functions for the voltage also the current controller both can be obtained as the following:

$$H_v(s) = \frac{K_{iv} + sK_{pv}}{Cs^2} \tag{3.23}$$

$$H_i(s) = \frac{K_{ic} + sK_{pc}}{Ls^2} \tag{3.24}$$

By taking into account the closed loop transfer function standard form denominator.

$s^2 + 2\zeta\omega_n s + \omega_n^2$, K_{pv}, K_{iv}, K_{pc}, and K_{ic} can be calculated.

3.5.2. Design of Two-Quadrature Converter Control Loops

As mentioned earlier in section 3.5 in terms of the single and two-quadrature DC-DC converter, it is been noticed that the two-quadrature DC-DC converter either works as a buck or boost converter. Therefore, it is able to use the same method of controller design that is used in the boost converter as explained in section 3.5.1 and link its cascade controller to be the buck converter. Whereas using the equivalent circuit as shown in chapter-II (Figure II-20); then resulting in the two-quadrature converter under buck mode operation with its control system can be described in the block diagram as shown in Figure III-9.

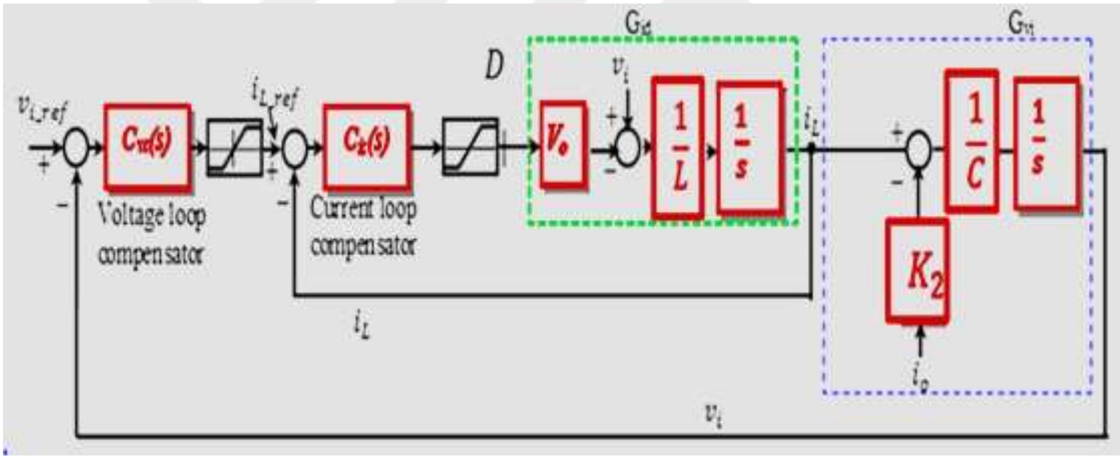

Figure III-9 The two-quadrature converter under buck mode operation.

Considering that: $K_2 = K_1$

The PSO strategy has been used to find out the suitable values of the three PI parameters in terms of Kp and Ki also set the limiting valve of saturation block (low and high limits) the PSO code works on running the simulation and set the values with minimum error is mentioned in Appendix (C-1).

3.6. WNN-PI Controller Based on PSO for BAT

The WNN_PI controller works on controlling the current boundary of the BAT that is based on the i_{BAT}^{max}, It is possible by analyzing the discrepancy between the DC-bus voltage signal and the DC-bus nominal voltage signal, which combines the capabilities of artificial neural networks for learning from processes and wavelet decomposition for identifying and controlling dynamic systems, as well as the ability to self-learn and adapt [72], [78]. This section modifies and implements the feedforward wavelet neural network and the proposed recurrent wavelet neural network with a tuning optimization system for the variables using the PSO method. The hybrid FCEV model's weights connection in the WNN and the PI controller's parameters (k_p and k_i) are adjusted live using the PSO method so that the voltage may be kept constant. Implementing a wavelet neural network faces two primary challenges. The PSO algorithm is first, and the network's design comes second. The Block diagram of PSO-based BAT with Feed-Forward function WNN-PI is shown in Figure III-10.

Next, we'll dive into the reasoning behind the WNN-PI controller's layout. Meanwhile, finding the i_{BAT}^{ref} via PI controller that tuned by PSO. Moreover, these currents are compared by the current boundary limiting block to find the requested i_{BAT}^{ref}, then compared with the output current of the BAT for producing the error signal which treated by the proposed PI-PSO controller to adjust the duty cycles (d1&d2) of the battery converter, which are limited between (0-1).

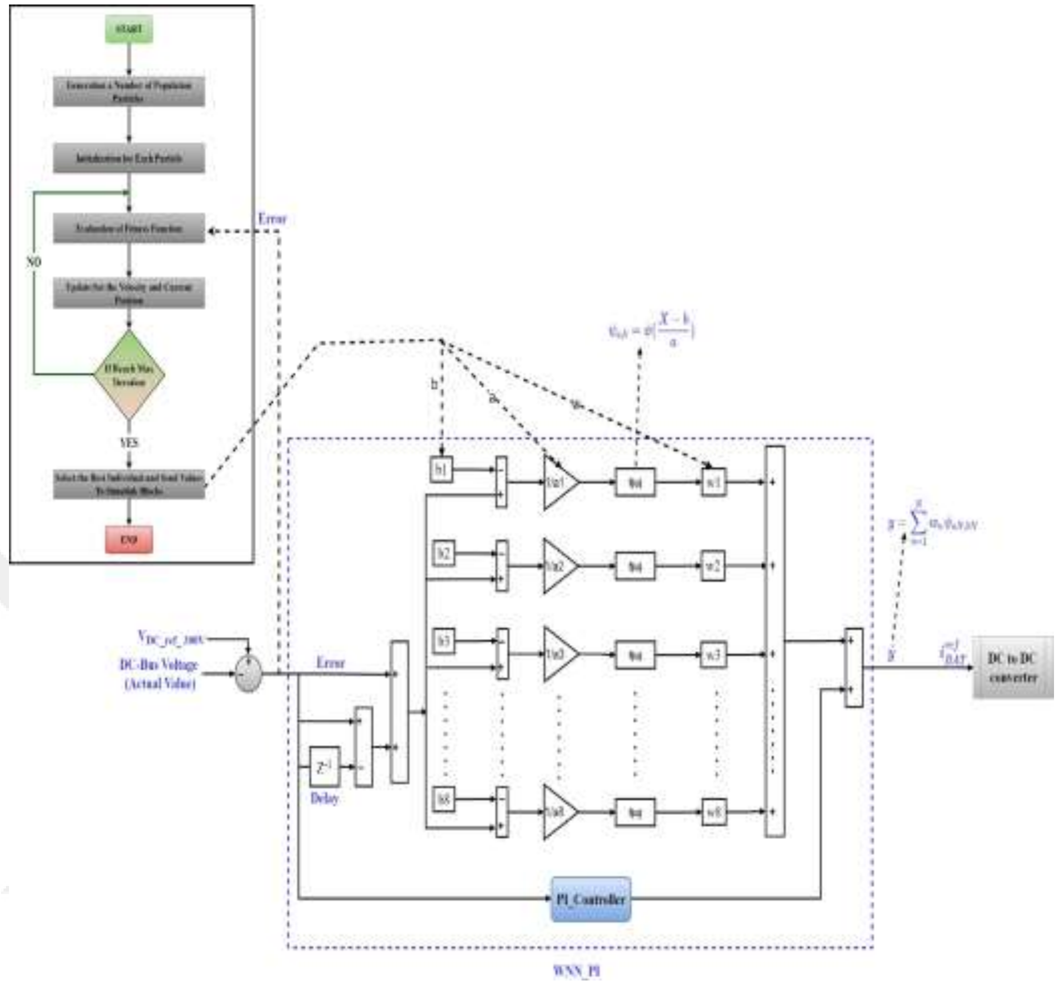

Figure III-10 The schematic representation of the WNN-PI BAT tuned by PSO algorithm.

The PSO algorithm has been discussed in section 3.2. Resulting in, adjusting the network parameters, to ensure the minimization of a cost function. Then, the cost fitness is expressed as shown in equation (3.1). When designing the WNN-PI controller, it is necessary to pick the kind of WNN, the number of layers and neurons, and the mother wavelet function. The proposed WNN-PI utilizes a single hidden layer with eight neurons and two input layers, one for the intended voltage (reference voltage) and the actual voltage. In addition, the following three varieties of mother wavelet functions are employed:

1. The Mexican hat function is shown below:

$$\psi(x) = (1 - x^2)e^{\frac{-x^2}{2}} \quad (3.25)$$

2. Below is seen the first partial derivative Mexican hat:

$$\psi(x) = (-x)e^{\frac{-x^2}{2}} \quad (3.26)$$

3. The Morlet's basic wavelet function is shown below:

$$\psi(x) = \mathrm{Cos}(w\,x)e^{\frac{-x^2}{2}} \quad (3.27)$$

The formula x is expressed as the desired signal, a variable value expressed as w; both are used to fulfill the requirement for admission. The parameter values of the WNNPI controller have been set by PSO and then values are presented in the chapter-IV of the Simulink implementation.

Note: All f the outcomes are specific to the Mexican hat function, as every other function yields the same answers as the Mexican hat function (therefore not given). Moreover, the control system for both converters meet that the currents of battery and fuel cell are under their rating currents and not passing over their rating currents; this point can be achieved by using developed architecture controllers which are designed and based on setting its variants by PSO whereas these architecture controllers been merged with the intelligent EMS scheme to be more efficient as well as high accuracy.

In the last two sections of chapter-III, presents a brief description and theory of the Fuzzy Logic Controller (FLC) and the Artificial Neural Networks (ANNs) respectively. which are the controllers that are used to develop the hybrid energy system. Appendix (A) shows the description of full models for the fuel cell, battery and ultracapacitor those are built on the MATLAB/Simulink platform [7], [83].

3.7. Fuzzy logic Control Algorithm

The state of any variable in Boolean logic can be either (0 or 1) or (Yes or No) and nothing in between, however, the FLC enables states in between. A variable's grade of membership function (MF) can be thought of as its ability to belong to the described term. As an example, consider the fuzzy variables X and Y, as well as the specified term (good). Then, based on their membership grades [84], one may determine how (good) are the x and y. Moreover, there are three basic steps that need to take to implements the Fuzzy Inference Systems (FIS) which are [84]:

1. Fuzzification knowledge base
2. Decision-making logic
3. Defuzzification interface/method

The FLC is depicted in Figure III-11 for FIS, along with the three main steps:

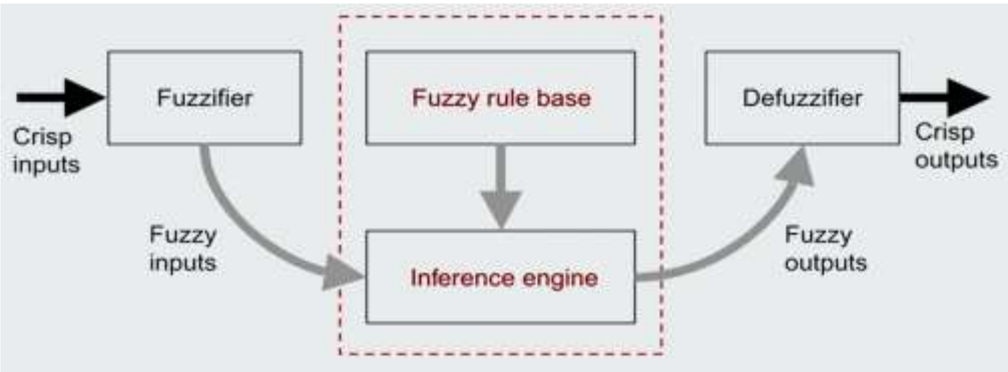

Figure III-11 The Fuzzy Inference System of the FLC.

3.7.1. Membership Function (MF)

The Input extent points are converted to membership values (or membership grades) between 0 and 1 using a curve known as a membership function (MF). The universe of speech [84] refers to the input extent.

Then, for any set X, the MF on X is any function between X and the real unit interval (0-1). Typically, the MF that symbolizes a fuzzy set is indicated by μA.

Gaussian, S-function, Triangular, trapezoidal, Dsigmoidal, Gbell, Pi-shaped, and Psigmoidal are some of the shapes of MFs. While the triangular-type is considered the simplest and most used MF, moreover it can be symmetrical or asymmetrical. Usually, the symmetrical triangles fuzzy sets are used due to they have good results and simple calculations. The choice of the MF is critical because it determines all the information that is included in the fuzzy set. They are described by their overlapping, shape, peak values, and continuity properties, which explain how the fuzzy system is designed and behaves.

3.7.2. Fuzzy Rules

Fuzzy logic is attempting to imitate human behaviors; by making decisions based on rules. The rules are represented by fuzzy rules, while the decisions and means of making decisions are represented by fuzzy sets. A number of if-then statements are used to operate the fuzzy rules. For example, If X is true, then Y is true, and if A is true, then b is true, where y and b are all sets of X and A.

3.7.3. Fuzzy Inference Methods

These two fuzzy inference approaches are:

1. Mamdani’s 2. Takagi-
Sugeno (TS).

The two types differ from one another in the outcome of ambiguous rules. The fuzzy sets are used as the rule consequent in Mamdani systems, but a linear function of the input variables is used in TS systems. Mamdani FIS is employed for the created EMS of this study.

3.7.4. FLC Advantages

There are several advantages of using FLC as control strategy:

1. The FLC is simple to comprehend and it is presented in natural language.
2. Flexible and able to deal with imprecise information.
3. Controlling nonlinear systems is quite advantageous.
4. Not required to use a mathematical model to control the system.
5. Utilized to help the expert consolidate his or her knowledge of the control technique.
6. FLC can be executed together with the traditional control strategies without any sort of incompatibility.

3.8. Artificial Neural Networks

As a data processing paradigm, Artificial Neural Networks (ANNs) are inspired by the way in which natural neural systems, like the human brain function. Artificial neuron is the main processing element in neural networks (or neurons). Generally, neurons are grouped in regular layouts and work in parallel. Moreover, they are normally arranged in layers, and allowed to have feed-back connections both within and across layers. The strength of each link is represented by a numerical value called (weight), which can be modified.

3.8.1. Artificial Neurons

The artificial neuron is essentially a mathematical simulation of a biological neuron in its most basic form. The fundamental building blocks for information processing in every neurological system are biological neurons.

The artificial neuron's mathematical model is based on the following hypothesis:

1. Data in the brain is processed by cellular components called neurons.
2. Signals, carrying the data, are sent through intercellular connections between neurons.
3. Every pair of nodes in a network is given a "weight" that determines how much of a signal is sent through that connection.
4. To generate an output signal, a neuron applies an activation function to a weighted sum of its input signals when a bias or fringe threshold is met.

Figure III-12 illustrates the construction of an artificial neuron.

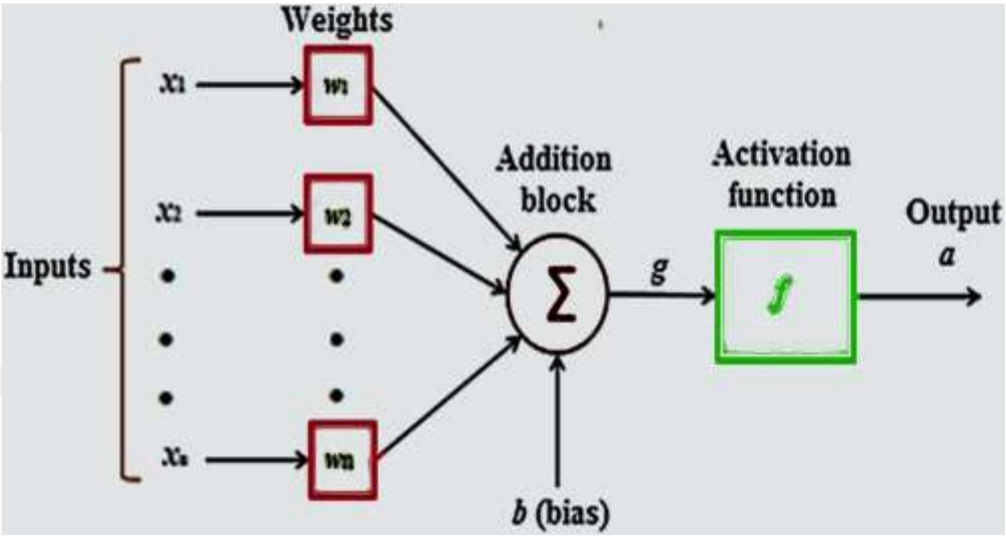

Figure III-12 The construction of an artificial neuron.

IV. CHAPTER FOUR VERIFICATION AND VALIDATION OF THE DEVELOPED EMS SCHEME

4.1. Introduction

This chapter shows the best power sources integration topology for the FCEV system of FC hybrid electric vehicle which is considered the main target of this study as obtaining sizes and efficiency as well as many other targets such as evaluating the performance of the proposed power flow management controller, improve fuel economy field, sturdiness, and optimum performance with minimizing cost. Overall, performance study of the energy resources with either Rule based Fuzzy Logics (FLC) or Artificial Neural Networks (ANNs) schemes and (WNN-PI & RWNN-PI) methods based on PSO to cover all the FC response, hydrogen consumption, change SOC of ESR, and efficiency. Therefore, the best analysis and evaluation have been done in this study by applying a different vehicle driving cycles by the Advanced Vehicle Simulator (ADVISOR) and the MATLAB/Simulink 2022a (64bit) environment for plug-in FC vehicle under the proposed EMS scheme as shown in

Figure IV-1 as a small car with total load 11kW. Moreover, the proposed design by Simulink models used (SimPowerSystems toolbox, embedded function block, and other default Simulink blocks) to make sure the findings are relevant in practice. Furthermore, the established based on realistic parameters of the power resources extracted from their datasheets; as well as the average mathematical models of the power electronic converters with their controllers are used.

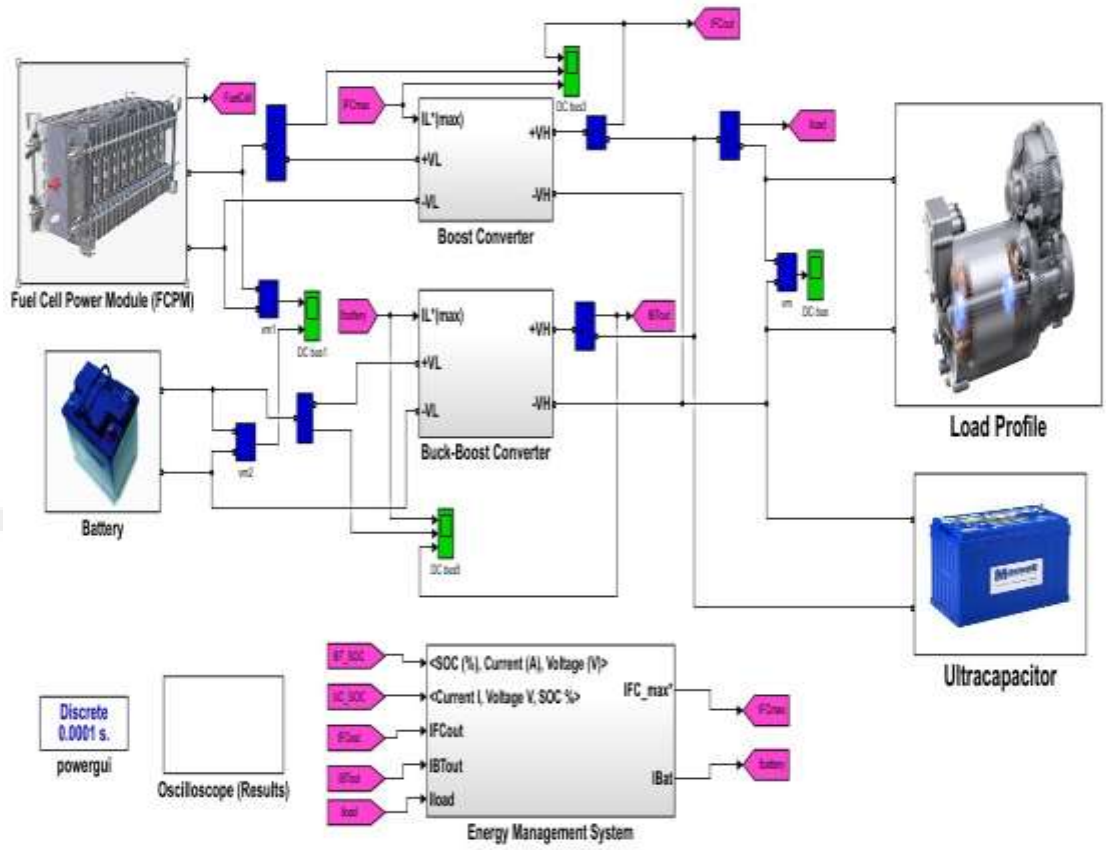

Figure IV-1 Overall block Simulink model.

4.2. Overview of ADVISOR Software

The ADVISOR® program and "Advanced Vehicle Simulator" is a MATLAB/Simulink environment based simulation software which has been designed for analysis and quantify of the performance, emission and the fuel economy of various vehicles such as HEVs, FCEVs, EVs and conventional vehicles. The ADVISOR has been produced by the National Renewable Energy Laboratory for the US DOE. Moreover, it provides a resource for assessing the results of several cuttingedge technologies for automobiles; and the software is released to the public via the

Internet. The ADVISOR provides the vehicle engineering community with easy and flexible use for different designs [85]. The main page of the ADVISOR program is illustrated in Figure IV-2.

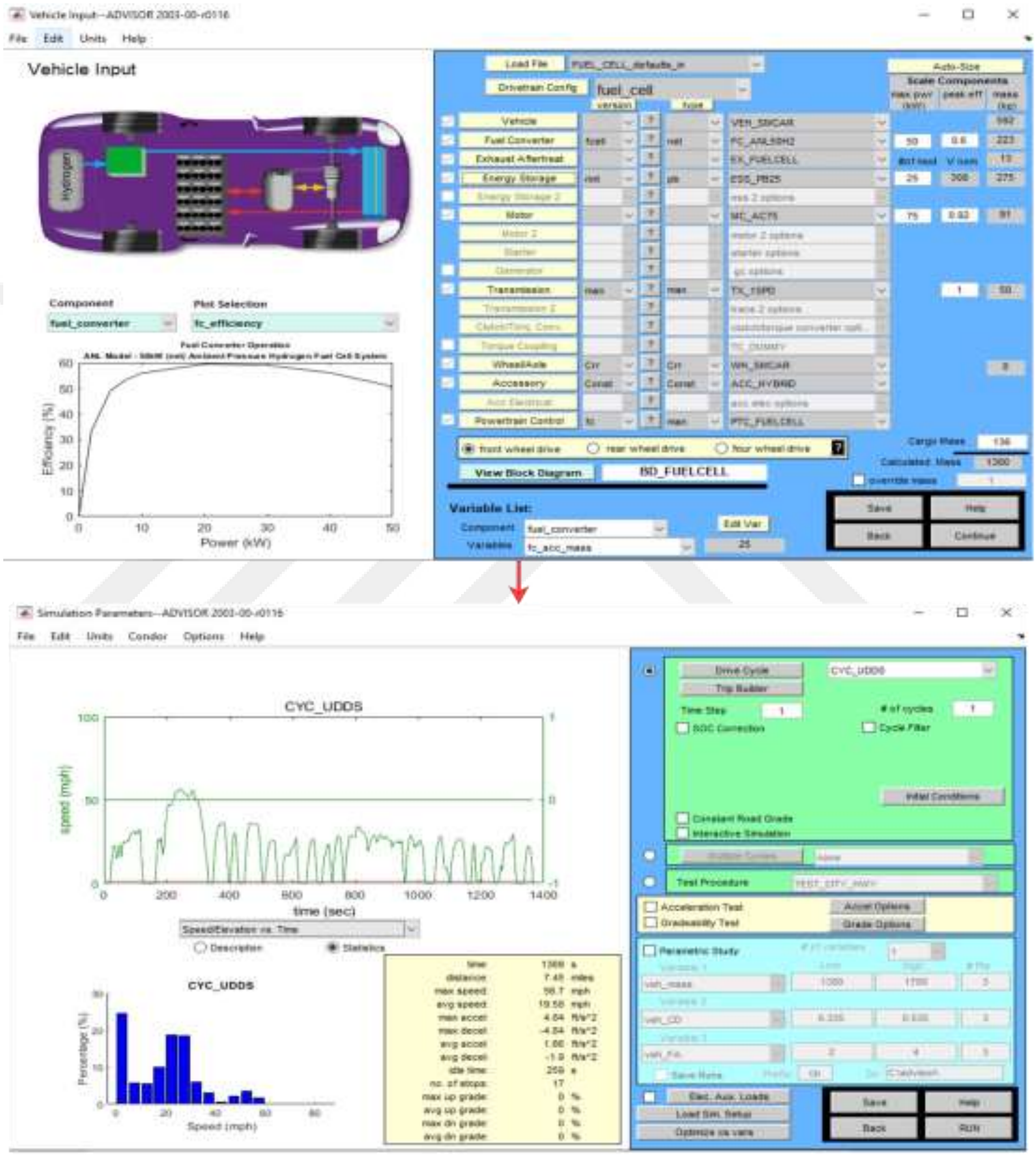

Figure IV-2 Window of ADVISOR Software.

The load power profile of the vehicle is required to complete the design parameters of the power sources (FC, UC, and BAT), and obtained the optimal performance of these power sources under the correct power flow of the Energy Management System (EMS) through evaluation of the proposed EMS scheme based on three driving cycles. The load power profile is used to estimate the distance travelled, speed and the weight of the electric vehicles.

The driving cycles are the Urban-Dynamometer-Driving-Schedule (UDDS), Federal Test Procedure (FTP), and Orange County Bus Cycle (OCC) driving cycles, while the ADVISOR analysis program is used to obtain the power-time and speedtime data for these driving cycles, which is then loaded into the Simulink lookup table block.

4.3. Introduction to FCEV Vehicle Driving Cycles

A driving cycle is a sequence of data points that plots a vehicle's speed against time [86]. Driving cycles are commonly employed in off-line simulations before real-world driving to assess a vehicle's fuel economy. Moreover, it is used to evaluate a vehicle's fuel consumption and pollution emissions in a standardized manner so that different vehicles can be compared. The modal cycles such as the European standard NEDC or Japanese 10-15 Mode, and the transient cycles such as the FTP or UDDS, are the two types of driving cycles. The main distinction is that model cycles are made up of straight acceleration and constant speed phases and are not indicative of real driver behavior, whereas transient cycles are made up of multiple speed fluctuations, which are typical of on-road driving circumstances [87]. The performance of the designed EMS is assessed using three driving cycles: UDDS, FTP, and OCC.

Figure IV-3 shows three lookup table blocks representing the acquired data of UDDS, OCC and FTP driving cycles in terms of speed and power with time by Simulink software. The output of each of them is divided by the DC link voltage (300 volts) and then injected into the independent current source to represent the effect of load changes on the plug-in hybrid FCEV.

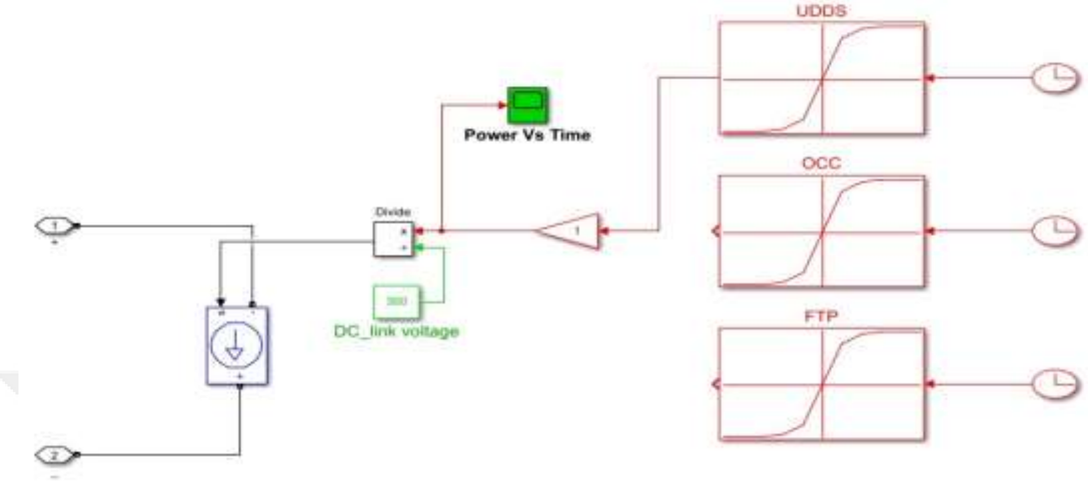

Figure IV-3 Simulink Model to plot the power demand.

ADVISOR provides numerous forms of driving cycles with various vehicle state situations. The proposed plug-in FCEV system will be designed, modelled, and simulated using the UDDS speed and power profiles as given in Figure IV-4 which is the reference cycle for the proposed plug-in FCEV.

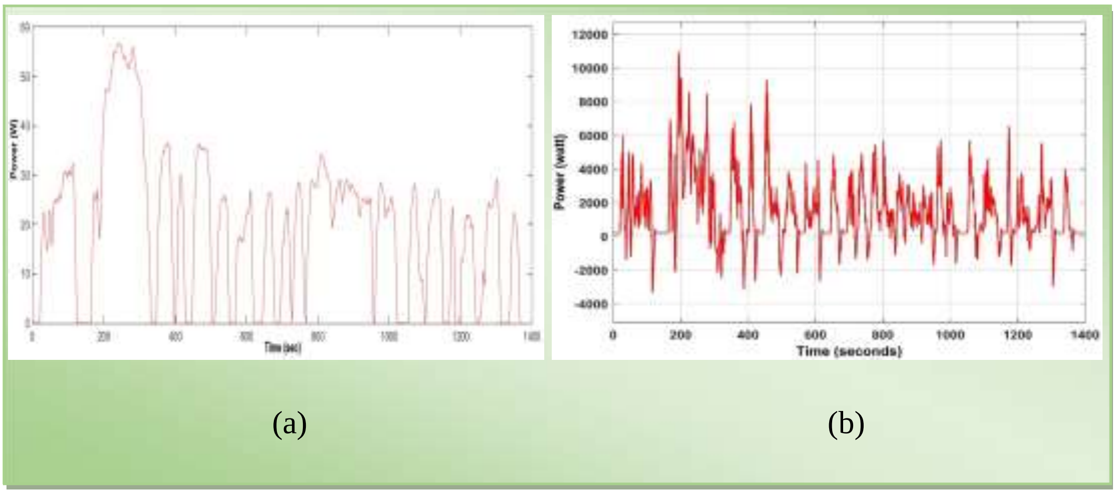

Figure IV-4 The profile of speed (a) and power (b) during UDDS.

Similarly, using ADVISOR and MATLAB/Simulink the speed-time and the powertime profiles of the OCC and FTP driving cycles which are acquired and plotted as shown in Figure IV-4 and Figure IV-5, respectively.

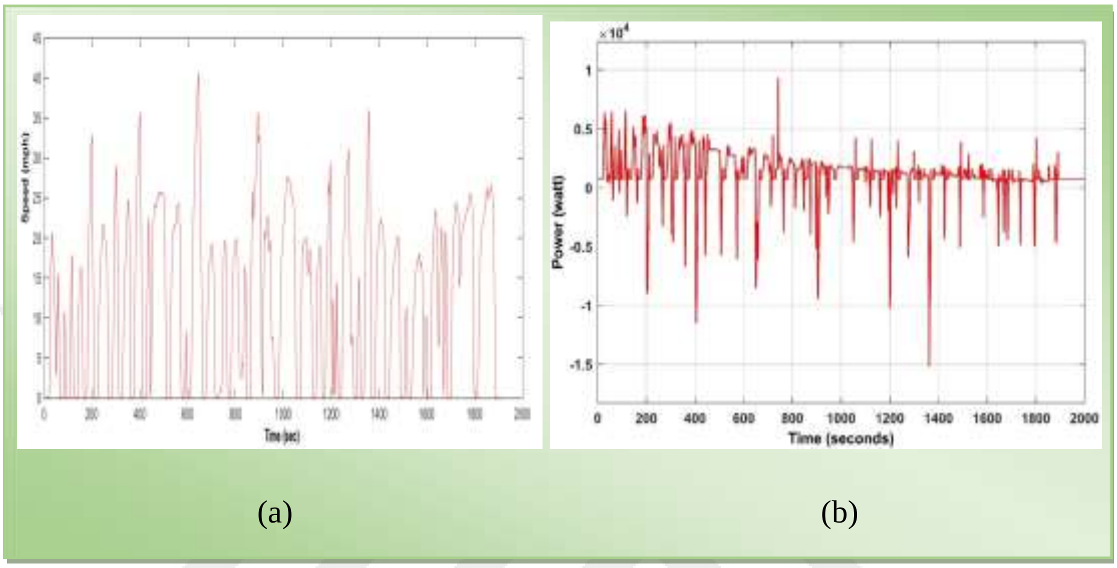

Figure IV-5 The profile of speed (a) and power (b) during OCC.

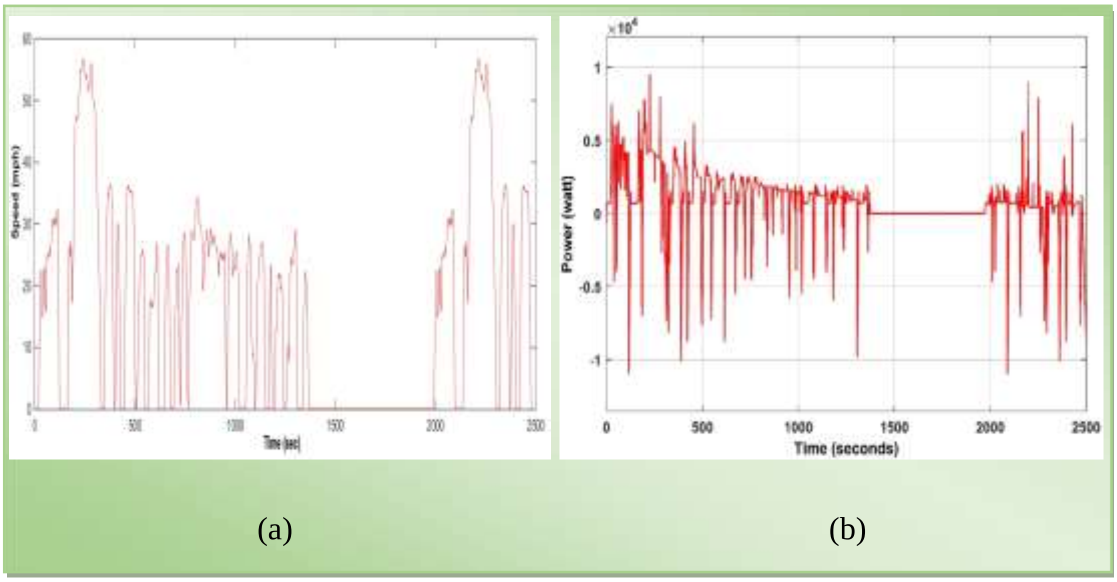

Figure IV-6 The profile of speed (a) and power (b) during FTP.

The UDDS, OCC and FTB driving cycles parameters obtained from the ADVISOR system model are illustrated in Table IV-1. While the major driving cycle UDDS is the primary example for studying FCEV performance since it is owing to the fact that UDDS has the worst variances in peak power consumption among the various driving cycle standards. Resulting in ensuring that the proposed EMS is efficient under any driving cycle.

Parameters	**UDDS**	**OCC**	**FTP**
Time	1369 sec	1909 sec	2477 sec
Distance	7.45 miles	6.54 miles	11.04 miles
Maximum speed	56.7 mph	40.63 mph	56.7 mph
Average speed	19.58 mph	12.33 mph	16.04 mph
Maximum acceleration	4.84 ft/s^2	5.95 ft/s^2	4.84 ft/s^2
Maximum deceleration	-4.84 ft/s^2	-7.52 ft/s^2	-4.84 ft/s^2
Average acceleration	1.66 ft/s^2	1.49 ft/s^2	1.68 ft/s^2
Average deceleration	-1.9 ft/s^2	-2.09 ft/s^2	-1.89 ft/s^2
Idle time	259 sec	407 sec	360 sec
Number of stops	17	31	22

Table IV-1 UDDS, FTP and OCC drive cycles parameters acquired from ADVISOR software.

Based on specific parameters of UDDS illustrated in Table IV-1 and Figure IV-4 (b), it can be noted that the selected maximum load power is up to 11 kW. So, according to this load the power demand of the FC, BAT and the UC have been designed in this work.

4.4. Power Sources Simulink Model and Designed Parameters

One of the critical criteria is that increasing the efficiency, lifetime of power resources and fuel cost all aimed as the steady operation of the FC system. As a result, the fuel cell should run and produce a steady-state power as average power rather than responding to peak or transient power demand. As illustrated the power load profiles of UDDS, FTP, and OCC, which indicate that the power profile of these driving cycles has numerous immediate and heavy fluctuations. Hence, the use of another resources with FC source, such as UC and BAT, in combination with the proposed load sharing algorithm is essential to obtain the required improvements in the FC system.

As shown in Figure IV-4 (b) the UDDS driving cycle with regards to the available power for a time span of 1400sec. After that, the following properties of UDDS loads can be determined as 7kW as an average power at the whole cycle and 11kW is the highest shoot which is shooting from zero to 11kW in just 10 seconds.

The nominal power ratings for the battery, ultracapacitor and fuel cell are taken into account to determine the size of the intended plug-in FCHEV system components. Additionally, a complete model for power sources were developed by extracting the actual technical needs of these resources and incorporating them into the Simulink model environment, making the system performance results as realistic as feasible in the real world. The designed plug-in FCEV is sizing methodology the three power sources used for the developed plug-in FCEV, which are listed below:

1. Fuel cell: Hydrogenics 12.5kW HyPM-HD12 PEMFC [88].
2. Battery: lithium-ion (Valence-Tech) U1-12XP [89].
3. Ultracapacitor: Maxwell Boostcap®BCAP1200 UC [90].

The Simulink model using SimPowerSystems in accordance with the previous power rating characteristics for the FC, UC, and BAT are given in the following sections below.

4.4.1. FC Simulink Model

In order to meet the load average power need, a 12.5 kW HyPM-HD12 PEMFC power module from Hydrogenics was used, with its characteristics listed in Table IV2. (The full details can be found in Appendix B-1). Estimated 88% as the efficiency of the fuel cell converter, then the FC can supply roughly 7.95kW for an average load power of 7kW. As indicated in [88].

Maximum operating point [I_{end} (A), Vend (V)]	[320, 39.2]
Nominal operating point [I_{nom} (A), V_{nom} (V)]	[250, 41.15]
Voltage @ 0 A and 1 A [V_0 (V), V_1 (V)]	[52.5, 52.46]
Selected Number of cells	65
Nominal Air flow rate (lpm)	732
Operating temperature (C^o)	45
Nominal stack efficiency (%)	50
Voltage undershoots (V) @ Peak O_2 utilization	2
Nominal composition (%) [H_2, O_2, H_2O (Air)]	[99.95, 21, 1]
Peak O2 utilization (%)	60
Nominal supply pressure [Fuel (bar), Air (bar)]	[1.16, 1]

Table IV-2 Main parameters of the HyPMHD12 PEMFC.

The parameters in Table IV-2 have been included in the FC Simulink model provided by SimPowerSystem. The FC model, (FC V-I) characteristics, and FC power curve are all respectively depicted in Figure IV-7. The FC's dynamic reaction is modelled in MATLAB/Simulink so that the generated results are as similar as possible to the actual fuel cell stack; therefore, a flow rate regulator has been constructed for this purpose, as shown in Figure IV-8, to regulate the utilization of H2 fuel and O2, then incorporated into the FC model as shown in Figure IV-7 (a). The mathematical modelling equations (A.3) and (A.4) that are discussed in Appendix (A-1) are used to create this model. Moreover, when compared to the practical characteristics of real actual FC as depicted in Appendix (B-1) Figure B-1, it is obvious that the modelled results are extremely similar to the practical results (real one).

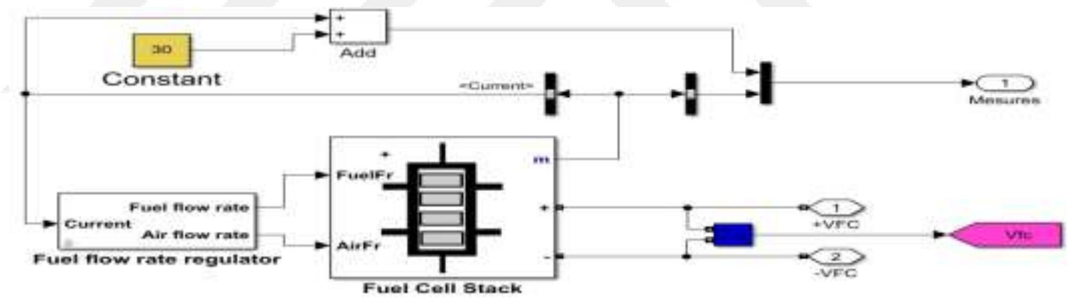

(a)

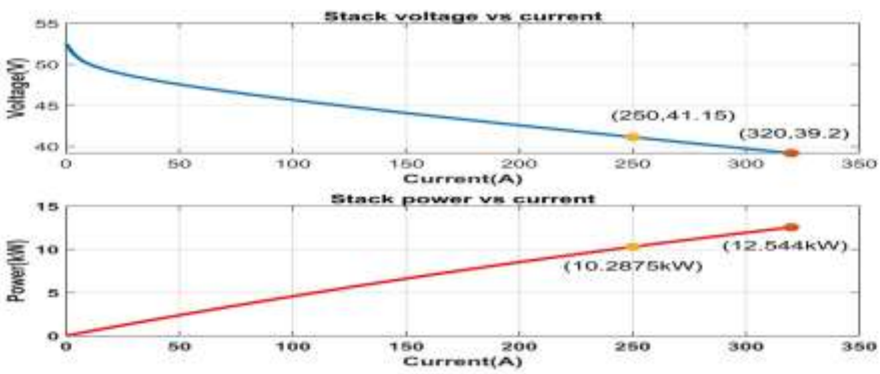

(b)

Figure IV-7 (a) shows the Simulink FC model and (b) Power curve of the FC.

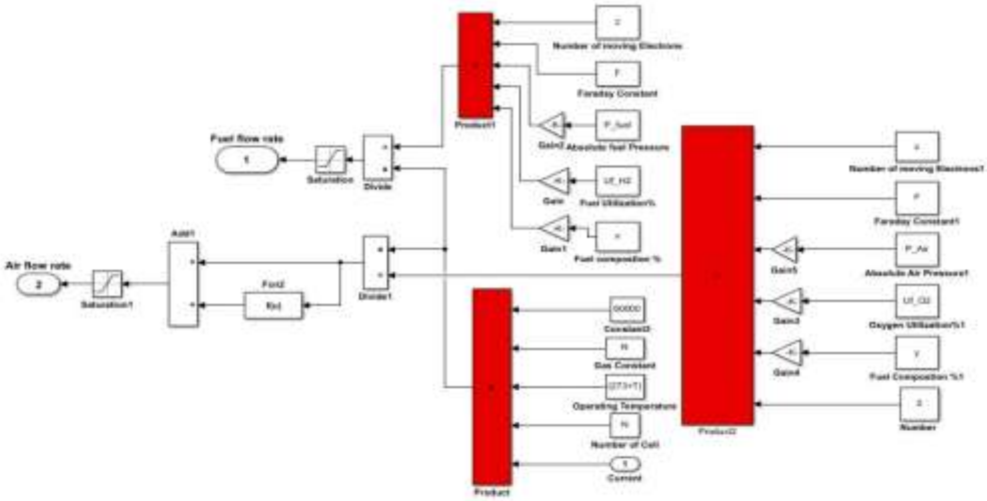

Figure IV-8 Developed model of the Fuel and air flow rates regulators.

4.4.2. BAT Simulink Model

Table IV-3 shows the BAT characteristics for each BAT package, which is taken from [89] and documented in Appendix B-2. In the Simulink, we modeled the battery that has 4 cells linked in series connection for the developed plug-in FCEV system. Each series string has a nominal voltage of 12.6V, thus a 48V can be achieved without exceeding the converter duty cycle's stable dynamic range. Additionally, the UCharge U1-12XP has a maximum capacity of 40Ah. This indicates that the total energy content of this BAT pack system is able to provide 1920Wh. As a result, the output power of the battery is 4.937kW. The BAT model characteristics is given in Figure IV-9, that used the practical BAT values that are shown in Table IV-3. Similarly, the mathematical modelling equations outlined in Appendix (A-3) are used to create this model.

Internal Resistance (ohms)	0.012

Rated Capacity (Ah)	40
Fully Charged Voltage (V)	55.88
Nominal Discharge Current (A)	17.4
Nominal Voltage (V)	48
Battery Voltage response time (sec)	10
Capacity (Ah) @ Nominal Voltage	36.17
Exponential Zone [Voltage (V), Capacity (Ah)]	[52.3, 1.96]

Table IV-3 U1-12XP lithium-ion (Valence-Tech) battery specifications.

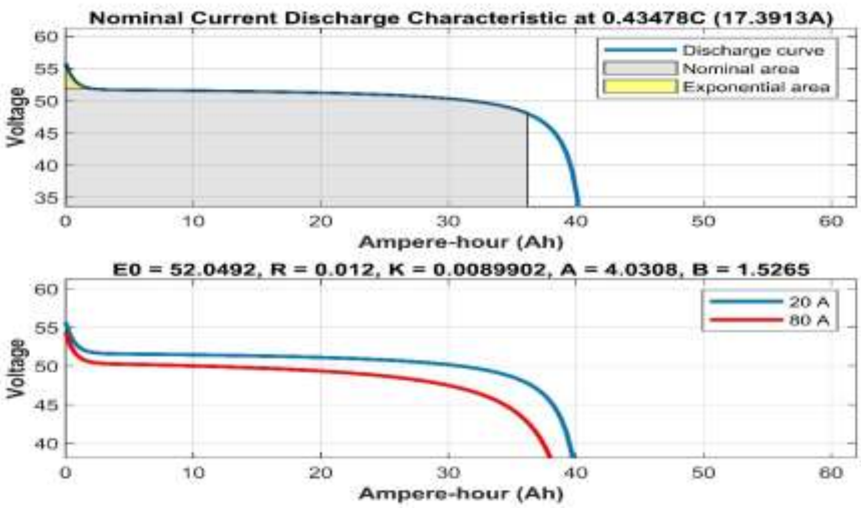

Figure IV-9 BAT model discharging characteristics.

Observed that the nominal discharge current at 48V no exceeds 17.4A as shown in Figure IV-9. However, at 80A the BAT can only supply 30Ah at the same nominal terminal voltage. Hence, this model expected accurately the performance of the

U112XP lithium-ion BAT as shown in Appendix (B-2), Figure B-2 which is very important to reduce the gap between the simulation and practical results.

4.4.3. Ultracapacitor Simulink Model

An UC has been added in parallel with the hybrid system to reduce the influence of peak/transient load demand. In this study, the ultracapacitor is BCAP1200 type. With regards to the DC-bus voltage that designed to has 300 volts then in order to have 300 volts from ultracapacitor is obtained by connecting 120 cells in series (n cells). Table IV-4 shows the most important specifications (the full details can be found in Appendix B-3).

Rated Capacitance (F)	10
Equivalent Series Resistance DC (Ω)	0.0696
Rated Voltage (V)	300
Maximum Voltage (V)	324
Number of Series Capacitor	120
Number of Parallel Capacitor	1
Operating Temperature (C^{o})	25

Table IV-4 Boostcap®BCAP1200 UC specifications for 120 cells in series connection.

A Simulink model, as illustrated in Figure IV-10, is created to assess the selected UC unit. The UC voltage behavior in response to a constant discharge current (in the order of 40A) in a time span of a few seconds is shown in the simulation results in

Figure IV-11. The modelled findings reveal that the developed UC model result approximately matches the calculated results of the BCAP1200 UC when compared to the experimental results in [90].

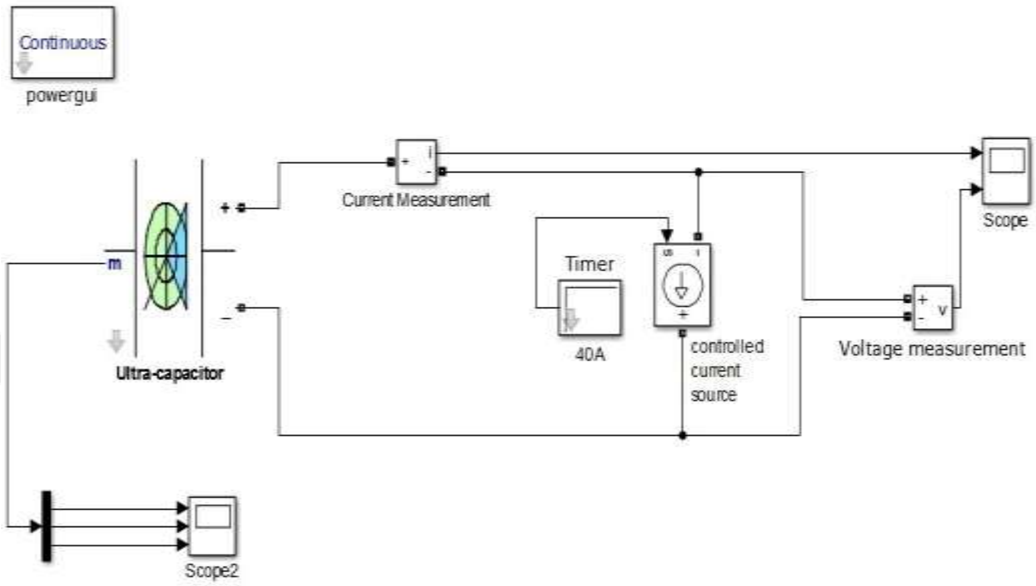

Figure IV-10 Simulink diagrams of the UC model discharging test.

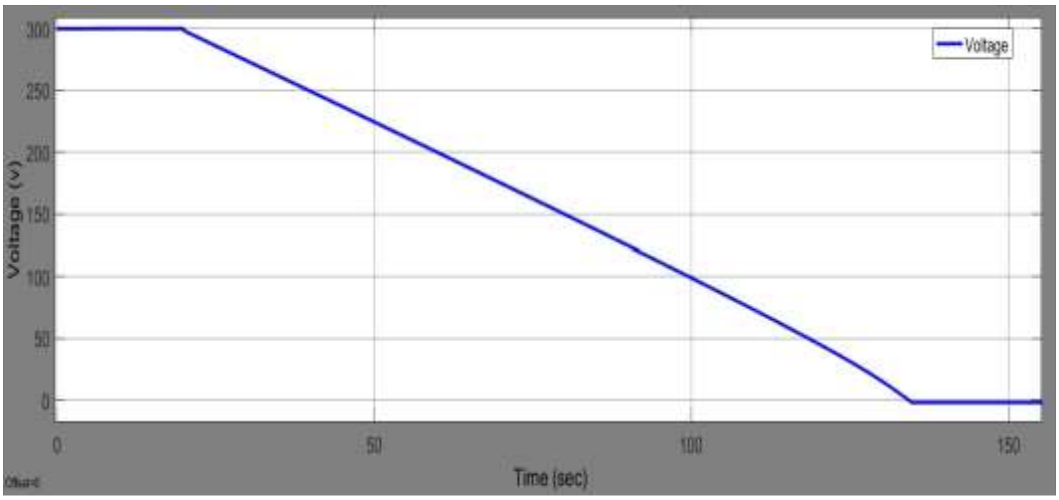

Figure IV-11 Discharge characteristics of the UC.

As previously stated, the design of the ultracapacitor unit is giving an 11kW by just 10sec. since the UC unit's maximum energy density of 5,800W/kg whereas indicated in [90]. Then, minimum rating of 101.85Wh with consider that 30% as the depth-of-discharge. Eq. (4.1) is used to obtain the minimal necessary energy required:

$$P_{min}\, in\ Wh = \frac{\text{peak power demand}}{depth - of - discharge} \times \frac{response\ time}{3600} \tag{4.1}$$

The capacitance of selected UC unit can be calculated as:

$$C = \frac{C_{cell}}{n_{cell\_s}} \times n_{cell\_p} \tag{4.2}$$

The UC unit capacitance equals 10F for $C_{cell} = 1200F$, $n_{cell\_s} = 120$, and $n_{cell\_p} = 1$. The comparable energy in joule for a DC output voltage of 300V is 450kJ. As a result, this UC unit can provide around 125Wh. Thus, the selected UC unit can easily meet the needed power requirement.

The UDDS driving cycle, as mentioned in section 4.3, has the highest power consumption needs. Then the plug-in FCHEV must meet the UDDS cycle criteria as well as the suggested EMS scheme used the planned ultracapacitor, battery and fuel cell power rating characteristics. Then, simulation findings are quite close to the measurement data acquired from the power sources datasheets, implying that the simulation models are valid and accurate.

4.4.4. Selection of FCEV Hybrid Topology

Additionally, the volume and weight of the created FCEV hybrid topologies have been evaluated in this study in comparison to the FCEV hybrid topologies given in (Figures II-4 and II-5 chapter-II). The approximate weight and volume of Hydrogenics 12.5kW HyPM-HD12 PEMFC are 85kg and 0.1137m3 respectively. While the Valence Technology U1-

12XP lithium-ion battery weighs 6.5kg and volume 0.004668m3 per unit. As a result, the total BAT weight and volume for the planned four units are 26kg and 0.0186m3, respectively. In the design of UC to achieve 300V, the Maxwell Boostcap®BCAP1200 UC, 120 cells were employed. Then, the weight per cell is 260g, whereas the volume per cell is 0.000214m3. Hence, the selected UC unit weighs 31.2kg and has a capacity of 0.02568m3. Thus, the overall plug-in FCEV system weighs 142.2kg and has a capacity of 0.1579m3. Moreover, Table IV-5 summarizes the BAT and UC characteristics of a selected FC hybrid topology in comparison to two other topologies which are depicted in (Figures II-4, II-5, and II-6 chapter-II). The FC and energy storage DC-DC converters' weight and volume are computed depending on the converter power requirements. As a result, the efficiency of each topology can be computed using equation (4.3) and the power ratings of power sources, as summarized in Table IV-6.

$$\eta\% = \frac{total\ P_{load}\ included\ converter\ efficiency}{FC\ power + BAT\ power + UC\ power} \tag{4.3}$$

For example, η for selected topology can be found as shown in (4.4):

$$\eta\% = \frac{(8 \times 0.88 + 4.937 \times 0.88 + 11)kw}{(8 + 4.937 + 11)kw} = 93.5\% \tag{4.4}$$

Topology	Selected Topology	Topology in Figure II-5	Topology in Figure II-4

Energy Storage	BAT	UC	BAT	UC	BAT	UC
Voltage (V)	48	300	300	48	48	48
No. of series Cells	4	120	24	19	4	19
Capacity (Ah)	42	0.339	6.67	2.122	42	2.122
Capacitance (F)	-----	10	-----	63.15	-----	63.15
Weight (kg)	26	31.2	156	4.9	26	4.9
Volume (m3)	0.0186	0.02568	0.1120	0.00407	0.0186	0.00407

Table IV-5 BAT and UC characteristics of selected topology vs other FCEV connection topologies.

The overall characteristics of the compared topologies are listed in Table IV-6.

	Selected Topology	Topology in Figure II-5	Topology in Figure II-4
Weight (kg)	198	326	211
Efficiency (%)	93.5	90.47	88

Table IV-6 Overall comparison between the three FCEV connection configurations.

As can be seen from the aforementioned data located in Table IV-6, the FC hybrid system's chosen topology provides a lightweight construction with improved efficiency and lower weight.

4.5. Simulink Model of the Power Conditioning Unit

The average models of the single and two-quadrature converters, as explained in chapter-II, are implemented as Simulink models in two Figures which are IV-12 and IV-13, respectively. In which the PSO approach is used to get their parameters, as indicated in Table IV-7 for fuel cell converter and Table IV-8 shows the parameters for battery converter, as well as the tables, show the values of saturation block (low and high limits). Moreover, the basic standard of the PI controller has been implemented in the Simulink model as shown in Figure IV-14. Furthermore, Appendix (C-1) shows the PSO codes for the BAT and for the FC; which are used to find the K_p and K_i. Where the converter's parameters in terms of the values of inductance and capacitance are listed in Table IV-9.

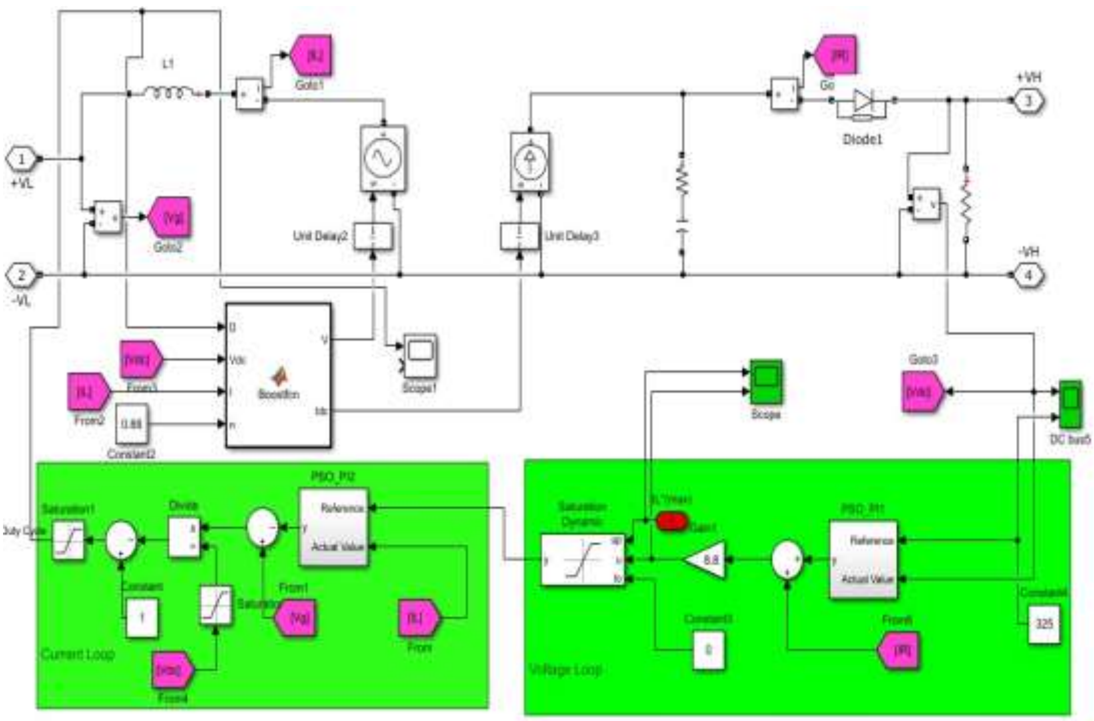

Figure IV-12 Cascade controller system by PSO for the fuel cell converter.

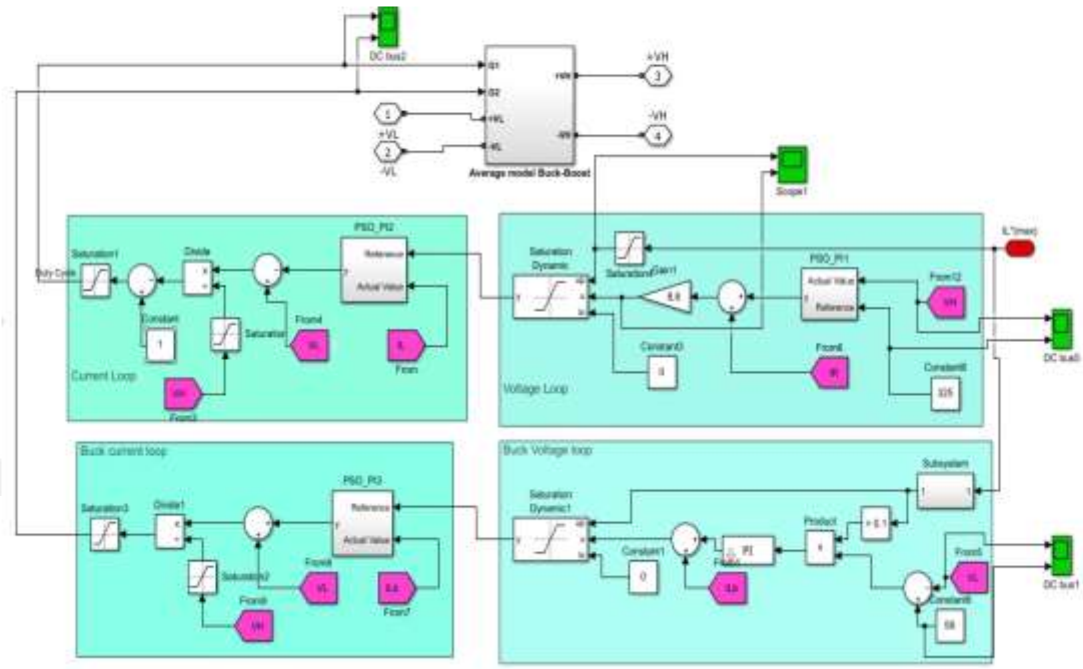

(a)

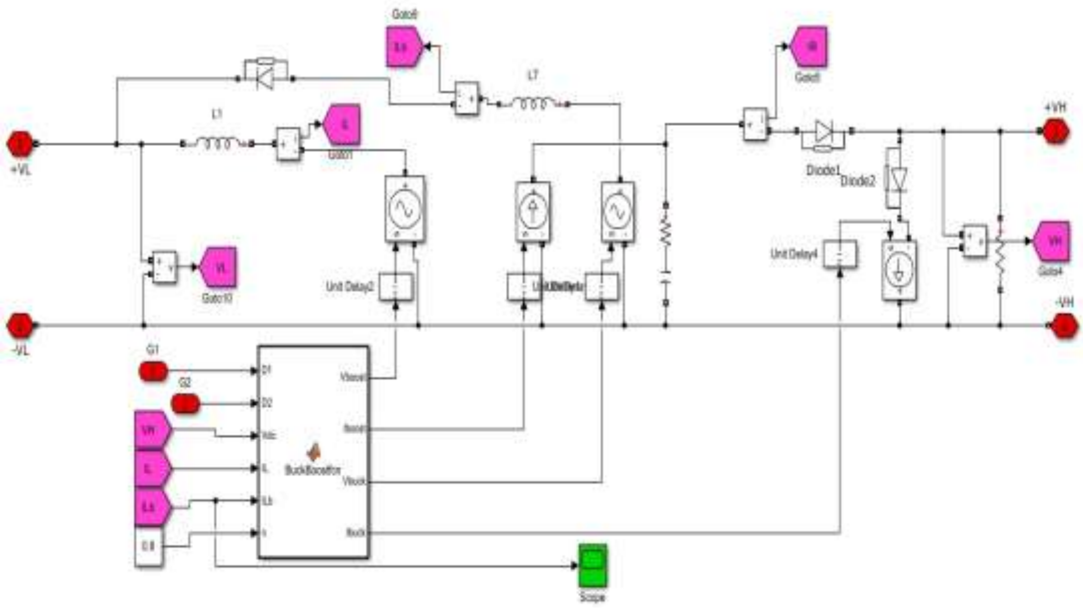

(b)

Figure IV-13 Battery converter (a) the cascade controller system by PSO, (b) average model Buck-Boost.

Boost mode Converter	@Voltage-Loop		@Current-Loop	
	K_{pv}	K_{iv}	K_{pc}	K_{ic}
	1029.7	38152	0.07×10-3	21.9988×10-3
	Saturation Block		Saturation Block	
	Upper	Lower	Upper	Lower
	0.5	-0.5	50	-50

Table IV-7 Fuel cell converter parameters of PI controller.

Buck Mode Converter	@Voltage-Loop		@Current-Loop	
	K_{pv}	K_{iv}	K_{pc}	K_{ic}
	10.6839	285.9535	11.1946	2907.3
	Saturation Block		Saturation Block	
	Upper	Lower	Upper	Lower
	1	-1	1	-1
Boost Mode Converter	@Voltage-Loop		@Current-Loop	
	K_{pv}	K_{iv}	K_{pc}	K_{ic}
	1028.9	36759	0.0712	21.9918
	Saturation Block		Saturation Block	

	Upper	Lower	Upper	Lower
	0.06	-0.06	50	-50

Table IV-8 Battery converter parameters of PI controller.

Parameters of FC Converter		Parameters of BAT Converter	
Parameter	Value	Parameter	Value
Inductance (Lboost)	100µH	Inductance (Lbuck-boost)	10µH
Capacitance (Cboost)	800µF	Capacitance (Cbuck-boost)	800µF

Table IV-9 The parameters of the proposed converters.

The D of the FC and BAT converters is controlled by the Embedded function block in Figure IV-12 and Figure IV-13 (b) (see their algorithm in Appendix C-2 (1) and (2)). Two output signals are connected to the BAT converter in Figure IV-13 (a) one to control the ON time of the buck switch and the other one to control the ON time of the boost switch.

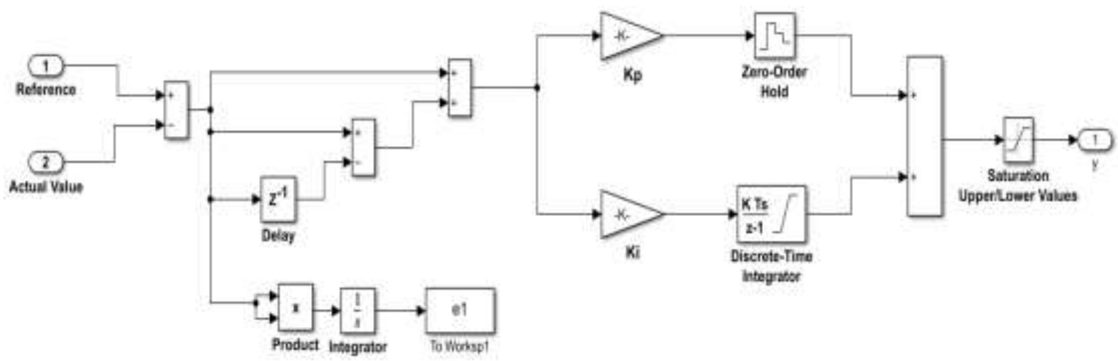

Figure IV-14 The Simulink model of PI tuned by PSO.

Overall, the two converters of FC and BAT depend on the current reference as shown in chapter-III Figure III-1; the BAT current reference i_{BAT}^{ref} is acquired by the WNN-PI controller, and the BAT reference current is fed to the BAT converter to manage the converter's output voltage and the battery's charging and discharging processes. So, the next section will explain the Simulink model of WNN-PI and the value of its parameters based on the algorithm, equations and blocks that have been mentioned in chapter-III. While the operation of the FC converter also depends on the current reference i_{FC}^{*} so the controller of power flow will be further explained in section 4.7 with all details of EMS controller.

4.6. Simulink Implementation of The BAT Current Reference Based on WNN-PI Controller

The actual DC link voltage is subtracted from the reference DC voltage 300V to get the error signal which is then fed to the PI controller of the voltage loop controllers through the WNN-PI controller as depicted in Figure III-10 chapter-III.

Figure IV-15 of the WNN-PI Simulink model demonstrates the usage of a feedforward wavelet neural network connected with a proportional-integral (PI) controller to regulate the current reference provided to the battery converter. Online, the PSO algorithm learns the relationship between the WNN and PI parameters and their translation, dilation, and weights. (Appendix C-1 shows the codes). The output of WNN is given by equation (3.9) chapter-III.

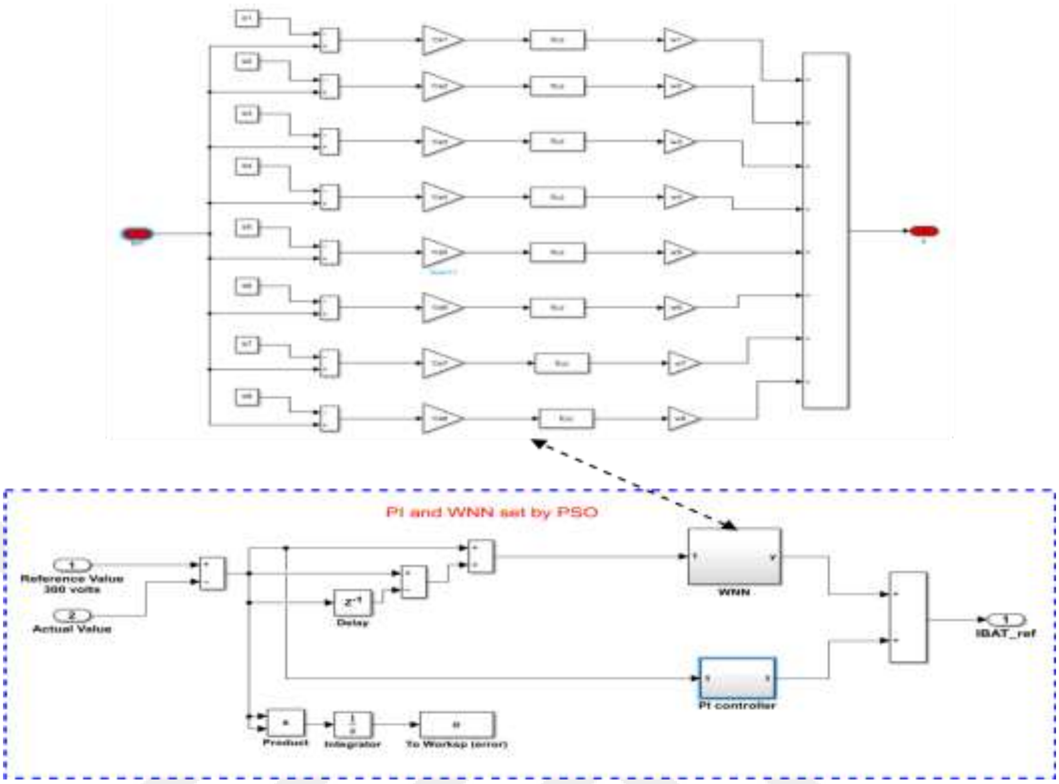

Figure IV-15 Battery controller scheme by wavelet and PI in Simulink model.

The parameters of PSO are mentioned in Table IV-10. Tables IV-11 and IV-12 show the optimal values for the PI controller parameters with saturation block values (low and high limits values) and the WNN parameters respectively.

PSO-Parameters	Value
"No of birds"	10
Iteration	10
Dimension	28
C1 & C2	1.4
Wmax	0.8
Wmin	0.2

Table IV-10 Variables value of PSO.

Variables	K_p	K_i
Values	0.7997	4.0057
Saturation Block	Upper	Lower
Values	80	-20

Table IV-11 PI parameters tuned by using PSO.

WNN Dilation variables		WNN Translation variables		WNN Weights variables	
a1	1.2457	b1	1.1851	w1	3.3513
a2	1.1478	b2	4.8012	w2	0.3165
a3	0.3275	b3	1.5728	w3	0.3119
a4	2.6528	b4	1.3352	w4	4.9613
a5	3.3322	b5	0.8062	w5	4.0091
a6	4.2591	b6	4.2511	w6	4.3895
a7	3.9728	b7	4.3493	w7	0.1699
a8	4.7074	b8	0.1326	w8	3.3935

Table IV-12 WNN parameters tuned by using PSO.

4.7. EMS Controller Model

4.7.1. Description of the Developed EMS Schemes

The FC output power is managed in the designed energy control system using the power needed and the SOC of the battery, as illustrated in Figure III-6 (a). The highfrequency component of the load power is eliminated using a low pass filter with a time constant of 25 seconds, resulting in the FC supplying almost constant (average) power. The FC reference power obtained from EMS controller is divided by the FC voltage Vfc and the efficiency of the converter (88%) to get the FC reference current

i_{FC}^{*}
( ).

Two EMS strategies, as illustrated earlier, are used in this study to control the FC output current, which are FLC and ANNs. There are two cases to evaluate the power flow of the proposed:

1. FLC and ANNs EMS with the Feed-Forward strategy of WNN.
2. FLC EMS with the Recurrent strategy of WNN.

Either the Feed-Forward or Recurrent strategies both are employed to control the BAT charging and discharging periods. The FLC control system is utilized first to control the FC reference current. Since the ANN needs data in terms of input and output for training it. Therefore, to obtain the required input/output data, the EMS has been implemented first by using the FLC scheme. Once the required data is obtained from FLC, the neural system has been trained as will be explained later.

4.7.2. Calculations and Power Flow Strategy

keeps the fuel cell power generator output under control and satisfies all the FCEV's requirements for normal and safe operation, the following consideration needs to take place:

- BAT charging power =1100W (From the data sheet the maximum charging current is 20A and the BAT charging voltage is 55v. So, the charging power (PBAT-charging) will be 20*55=1100W)
- SOCmin is once below 60%, SOCmax is once reach 90%, SOCnom1 is equal 85%, and SOCnom2 is once up 60%

Also, we proposed a three value of fuel cell power output to be control and achieve an efficient run; where consider as Pfc_min is from zero till reach 0.49kW, and Pfc_max is from 1.59kW till reach 9kW, then the optimal power output as average power Pfc_opt is from 0.5kW till reach 1.6kW. As mentioned earlier, there are two input resources P_{fc} and SOC of the BAT, then through EMS satisfy the output power of FC to get

the current reference for feeding the buck converter with developing controllers which in return optimal power flow and reduce the risk of shortening the lifespan of the battery and fuel cell by avoiding the consequences of abrupt dramatic rapid in the load power. The flow chart IV-16 shows the optimal power flow based on the calculations and rules mentioned above.

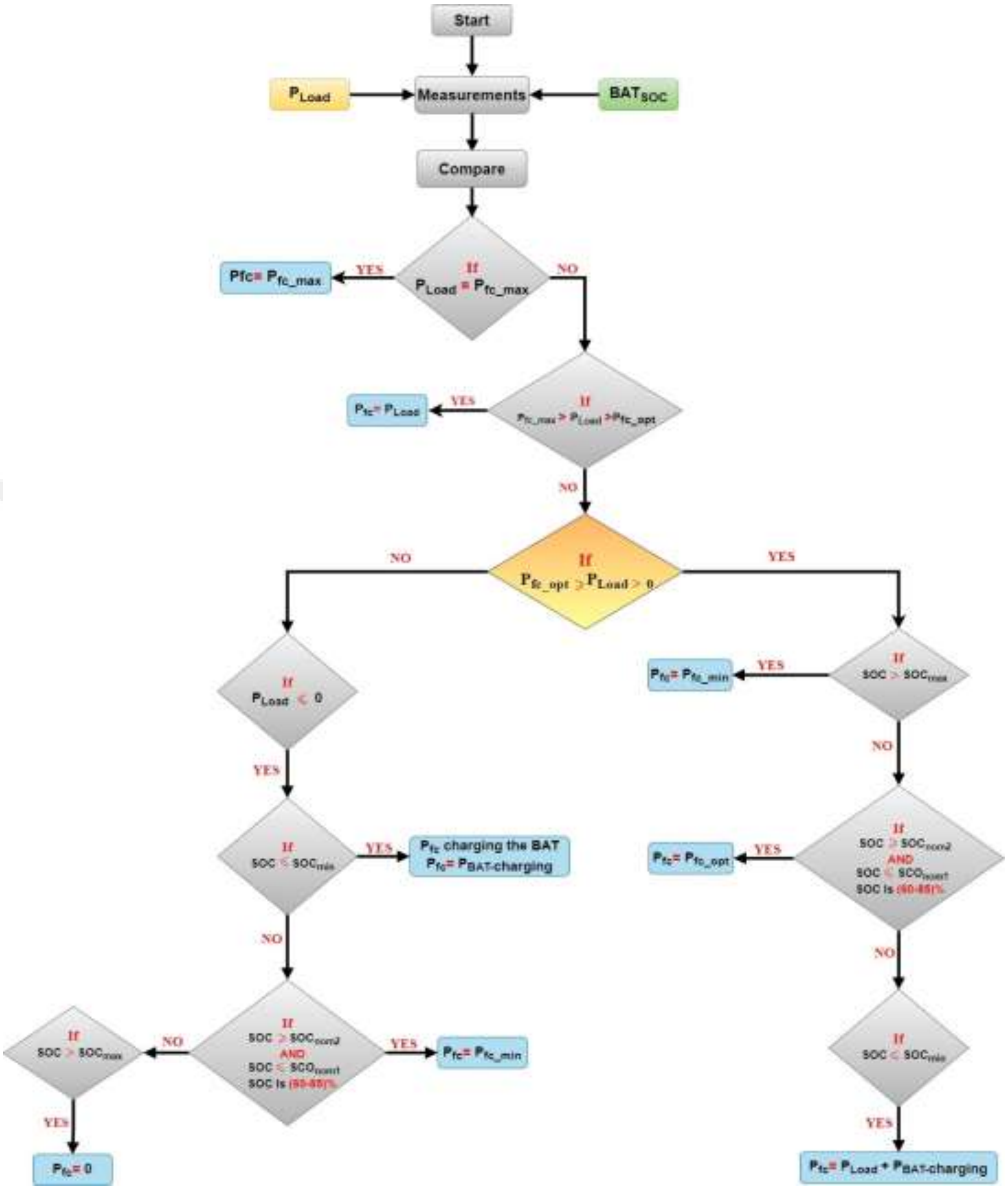

Figure IV-16 The optimal power flow based on the calculations and rules.

4.7.3. Fuzzy Logic Control

In this subsection, we use the fuzzy logic utilized to keep the output power of the fuel cell within its specified parameters. The fuel cell reference power is calculated using a set of if-then rules that take into account both the power needed and the state of charge for the battery, and membership functions. As can be seen in Figure IV-17, the FLC used in this study took in data from two sources but only produced a single output. When the power demand is sent into the fuzzy logic block, it is filtered to eliminate the high-frequency components in a manner similar to that of an ANNs

controller.

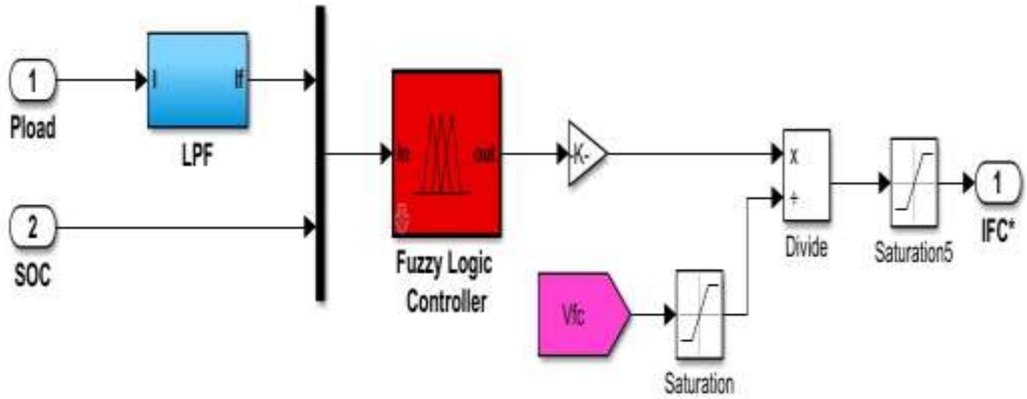

Figure IV-17 The fuzzy logic control EMS model.

Based on the flow chart IV-16 and the calculations the FLC regulates the power requested from the FC. The developed FLC has been implemented using a trapezoidal memberships function (trapmf) as shown in Figure IV-18.

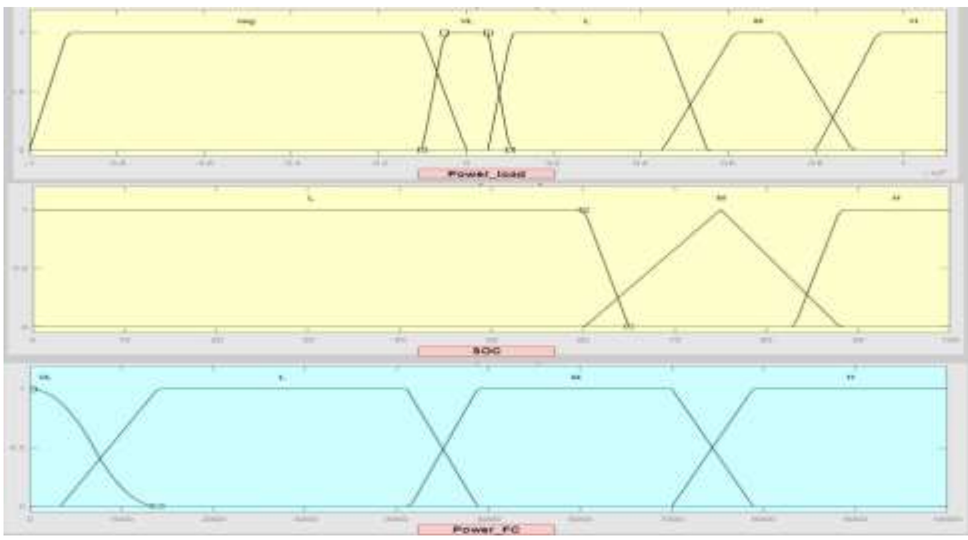

Figure IV-18 Fuzzy membership-functions.

Table IV-13 shows the fuzzy rules, thus designed to achieve the main target which is the power flow management in accordance with lower FC consumption.

where: H = high, M = medium, L = low, VL = very low, NEG = negative

The Mamdani's fuzzy inference method is utilized for defuzzification. The implemented fuzzy rules have 2 portions which are the distributed power during the car is accelerating and decelerating.

Inputs		**Output**
IF (BAT_{SOC}) IS	**AND (P_{load}) IS**	**THEN (P_{fc}) IS**
H	H	H
H	M	M
H	L	L
H	VL	VL
H	NEG	VL
M	H	H

M	M	M
M	L	L
M	VL	VL
M	NEG	VL
L	H	H
L	M	H
L	L	M
L	VL	L
L	NEG	L

Table IV-13 The fuzzy rules for proposed EMS.

Where fuzzy is implemented by using the Simulink block from the Toolbox of fuzzy logic in MATLAB/SIMULINK (version r2022a). With the assistance of MATLAB/SIMULINK FIS and GUI tool, the FLC design is successfully completed. This tool can be used to generate an input or output variable, membership functions, and rules without needing to generate a sophisticated code for the fuzzy logic system.

4.7.4. EMS based ANNs

ANNs has been used to control the output power of fuel cell based on that data of FLS. The neural control system has two inputs which are the load power and the SOC of the battery. The output of ANNs is the FC reference power. The parameters of the ANNs have been defined as the following:

1. The network that used is “feedforwardnet” training algorithm that used is the “Levenberg-Marquardt” method to train the neural network.
2. The number of epochs is 1000 epoch.
3. Three hidden layers have been used and the neurons of each layer are (80, 60, 30), which are chosen by the trial and error theorem.
4. Training goad (MSE) is 10^{-30}

A 70% of the data for training, 15% for testing and 15% for validation.

The codes that used to create this network and the Network diagram are shown in (Appendix C-4 shows the codes).

After several training times, the best-training network is discovered in terms of training data, testing data as well as validation to be 100%. Figure IV-19 depict the results of the trained network.

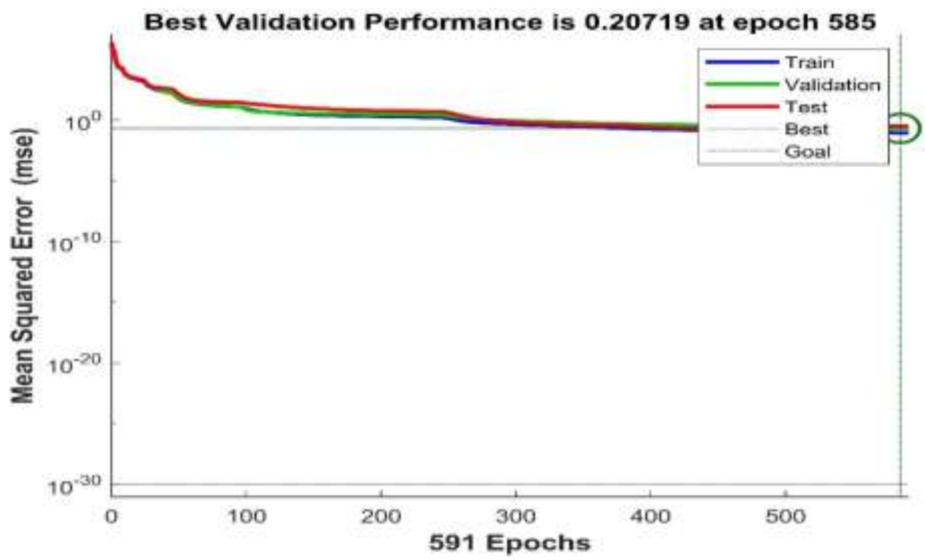

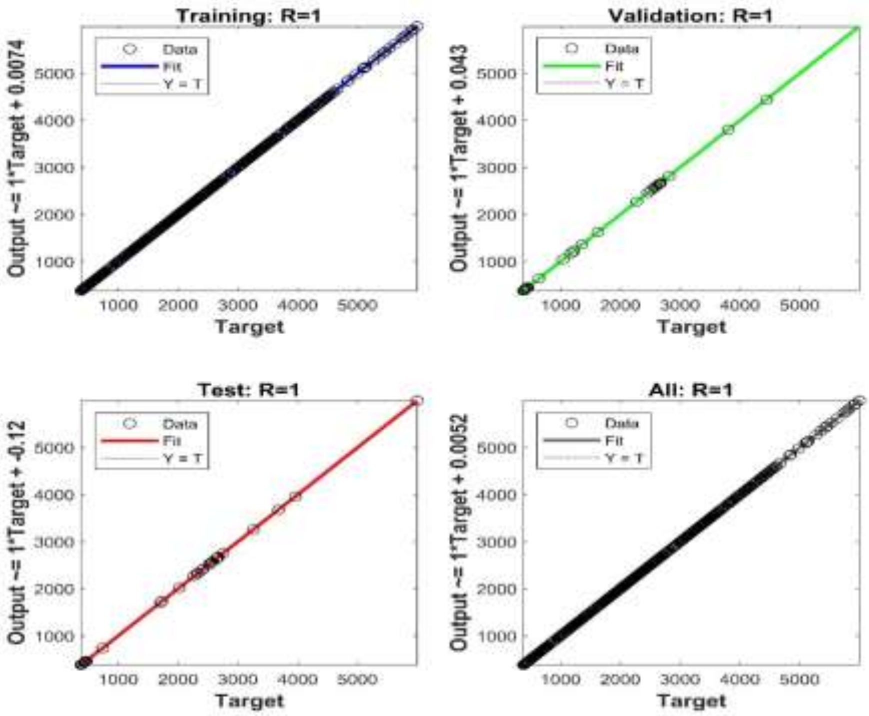

Figure IV-19 The results of the training process.

4.8. Verification of Our proposed EMS Control Strategy

As was previously stated, the planned EMS would perform checks using all three drive cycles: FTP, OCC, and UDDS. To evaluate the performance of the plug-in FCEV. Thus, comparing the results of the proposed controllers which are FLC and ANNs with WNN-PI in two cases.

4.8.1. Case one evaluates the system by FLC and ANN with the Feed-Forward strategy of WNN-PI

4.8.1.1. Case one during UDDS drive cycle

Figure IV-20 depicts the results of a comparison between the output power of the power sources as they are monitored during a UDDC driving cycle (a-f). As can be seen in Figure IV-20, the suggested control system is working properly, hence allowing the fuel cell system to provide steady-state load power without confronting rapid changes of load as observed in Figure IV-20 (a). Also, the battery assists the fuel cell to provide power to the load by reacting to its medium-frequency component. When the BAT SOC drops below 60%, the fuel cell's excess power attempts to recharge the BAT. Meanwhile, as predicted from its characteristics and seen in Figure IV-20 (c) and (f) below, the ultracapacitor is delivering the high-frequency components of the power demand (rapid changes).

Based on the data statistics of Figure IV-4 (b) of power profile the peak point of power needed is 10940W, where observed that supplies of power from resources are responding to the same time (195sec), hence fuel cell power peak output is 2725 (W) (see Figures IV-20 (a, b)) but the remaining power to meet the power demand is 8215 (W), therefore it is provided by the ultracapacitor and battery output power (see Figures IV-20 (c, d), (e, f)), BAT supply 2529 (W) and UC 5730 (W) at the time 195 seconds; thus the power respond to the load power is total 10984W at time 195 seconds.

Figures IV-20 (c) and (d) illustrate the BAT charge and discharge power. Where the battery power output is responding to the load demand that has low variations portion. BAT recharging by the negative power as shown in Figures IV-20 (c) and (d) represents the power captured from either the ultracapacitor or fuel cell system. Overall, the battery run in a safe manner and extends the battery's lifetime.

The changes in UC discharging and charging output power as a result of the sudden load power demand, as shown in Figures IV-20 (e) and (f). Resulting, the UC successfully and effectively supplies the variations and confronting the rapid changes of load, so assisting in the improvement of the established FCHEV operation.

Overall, the findings of the EMS based on ANNs scheme as shown in Figures IV-20 (b), (d) and (f) are very similar to the FLC results as shown in Figures IV-20 (a), (c) and (e). This is mean that the ANN working properly due to the trained was correct and small mean square error attained. In terms of the DC voltage bus as shown in Figures IV-21 (a, b) by FLC and ANN, respectively.

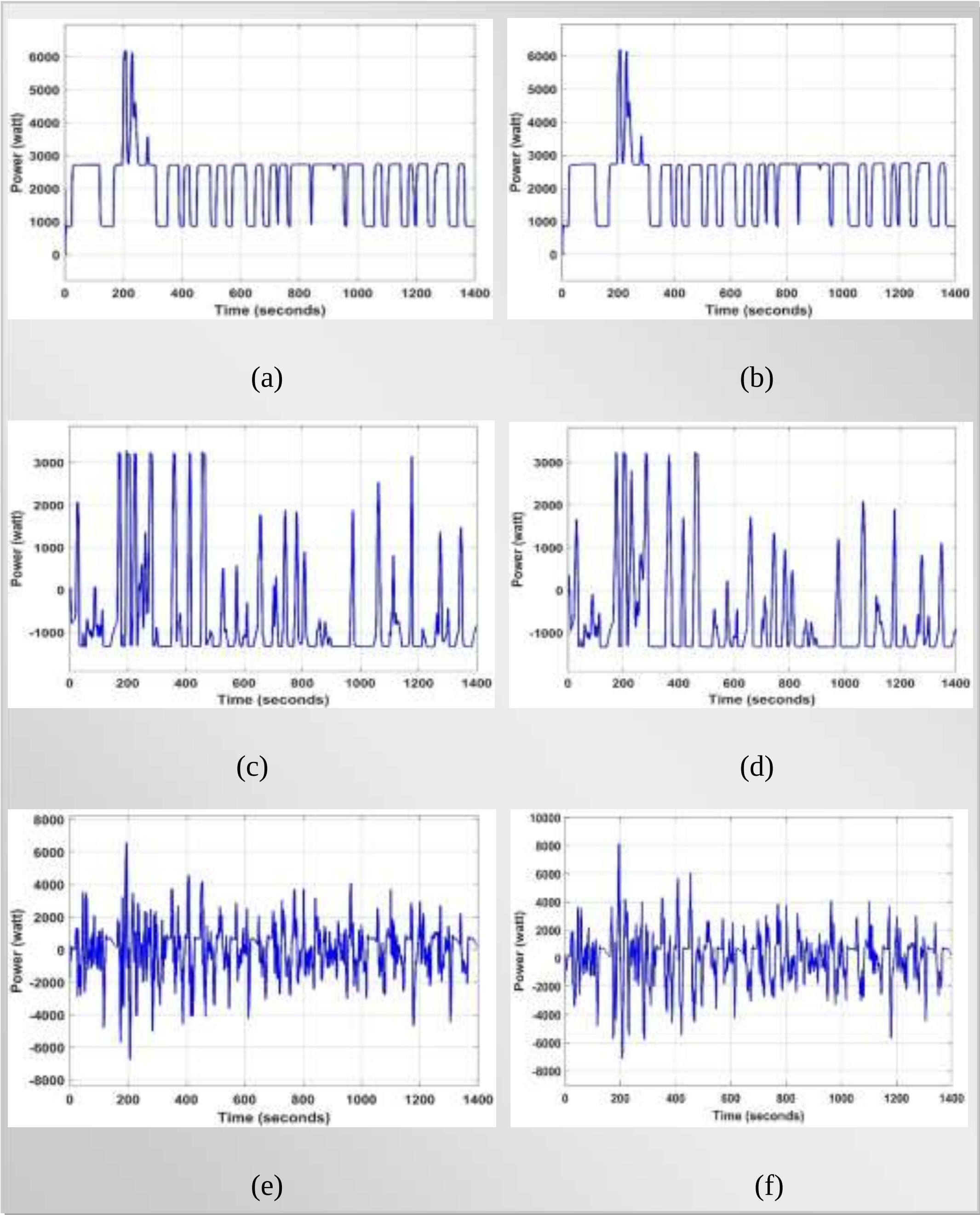

Figure IV-20 Output power of power sources via FLC (a, c, and e) and ANNs (b, d, and f) Schemes: (a and b) fuel cell, (c and d) battery, and (e and f) ultracapacitor.

The proposed advanced controller has limited the DC voltage bus, as can be seen in Figures IV-21 (a) and (b), show the DC-bus voltage that stays within the specified range of 290V to 325V (design DC-bus voltage). If the DC-bus voltage is higher than the set point (300V), the battery converter will enter buck mode which decrease the voltage also and charge the battery. The voltage of DC-bus was maintained at an acceptable level by adjusting the duty cycle for the buck and boost converter of BAT and for the boost mode of the FC converter as illustrated in Figures IV-22 (a, b, and c) respectively during controller FLC EMS with feed-forward WNN-PI. Overall, the DC link voltage is between 295.88V and 306.2V based on FLC and between 295.22V 307.16V based on ANNS (see Figures IV-21 (a, b)).

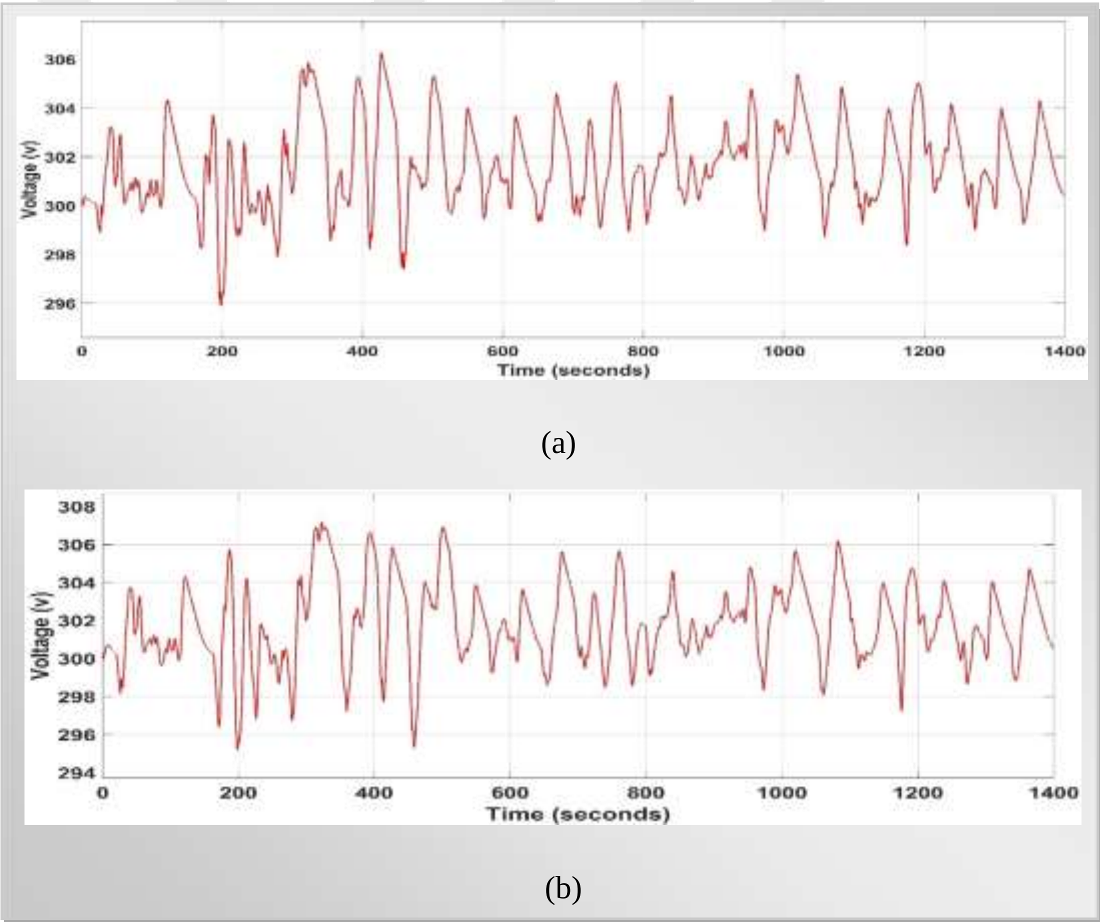

Figure IV-21 The variations of the DC link voltage (a) by FLC (b) by ANN.

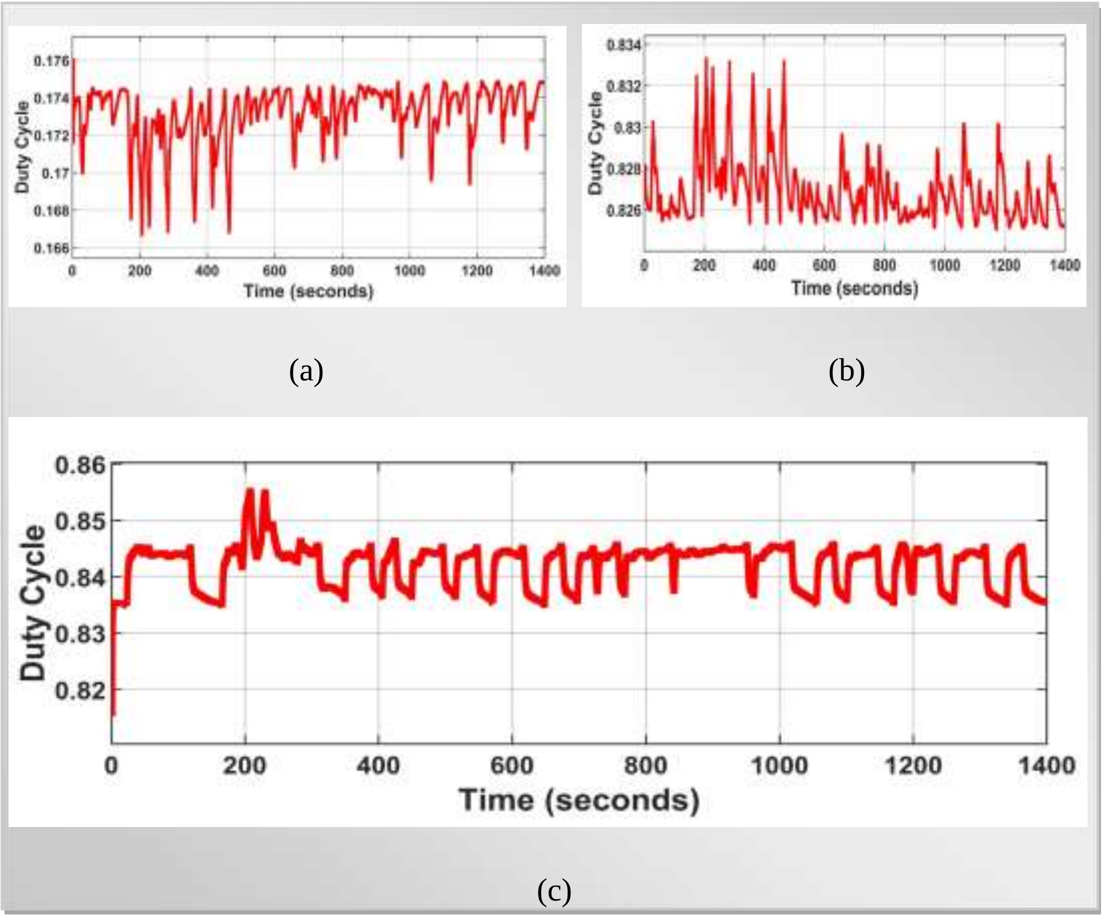

Figure IV-22 Buck duty cycle, boost duty cycle for BAT by FLC (a and b). Boost duty cycle for FC by FLC (c).

The duty cycle of the fuel cell converter's switch varies between 0.8153 and 0.8552 even when the power needed is high, whereas the duty cycle of the boost switch in the battery converter varies between 0.825 and 0.8334, and the duty cycle of the buck switch changes between 0.1666 and 0.1761 as shown in Figure IV-22 (a, b and c). Observed that all duty cycles not being above 90%, then all values are acceptable. Moreover, the duty cycles of the BAT and FC by ANN are very close to FLC results as show in Figure IV-23 (a, b and c).

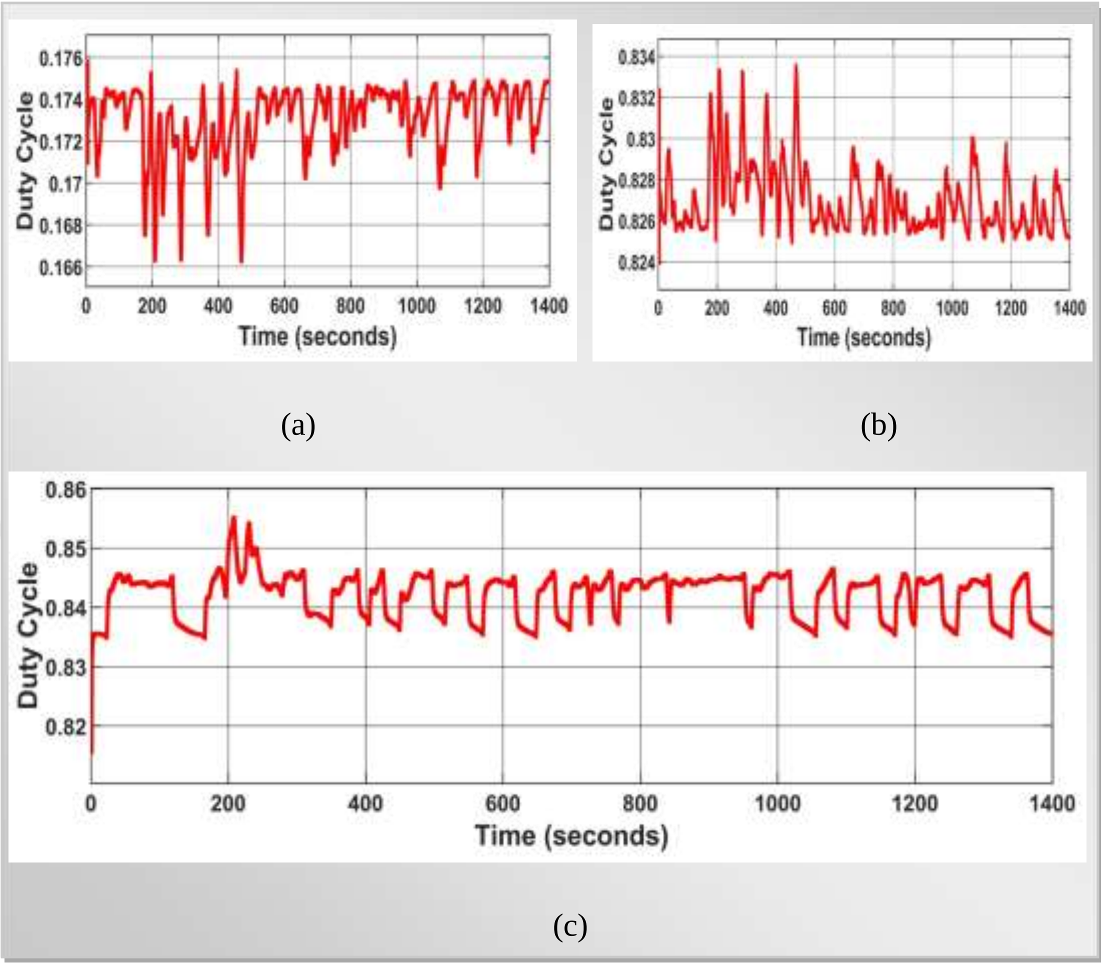

Figure IV-23 Buck duty cycle, boost duty cycle for BAT by ANN (a and b). Boost duty cycle for FC by ANN (c).

The developed EMS algorithm as described and calculated in section 4.7.2 maintains the designed SOC values of BAT and UC, where the BAT SOC is set to be between 60% and 90%.

It is obvious from Figures IV-24 (a, b) and (c and d) that the proposed EMS meets SOC of BAT limits, which is between 67.23% and 75.41% by FLC, while

67.28% and 75.66% by ANN as shown in Figures IV-24 (a and b); yet the ultracapacitor's charge level shifts between 83.51% and 86.56% by FLC, 83.32% and

86.82 by ANN, as shown in Figures IV-24 (c) and (d).

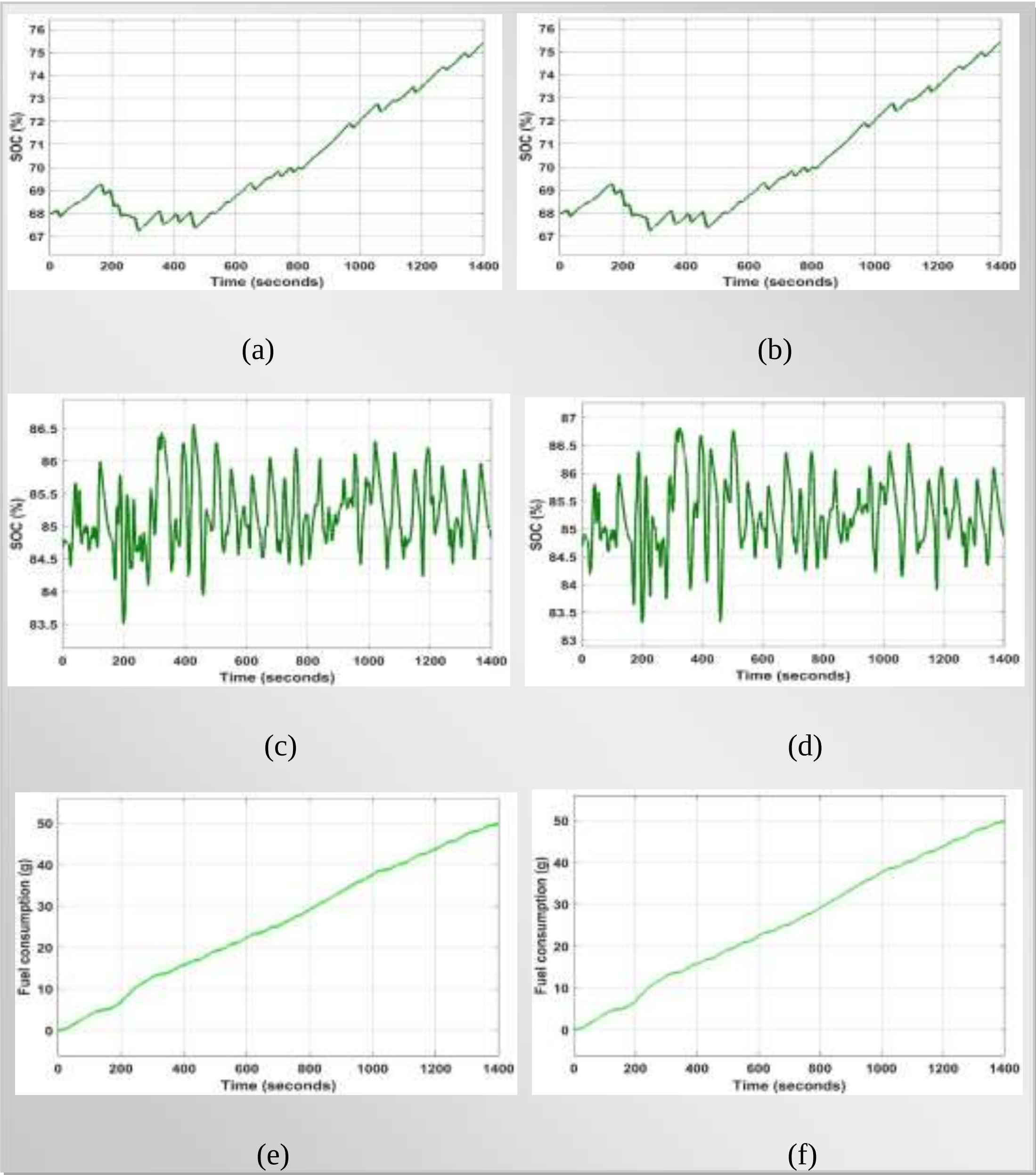

Figure IV-24 SOC of BAT and UC by FLC (a, b); by ANN (c, b). Fuel consumption (g) by FLC and by ANN (e, f).

It is the responsibility of the EMS that has been created to ensure that the ultracapacitor and battery have a sufficient charge during the acceleration phases of the FCHEV. Meanwhile, optimizing the energy flow in order to cut down on the use of H_2. In addition, it is possible to draw the conclusion that the ultracapacitor and battery offer the needed load power requirement in a satisfactory manner. Additionally, fuel consumption is decreased, leading to an improvement in overall efficiency.

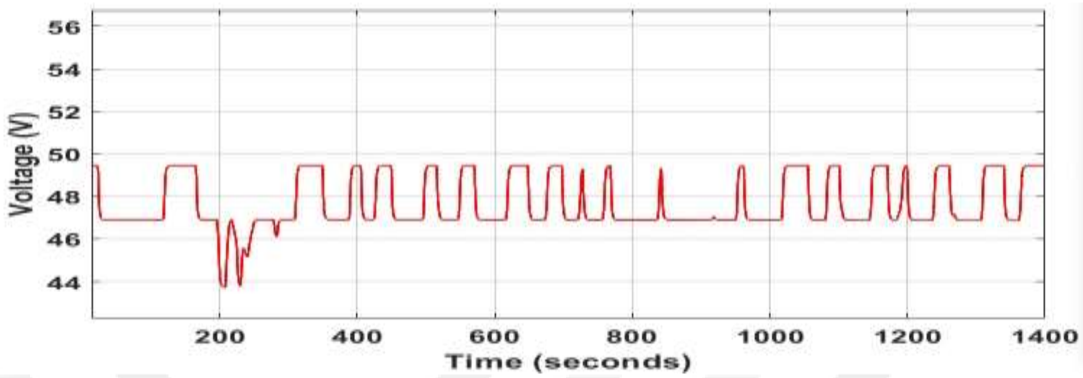

Figure IV-25 The voltage of the fuel cell controlled by FLC during the UDDS.

The desired voltage region for FC operating is clarified in chapter-I also as illustrated in Figure IV-7 (a), which states that if the FC voltage varies between 52 and 39.2V. It can be observed that FC for the proposed design is working under the Ohmic region which is the desired region (see Figure IV-25), hence each cell of the fuel cell system is between 0.67V and 0.76V, whereas the voltage of fuel cell system changes in the permitted ranges between 43.74V and 49.44V, as shown in Figure IV-25, this is the biggest fluctuations in FC voltage occurred between 195 and 350 seconds which is the period of maximum power demand. The FC fluctuations were decreased as a result of the EMS controller's optimal operation, which is why using of energy storage sources. Moreover, since the proposed system with FLC and the optimum feed-forward WNNPI methods are used it can be observed the efficiency of FC has been increased in terms of power as shown in Figure IV-26. The fluctuations in BAT voltage under varied UDDS cycle power demands as shown in Figure IV-27. It is apparent that the BAT voltage changes in a very limited range between 50.08V and 52.69V without causing the battery to overcharge.

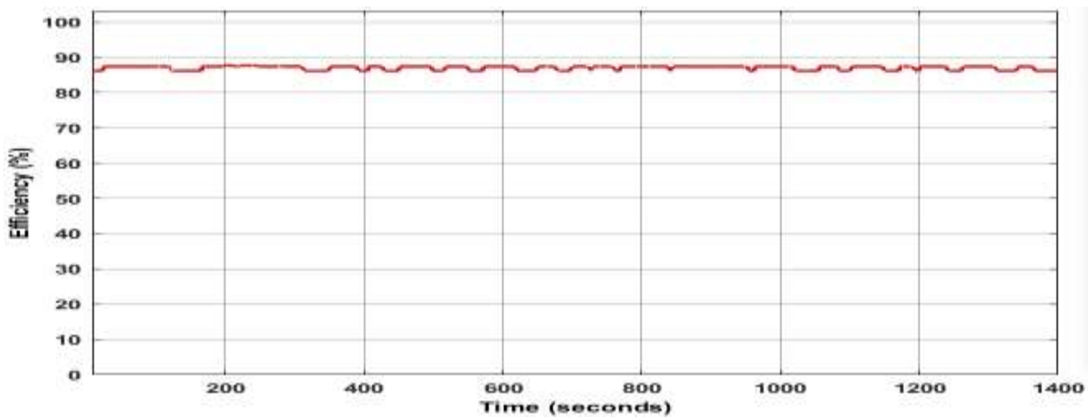

Figure IV-26 The efficiency of FC stack under various UDDS power demands based on the FLC.

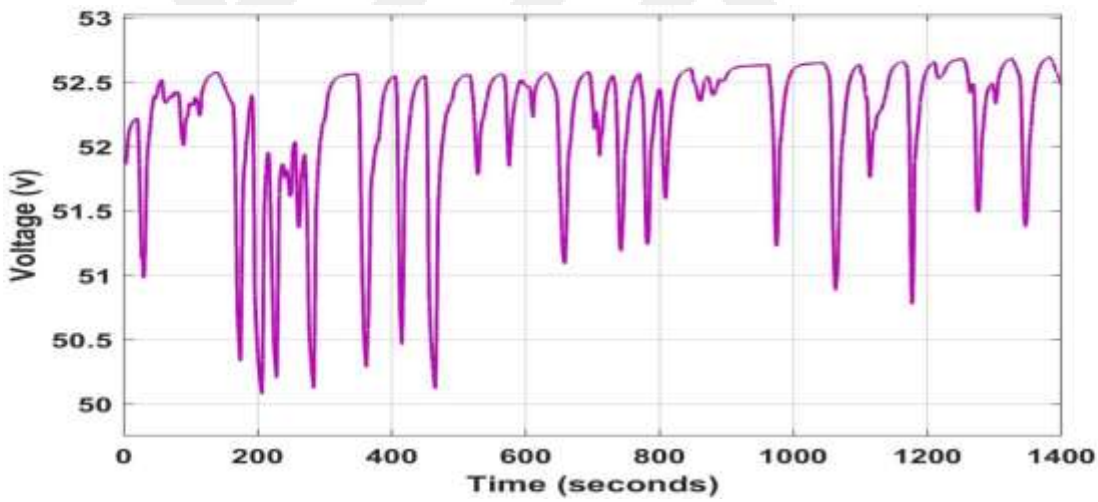

Figure IV-27 The voltage of the battery during the UDDS driving cycle.

Figures IV-28 (a, b, c, and d) illustrate the converters current of battery and fuel cell in terms of input and output during UDDS. These results demonstrate that all currents stay within their output rating currents, which are limited to 250A and 80A, respectively, even during times of peak load demand. Additionally, the highest discharging current of BAT is 80A, whereas the peak charging current is 20A, as indicated in BAT's datasheet in Appendix B-2.

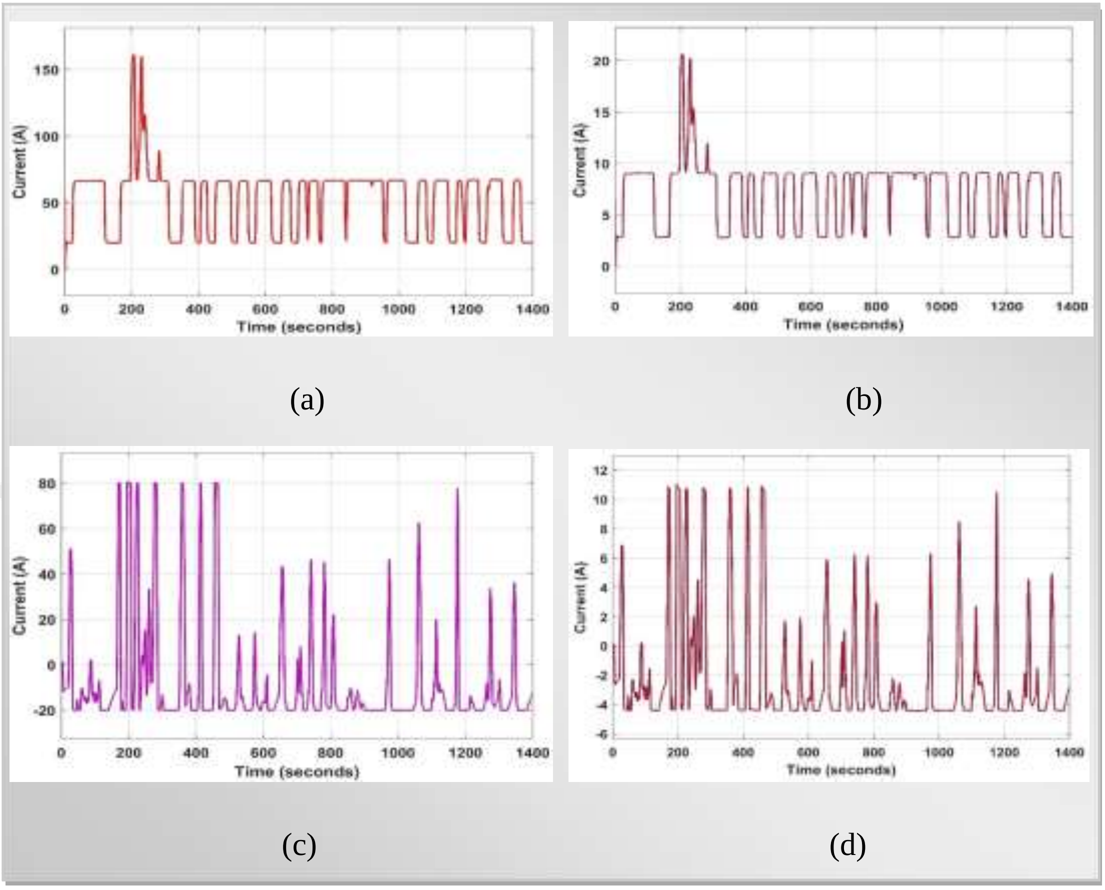

Figure IV-28 The currents of the fuel cell and battery during UDDC (a) input current of the fuel cell, (b) output current of the fuel cell, (c) input current of the battery, and (d) output current of the battery.

Overall, the results of maximum input and output current for the FC are 161.2A and 20.67A, respectively. While the maximum input and output current for the BAT are 80.79A and 11.05A, respectively. The BAT recharge at time 286.9 seconds with 20.03A while the UC recharge at time 206.5 seconds with 22.38A; which confirms that the battery responds after recharging UC first due to the UC has the fastest response accordingly to its characteristics.

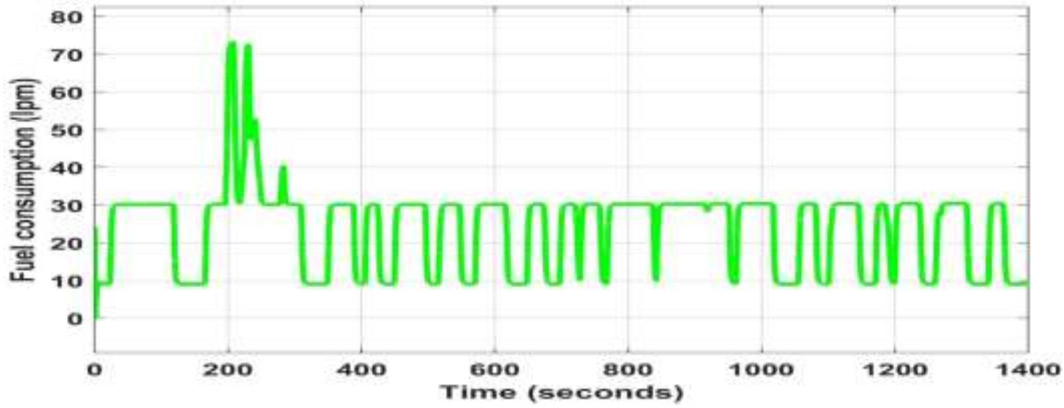

Figure IV-29 The quantity of H_2 usage during the UDDS driving cycle controller FLC.

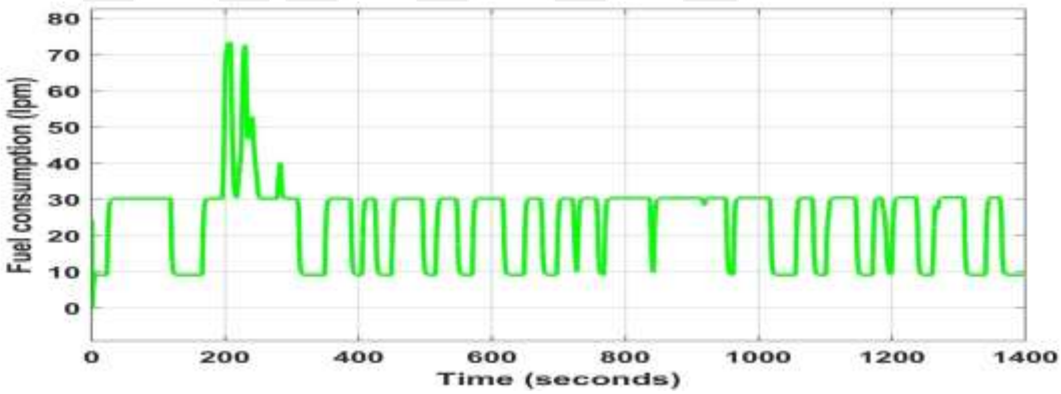

Figure IV-30 The quantity of H_2 usage during the UDDS driving cycle controller ANNs.

Figure IV-29 and Figure IV-30 depict the hydrogen flow volume in liter per minute (lpm) collected to fulfill the UDDS power needed. It's worth noting that the H_2 consumption at maximum load, as shown in Figure IV-29 by FLC is 73.32 lpm, while Figure IV-30 by ANN is 73.31 lpm.

The acquired findings of Case one (ANNs and FLC EMS with Feed-Forward WNN-PI) during the UDDS cycle were summarized in Table IV-14.

Parameters	FLC	ANNs
DC link voltage (V)	295.88 – 306.2	295.22–307.16
FC voltage (V)	43.74–49.44	43.74–49.44
Max-Input current to converter of FC (A)	161.2	161.2
Max-Output current form converter of FC (A)	20.67	20.72
Battery voltage (V)	50.08–52.69	50.09–52.7
Max-Input current to converter of BAT (A)	80.79	80.35
Max-Output current from converter of BAT (A)	11.05	10.97
Battery SOC (%)	67.23–75.41	67.28–75.66
UC SOC (%)	83.51–86.56	83.32–86.82
Average of FC stack efficiency (%)	87.4	86
Maximum fuel consumption (lpm)	73.32	73.31

Table IV-14 The results of Case one (ANNs and FLC EMS with Feed-Forward WNN-PI) during the UDDS cycle.

4.8.1.2. Case one during OCC and FTP drive cycles

This subsection presents the simulation results of the proposed design during other standards driving cycles such as OCC and FTP. Since the intelligent EMS system working properly in UDDS. Thus, different simulation results for the FCHEV system based on FLC with feed-forward WNN-PI under the OCC and FTP demands are shown in Figures IV-31 and Figure IV-32. Moreover, apparent that the FLC with feed-forward WNN-PI improves the FCEV's performance under OCC and FTP while staying within the current design restrictions.

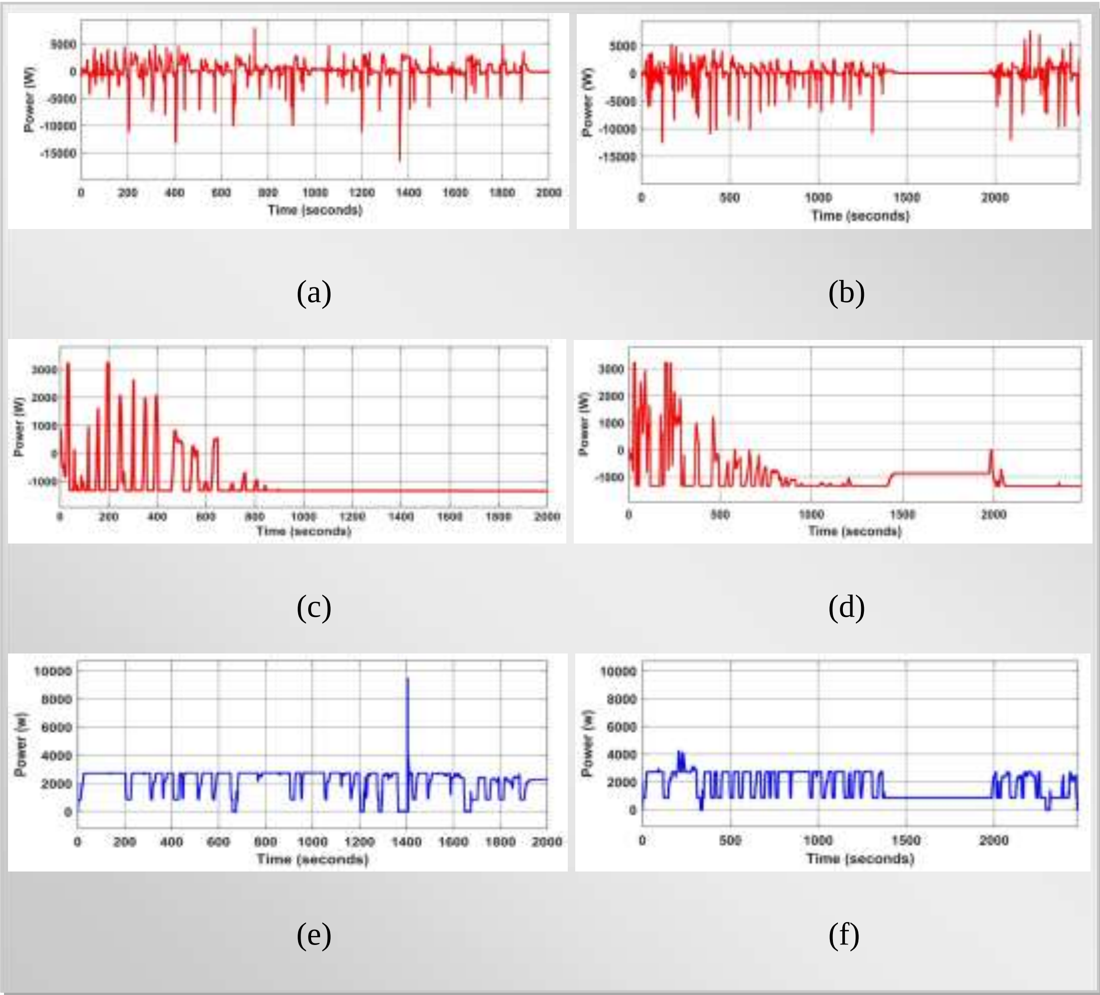

Figure IV-31 FCEV system performance under OCC (a, c, and e) and FTP (b, d, and f) drive cycles (a, b) UC power; (c, d) BAT power and (e, f) FC power.

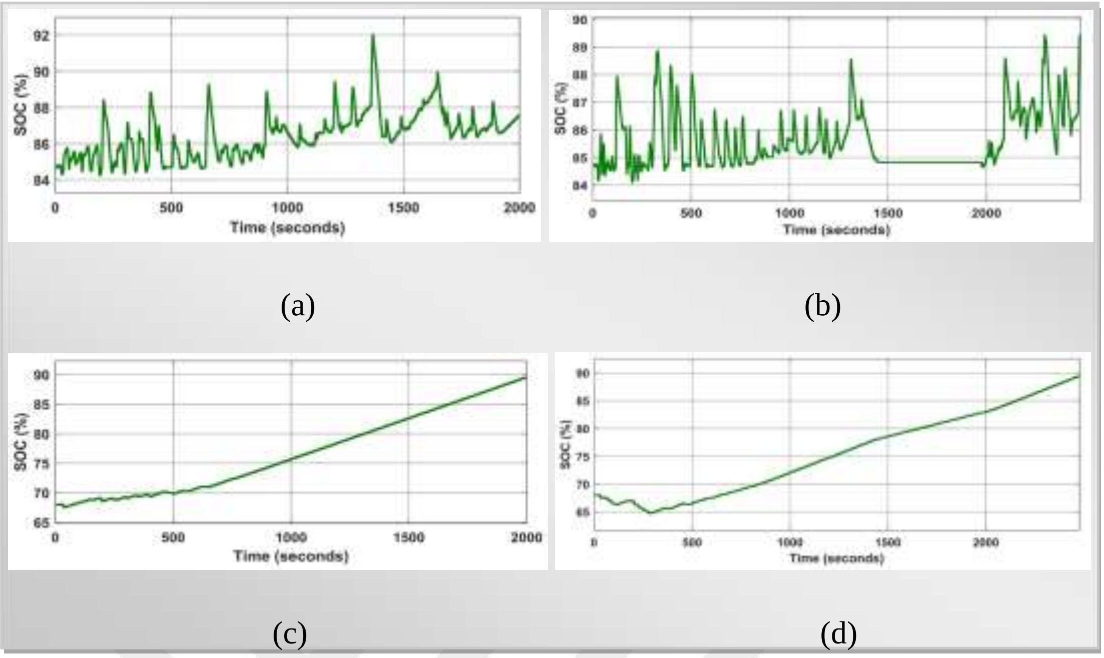

Figure IV-32 FCEV system performance under OCC (a, and c) and FTP (b and d)

drive cycles; (a, b) UC SCO and (c, d) BAT SOC.

The acquired findings of Case one (FLC EMS with Feed-Forward WNN-PI) during the OCC and FTP cycles were summarized in Table IV-15.

Parameters	OCC	FTP
DC link voltage (V)	298.5–324.5	298–316
FC voltage (V)	45.16–49.44	45.5–49.44
Max-Input current to converter of FC (A)	239.8	106
Max-Output current form converter of FC (A)	30.92	14.09
Battery voltage (V)	50.19–53.15	50.04–5.13
Max-Input current to converter of BAT (A)	80.30	80.44
Max-Output current from converter of BAT (A)	10.86	10.91
Battery SOC (%)	67.56–89.56	64.73–89.84
UC SOC (%)	84.26–92.02	84.11–89.82
Average of FC stack efficiency (%)	87.39	86.81
Maximum fuel consumption (lpm)	109.1	48.21

Table IV-15 Case one results (FLC EMS with Feed-Forward WNN-PI) during the OCC and FTP cycles.

4.8.2. Case two evaluates the system by FLC with the recurrent strategy of WNN-PI

This part of the thesis introduces the Recurrent Wavelet Neural Network, known as an RWNN, which functions in the same way as a feed-forward approach but also includes a signal from the output to the input called feedback. Furthermore, the feedback signal is generated by connecting the signal from the output layer to the input layer with delays; this technique is known as “partially feedback”. Moreover, the RWNN linked with the PI controller (RWNN-PI) for controlling the battery as shown in the Simulink model in Figure IV-33. Meanwhile, the RWNN and PI parameters are learned online in the PSO algorithm (see Appendix C-3).

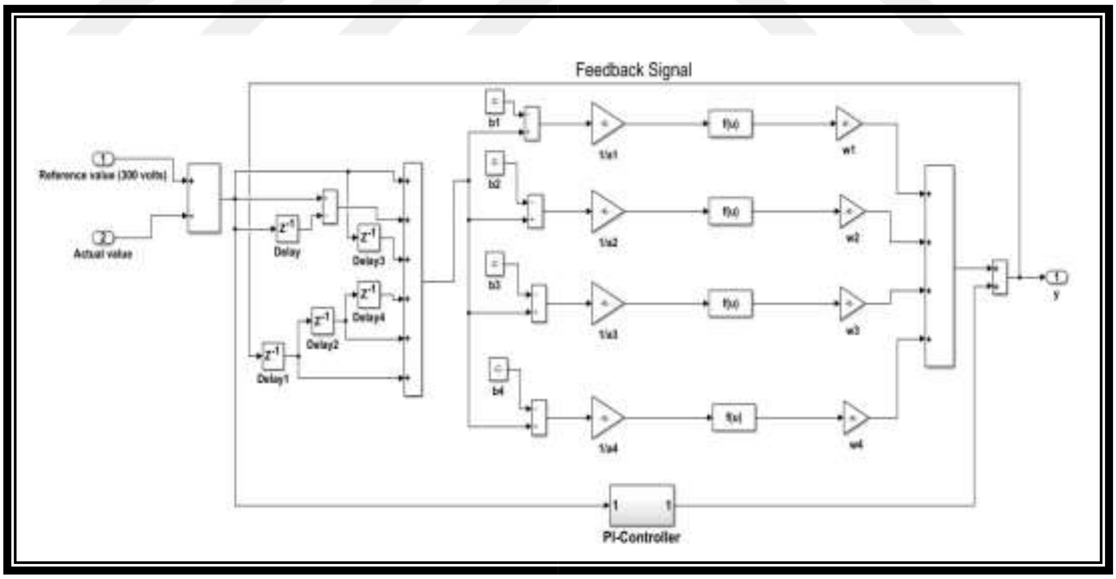

Figure IV-33 Simulink model of RWNN-PI controller.

The output of RWNN is described in subsection 3.4.2 and given by equations (3.14) and (3.15). Table IV-16 lists the PSO setting values. Variables for the PI controller and the RWNN are shown in their optimum values in Tables IV-17 and IV-18,

respectively.

PSO-Parameters	Value
"no of birds"	10
Iteration	10
Dimension	12
C1 & C2	1.4
Wmax	0.8
Wmin	0.2

Table IV-16 PSO Variables value.

Variables	K_p	K_i
Values	25.9874	1.1762

Table IV-17 PI parameters tuned by using PSO.

RWNN Dilation parameters		RWNN Translation parameters		RWNN Weights parameters	
a1	11.0776	b1	-0.7579	w1	14.7592
a2	-21.9609	b2	0.4560	w2	11.2434
a3	6.8087	b3	7.8331	w3	-0.1116

a4	13.3339	b4	3.9727	w4	29.1614

Table IV-18 RWNN parameters tuned by using PSO.

4.8.2.1. Case two during UDDS drive cycle

In this section, evaluate the proposed FLC EMS, as well as BAT converter controller by the RWNN-PI technique, which has been done during the UDDC driving cycle. Consequently, the results show that the properly respond of resources FC, BAT and UC and the overall system is working properly and more efficient than the FeedForward strategy of WNN-PI. Monitoring the fuel cell, battery power output and ultracapacitor states respectively as illustrated in Figure IV-34 (a-c).

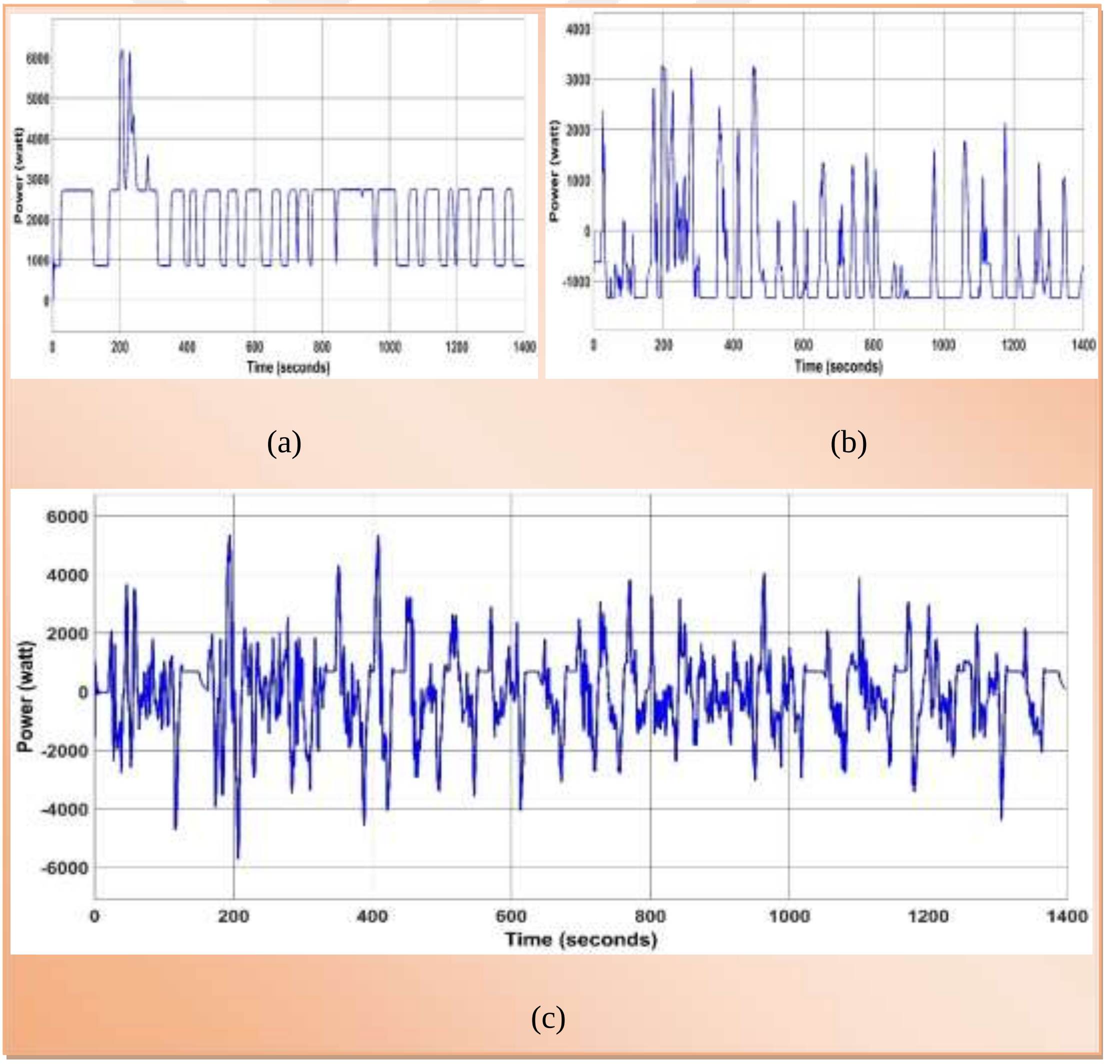

(a) (b)

(c)

Figure IV-34 Power distribution for three resources power of the power train FCEV, based FLC and RWNN-PI technique; (a) FC power, (b) BAT power, (c) UC power.

As shown in Figure IV-34 the control system has a successful response to cover the highest power demand and meet the power required calculation; where the fuel cell maximal power is 2725 (W) till reaches 6187 (W); then the UC has the fast respond into sudden load changes according to its characteristics so delivers 5345 (W); while BAT supply a stable power with 3225 (W). The total power is 11.295 kW at the time 195 seconds of the power profile. Moreover, the DC voltage link is between 295.4(V) to 305.7(V); thus, the advanced controller of RWNN-PI has limited the DC-Bus more than the WNN-PI as well as the DC-Bus is more stable at the 300 volts which is the desired voltage of the EMS design. Figure IV-35 shows the DC-Bus voltage that controlled by FLC EMS with RWNN-PI strategy.

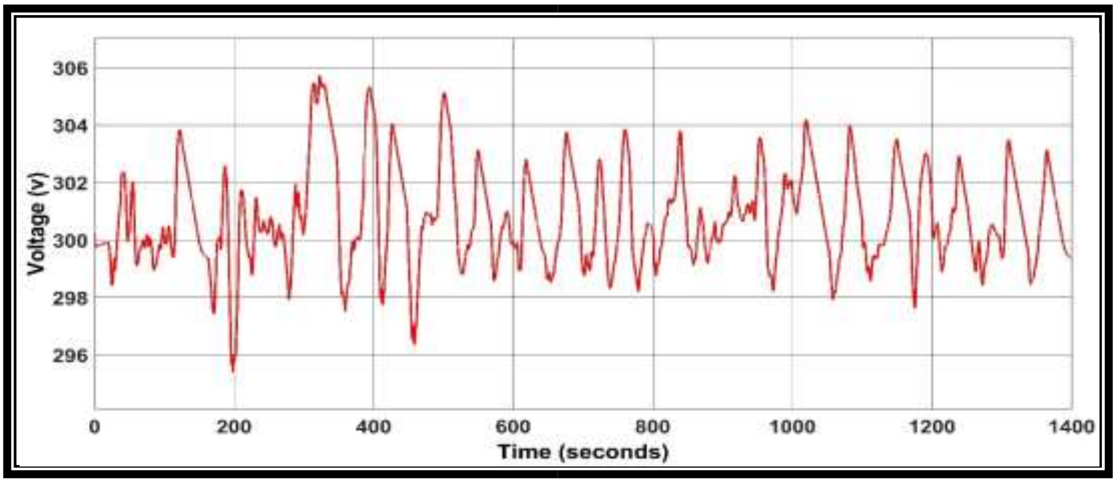

Figure IV-35 DC-Bus voltage of FCHEV.

Regarding the efficient working of the DC-DC converters, the DC-Bus has been more stable, power of FC, BAT and UC are efficient to desired power as well due to the duty cycles of converters being more controlled. Hence, the highest values of the converters at the highest power demand are listed below:

1- Between 0.8152 and 0.8547 is the range of values that the duty cycle for the fuel cell converter switch.
2- In the BAT converter boost mode, the duty cycle switches vary between 0.8082 and 0.8505.
3- In the BAT converter buck mode, the duty cycle switches vary between 0.1668 and 0.1788.

Figure IV-36 (a-c) shows the duty cycles of the converters; where (a) is the BAT buck duty cycle, (b) is the BAT boost duty cycle, and (c) is the FC boost duty cycle. it is observed all duty cycle values are acceptable since values are not above 90%. Also, figured out that the duty cycles of converters switch by RWNN-PI are more stable and efficient than the duty cycles of converters switch by Feed-Forward WNN-PI. As a result, a longer lifetime for converters switches.

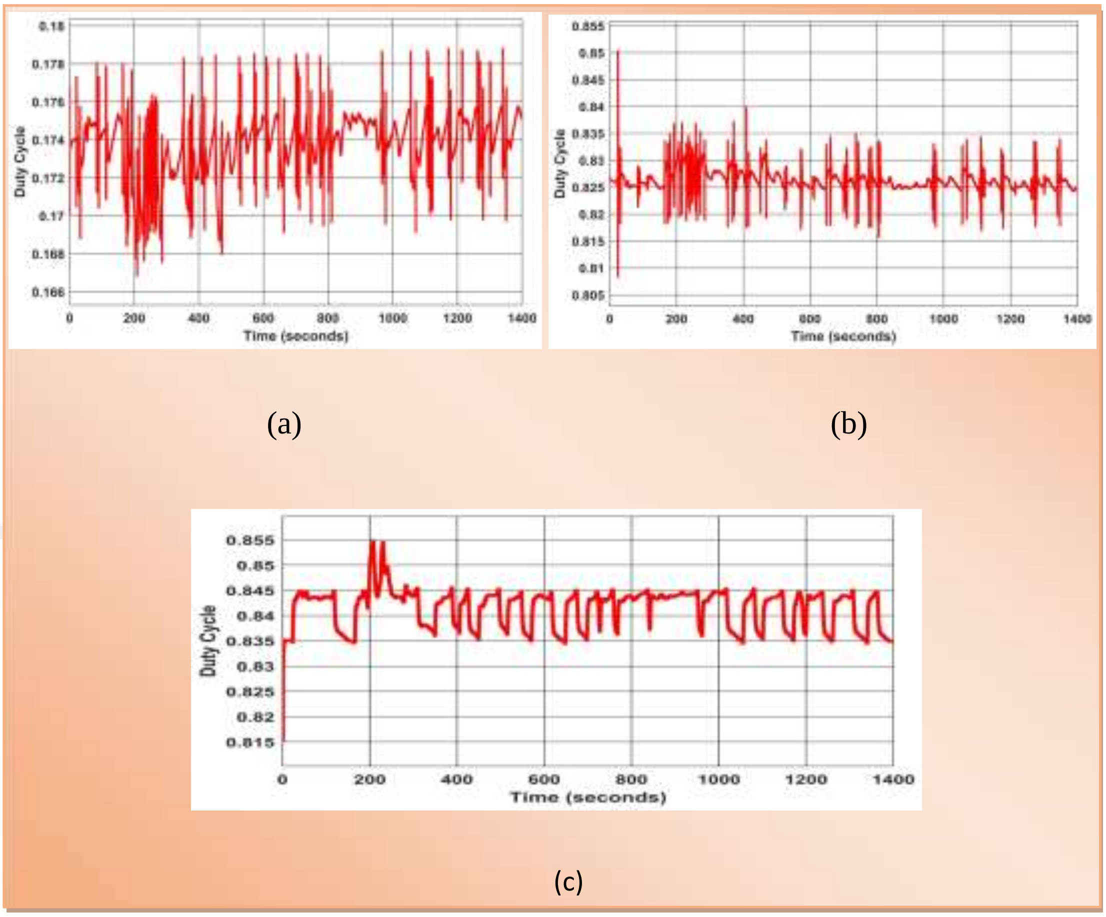

Figure IV-36 Duty cycles, BAT Buck and Boost (a and b), FC Boost duty cycle (c).

As previously stated, the BAT SOC is set to be between 60% and 90%, it can be evident from Figures IV-37 (a, b), where the BAT SOC is between 67.43% and 75.87% as shown in Figure IV-37 (a). While the UC SOC is between 83.36% and 86.39% as shown in Figure IV-37 (b). Therefore, the proposed RWNN-PI successful meet the SOC requirement and keeps the charge-discharge of BAT and UC as required for FCEV's acceleration-deceleration periods with highly efficient respond more than Feed-Forward WNN-PI.

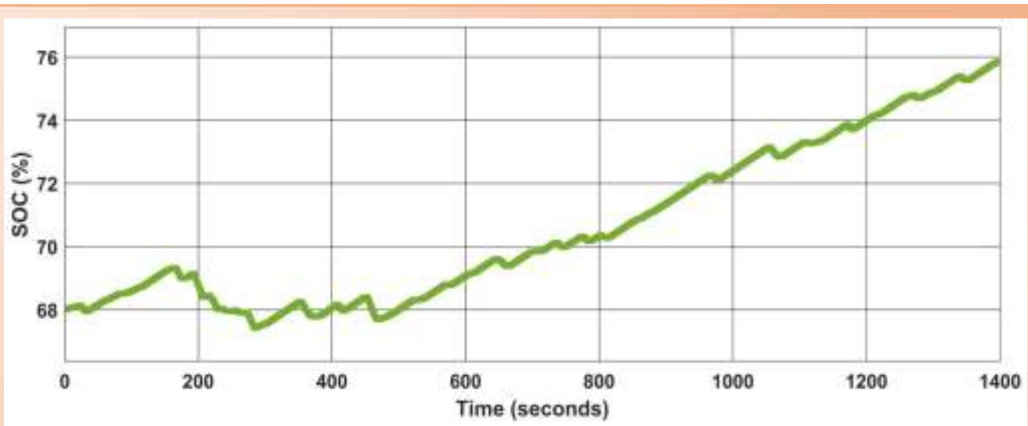

(a)

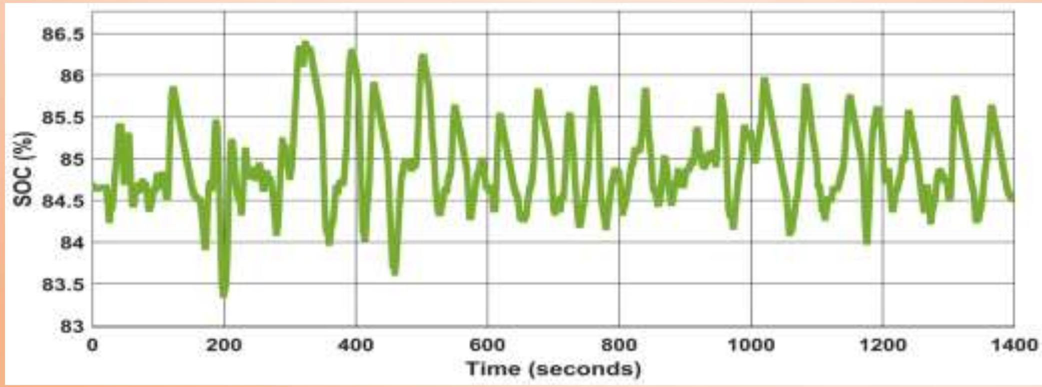

(b)

Figure IV-37 FCEV system performance of state of charge (a) BAT and (b) UC.

It is evident that the suggested designs of the fuel cell operate in the desired range, throughout the UDDS cycle. Hence, 43.74V to 49.44V is the fuel cell voltage range, as shown in Figure IV-38 (a). While the voltage range of the battery is between 50.09 and 52.71 as shown in Figure IV-38 (b) whereas apparent the voltage of the battery changes in a very limited; then, the BAT voltage here is better than the one obtained by Feed-Forward WNN-PI.

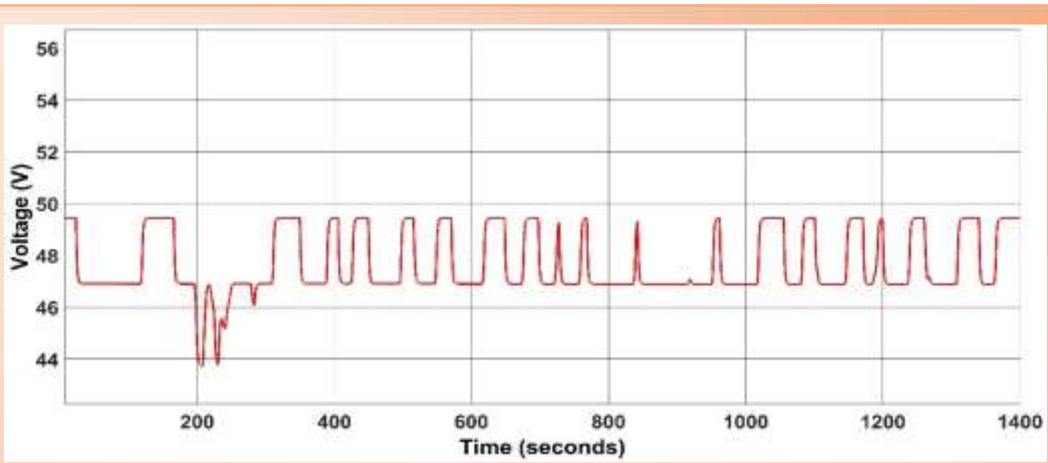

(a)

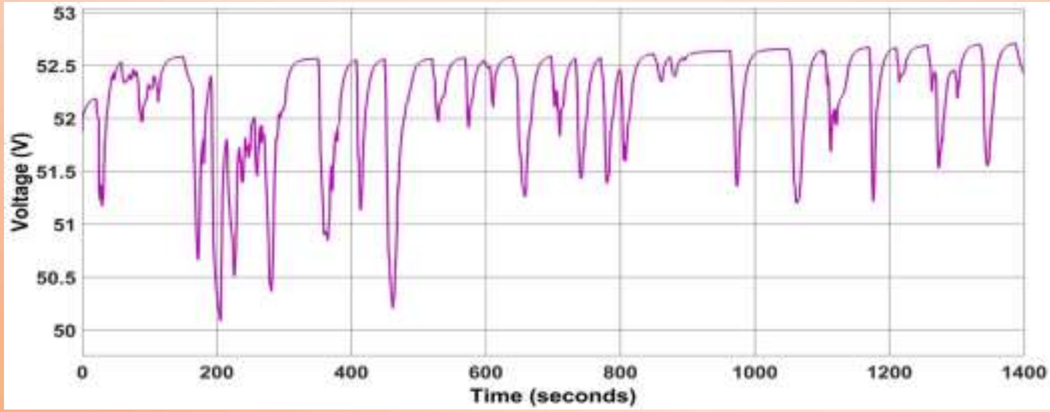

(b)

Figure IV-38 The voltage of FC and BAT during UDDS by FLC EMS with RWNN-PI strategy (a) FC voltage, (b) BAT voltage.

Figures IV-39 (a, b, c, and d) illustrate the converter's current of the battery and fuel cell in terms of input and output during UDDS. Also, as same as case one, all currents stay within their output rating currents, which are limited to 250A and 80A, respectively.

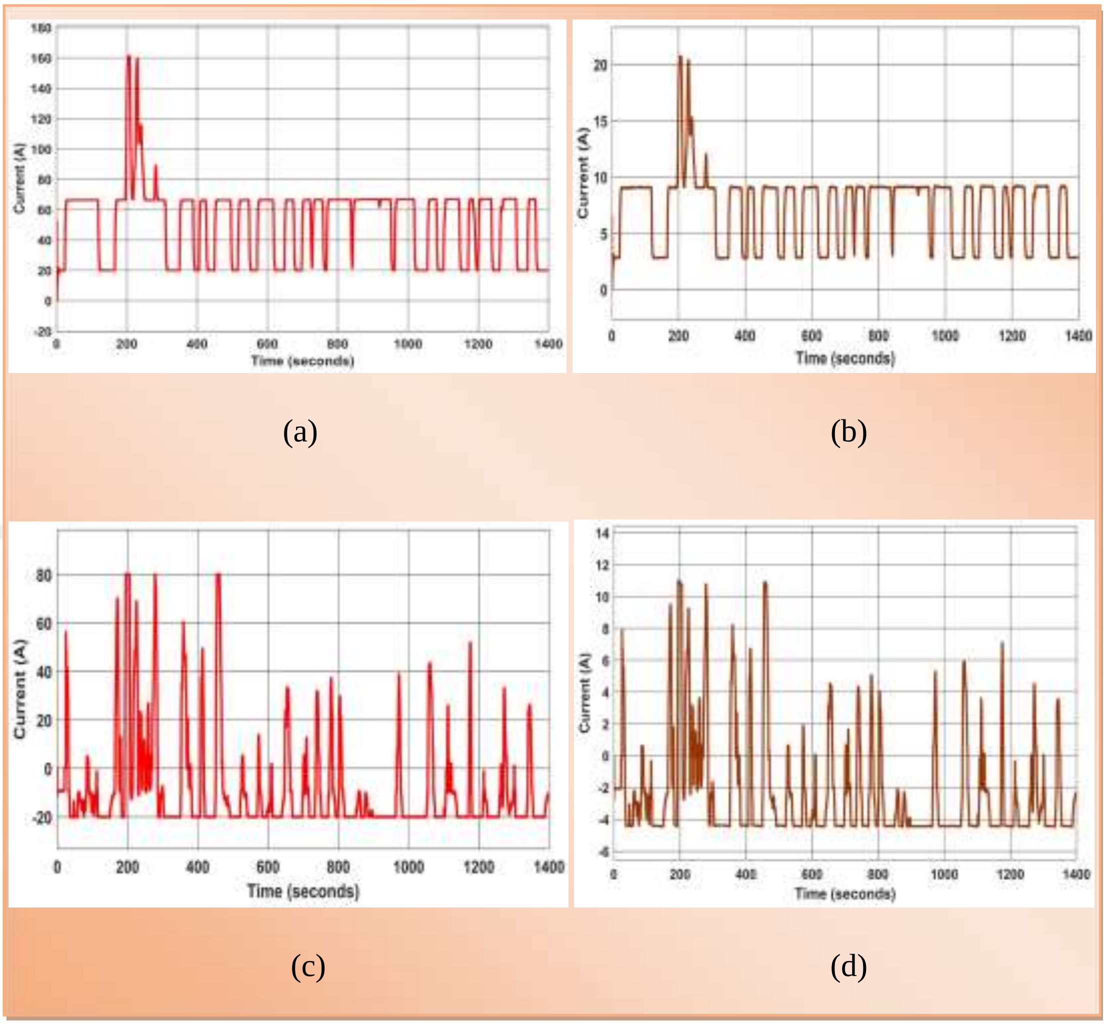

Figure IV-39 The currents, (a) input and (b) output of the fuel cell converter, (c) input and (d) output of the battery converter.

Figure IV-40 (a) and (b) depict the hydrogen flow volume in liter per minute (lpm) and in gram that collected to fulfill the UDDS power needed. Overall, the RWNN-PI method and the proposed EMS algorithm are more efficient than the case-one for the proposed FCHEV. Meanwhile, the power flow is more optimized as well which caused H2 usage is less. Fuel consumption is also lowered, resulting in improved overall efficiency. Figure IV-41 shows the FC efficiency.

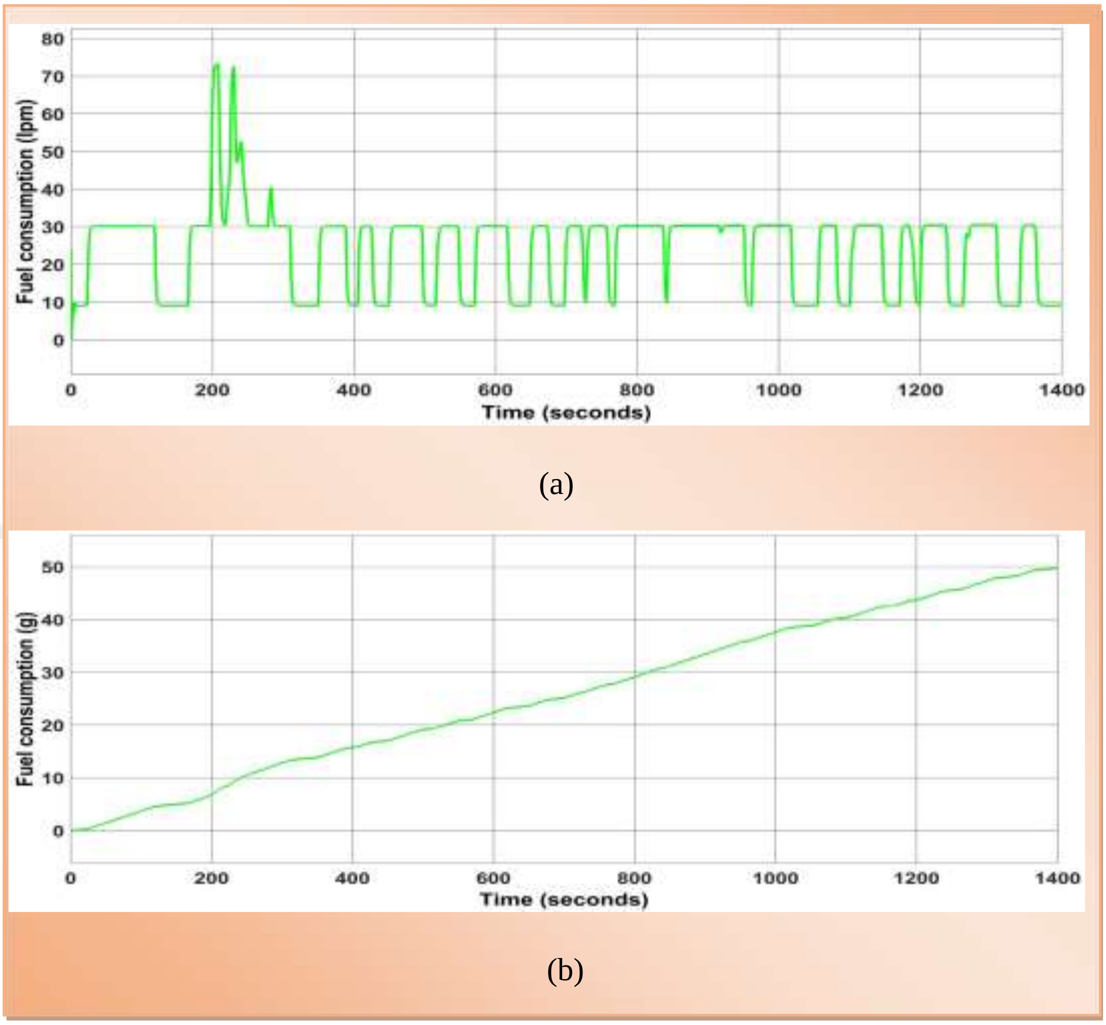

Figure IV-40 The quantity of H_2 usage during the UDDS driving cycle (a) in liter per minute and (b) in gram.

The acquired findings of case two (FLC EMS with RWNN-PI) during the UDDS cycle were summarized in Table IV-19.

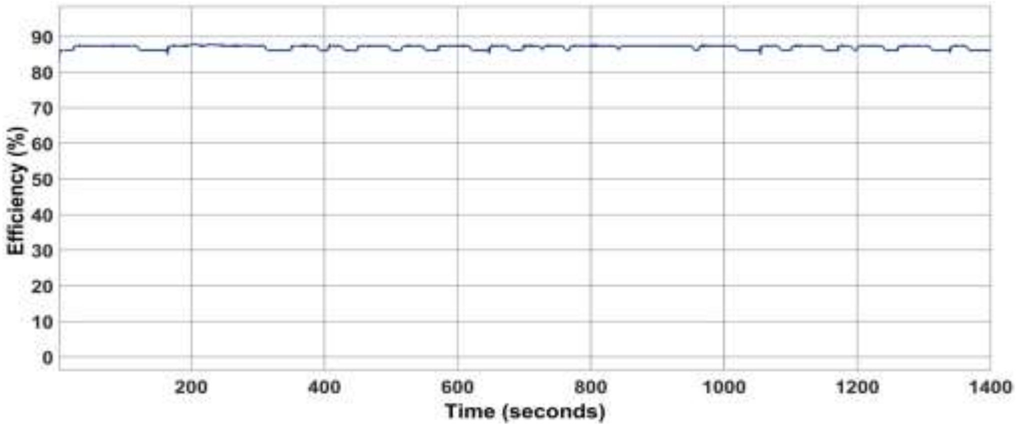

Figure IV-41 The efficiency of FC stack under various UDDS power demands.

Parameters	FLC with RWNN-PI
DC link voltage (V)	295.4 – 305.7 Mean value 300.5
FC voltage (V)	43.74–49.44
Max-Input current to converter of FC (A)	161.2
Max-Output current form converter of FC (A)	20.7
Battery voltage (V)	50.09–52.71
Max-Input current to converter of BAT (A)	80
Max-Output current from converter of BAT (A)	11
Battery SOC (%)	67.43–75.87
UC SOC (%)	83.36–86.39
Average of FC stack efficiency (%)	87.42
Maximum fuel consumption (lpm)	73.33 Mean value 23.98

Table IV-19 The results of case two (FLC EMS with RWNN-PI) during the UDDS cycle.

4.8.2.2. Case two during OCC and FTP drive cycles

The performance study of the system under the OCC and FTP driving cycle requirements is presented in this subsection along with the simulation results.

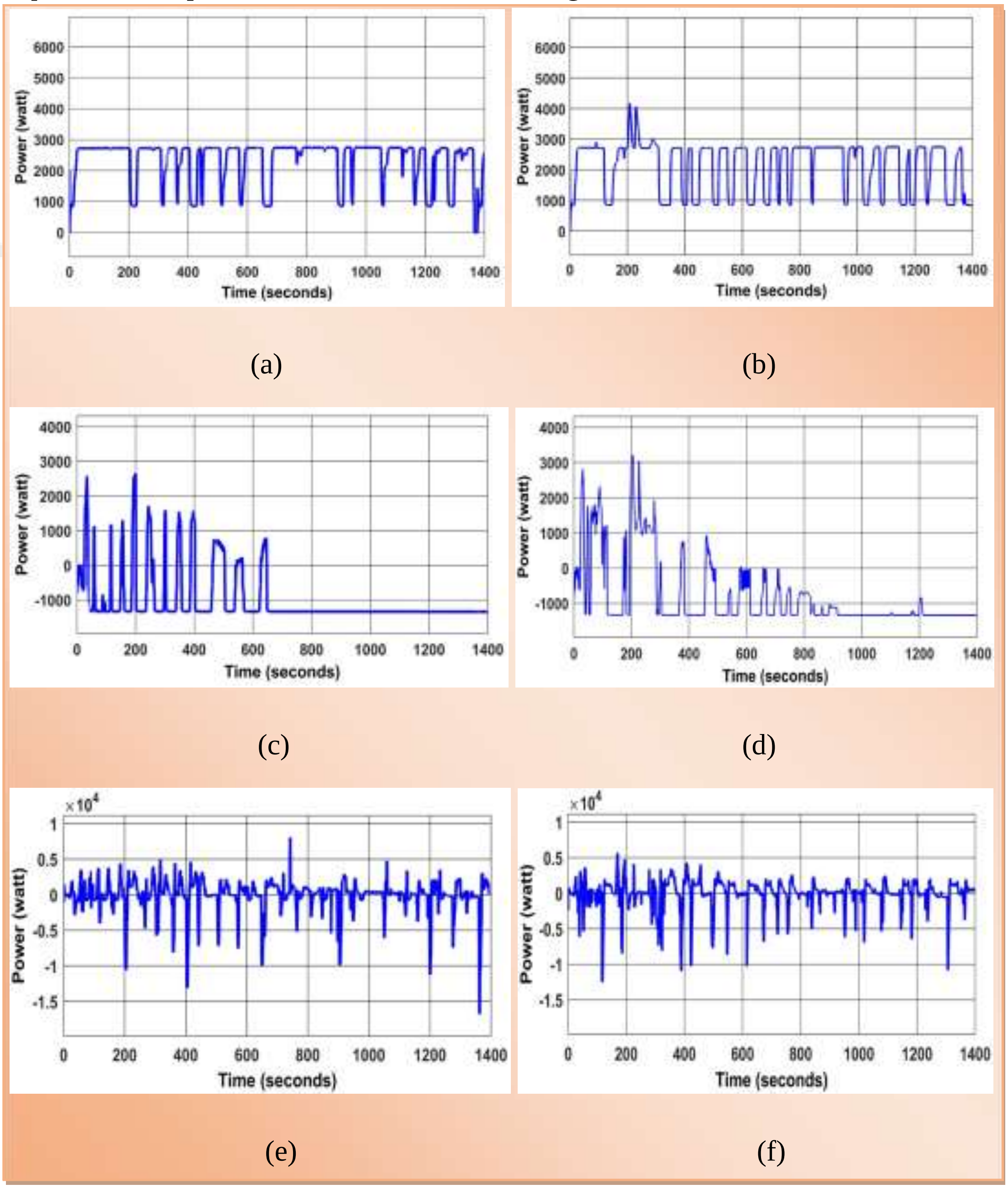

Figure IV-42 Simulation results of output power sources FCHEV system performance under OCC (a, c, and e) and FTP (b, d, and f) drive cycles (a, b) fuel cell; (c, d) battery and (e, f) ultracapacitor.

Because was evident based on the prior results that the FCHEV by FLC with RWNNPI displayed an excellent performance in terms of BAT, FC and UC responses, H2 consumption, efficiency and converters currents have been controlled more efficiently. Figures IV-42 (a-f), IV-43 (a-d) and IV44 (a-d) show the evaluation results over OCC and FTP demands. It can be observed from Figures IV-42 (a-f) that powers are more stable in case two and overcome the overshot issue. Moreover, Figures IV-43 (a-d) shows the input/output currents for converters of FC and BAT under OCC drive cycle, observing that currents are more stable and lower than the currents in case one of OCC drive cycle.

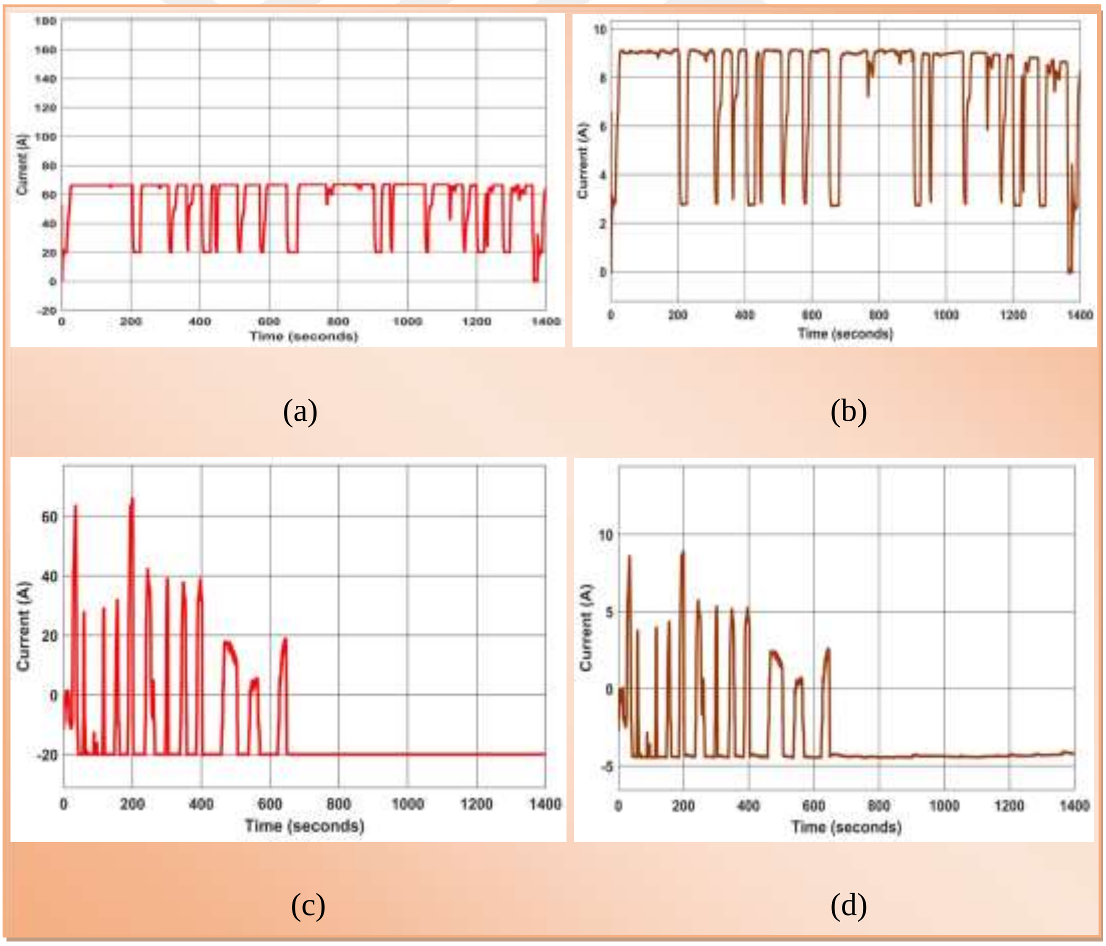

Figure IV-43 The input and output currents for converters of FC and BAT under OCC drive cycle; (a and c) input current of FC and BAT respectively, (b and d) output current of FC and BAT respectively.

As shown in Figure IV-44 (a-d), by comparing the input/output currents for FC and BAT converters under the FTP drive cycle, finding that the currents are lower than the currents in case one and more stable than the currents in case one of FTP drive cycle.

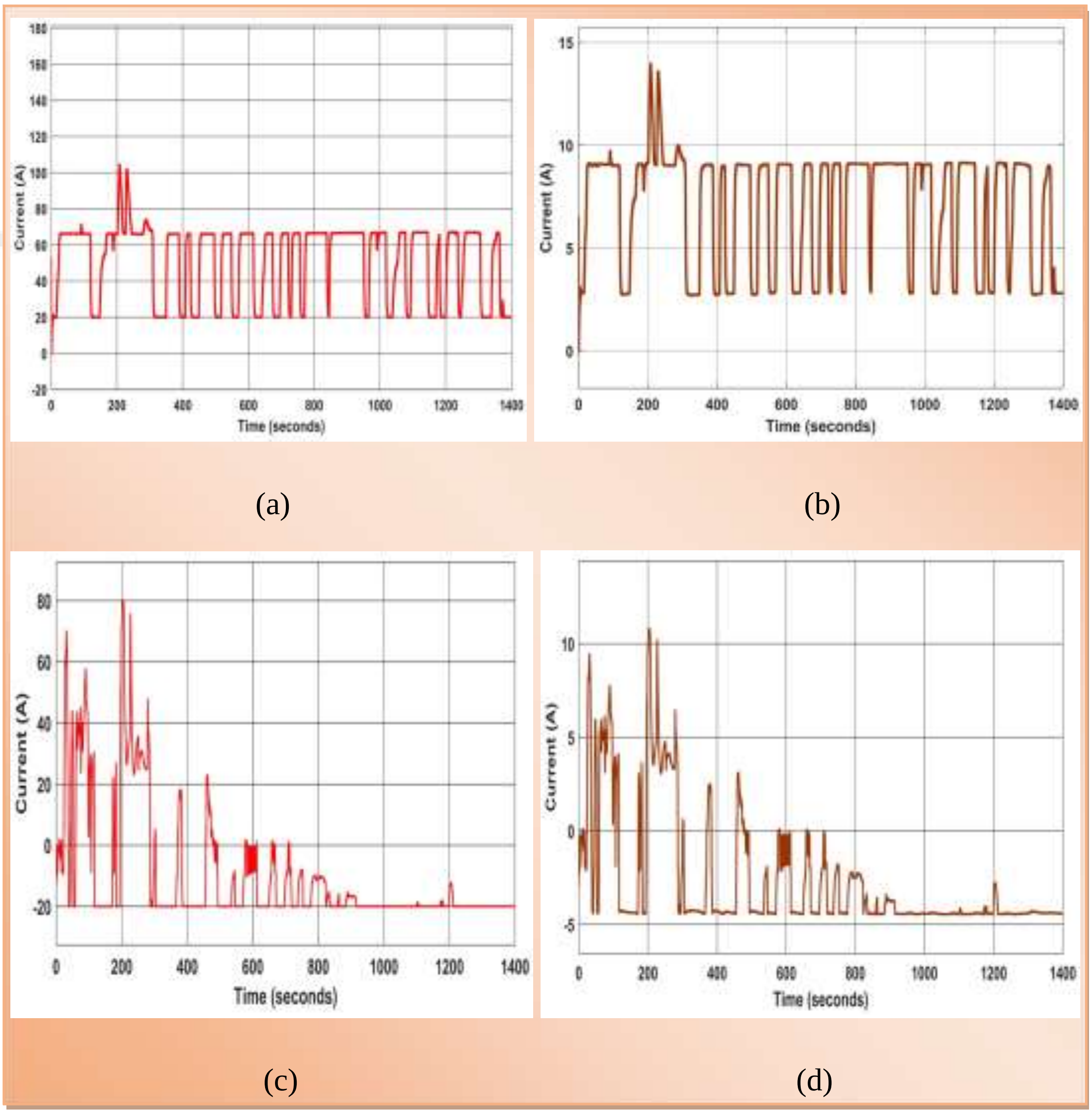

Figure IV-44 The input and output currents for converters of FC and BAT under FTP drive cycle; (a and c) input current of FC and BAT respectively, (b and d) output
current of FC and BAT respectively.

Overall, comparing the results of case two during the OCC and FTP drive cycles based on the FLC EMS with RWNN-PI controller is more efficient than the results of case one in terms of all drive cycles. Thus, a summary of the acquired findings of case two is in Table IV-20 as shown below.

Parameters	OCC	FTP
DC link voltage (V)	297.4 – 327.9 Mean value 304.6	297 – 314 Mean value 302
FC voltage (V)	46.9 – 49.44	45.55 – 49.44
Max-Input current to converter of FC (A)	67.09	104.4
Max-Output current form converter of FC (A)	9.178	13.96
Varies duty cycle of FC converter switch	0.8151 – 0.8530	0.8152 – 0.8477
Battery voltage (V)	50.51 – 52.85	50.19 –52.76
Max-Input current to converter of BAT (A)	80	66.24
Max-Output current from converter of BAT (A)	8.934	10.78
Varies duty cycle of BAT converter boost mode	0.8141 – 0.8388	0.8159 – 0.8386
Varies duty cycle of BAT converter buck mode	0.1612 – 0.1786	0.1673 – 0.1785
Battery SOC (%)	67.72 – 81.5	64.8 – 877.75
UC SOC (%)	83.94 – 93.03	83.82– 88.88
Average of FC stack efficiency (%)	87.41	87.41

Maximum fuel consumption (lpm)	30.52 Mean value 25.75	47.47 Mean value 23.52

Table IV-20 The results of case two (FLC EMS with RWNN-PI) during the OCC and FTP drive cycles.

4.8.3. Discussion of cases one and two results

The proposed control system for hybrid FC vehicle for EMS by FLC that linked with two strategies of wavelet which are Feed-Forward and Recurrent as (WNN-PI and RWNN-PI) has successfully and effectively achieved the following points:

1. FC generator provides steady-state load power without confronting rapid changes and the BAT responds to the load medium-frequency component and assists the fuel cell. While the ultracapacitor is responsible for delivering the power needed with highfrequency components (it responds rapidly to unexpected changes in load).
2. The proposed FC design is working under the Ohmic region which is the desired region. Additionally, the BAT voltage changes in a very limited range, without causing the battery to over-charge or over-discharge.
3. Ensured the BAT runs in a safe manner and extends the lifetime. Given that the battery does not respond to unexpected load fluctuations also the algorithm aims to set the BAT SOC between 60% and 90%. Then, the regenerative braking system, along with FC and UC excess power successfully recharged the BAT.
4. The converters for FC and BAT do not produce more current than their output ratings.
5. The DC-bus voltage stays within the specified range of 290V to 325V (design DCbus voltage).
6. All duty cycles of the converters are acceptable since the values are not above 90%.
7. The EMS has been evaluated by FLC and ANNs and both controllers are working properly. Moreover, the findings of the EMS based on the ANNs scheme are very similar to the FLC results due to the ANNs was trained correctly and a small mean square error was attained.
8. Overall, combining the FCEV with energy storage technologies which are the BAT and UC aimed to improve the responsiveness of the fuel cell and extends the power sources lifespan. Moreover, achieved that the usage of the H_2 was reduced, the fuel cell system size was reduced as well, and the efficiency of the is increased.

Recurrent wavelet (RWNN-PI) approach was used in case two. Hence, it successfully and effectively during the three drive cycles achieved better results than WNN-PI, in terms of the points listed below:

- The power of the resources FC, BAT and UC are more stable and do not show any overshooting and their values are lower than the WNN-PI technique. Consequently, a better power flow has been achieved.
- The DC-Bus is more stable at 300 volts which is the desired voltage of the EMS design.
- The duty cycles of converters are more stable and efficient as well as reducing the input/output currents of the converters. As a result, a longer lifetime for converters switches and a long lifespan of the BAT and UC.
- Meets SOC requirements and keeps the charge-discharge of BAT and UC as required for FCEV's acceleration-deceleration periods with a highly efficient response more than Feed-Forward WNN-PI.

V. CHAPTER FIVE CONCLUSIONS AND SUGGESTIONS FOR FUTURE WORK

5.1. Conclusion

This study provides a coupling intelligent controllers system for energy management technique that controls a hybrid plug-in FCEV system. The goal of this study was to create the next development of an EMS scheme using a combination of batteries, ultracapacitor and fuel cell resources aimed at minimizing the fuel usage of the FCHEV powertrain and boosting the system's efficiency. In the design system, the created EMS scheme took into account the output characteristics of the power resources, as well as their dynamic responsiveness and restrictions.

Following is a summary of the main findings that can be drawn from this study:

- The power needs of the vehicle over a variety of driving cycles were taken into account during the development of the fuel cell plug-in electric automobile. The main source is the power of the fuel cell, batteries, and ultracapacitors as support sources. Moreover, power electronic converters were used with its controller.
- ADVISOR, developed by the National Renewable Energy Laboratory, was utilized to model acceleration and grade test procedures for analyzing hybrid vehicles' dynamic features and obtaining their electrical load power profile. This application was used to extract a variety of load power profiles, including UDDS, OCC, and FTP, which were then used to simulate FCHEV and evaluate the effectiveness of the proposed intelligent EMS.
- The fuel cell vehicle powertrain uses a variety of FC, BAT, and UC connection topologies, which are evaluated and contrasted (compared). The connection system's architecture was chosen based on overall system efficiency, power controllability, and system mass. According to the findings of the comparison, the chosen topology, which is based on a combination of passive and active connections, provides a lightweight structure with high efficiency and lighter weight.
- The purpose of obtaining precise findings that are close to reality, a thorough model for the FCHEV system's components has been developed. With a few additions and modifications, the FC, BAT, and UC models that were already included in Simulink's SimPowerSystem were used. Then, modeling these sources based on their manufacturer

datasheets. As the result, the properties of the power sources have thus been acquired in a manner that is close to their actual qualities.

- Based on the average modeling methodology, the power converters were modeled. In contrast to the switching model, average models take less time to simulate a system. Dependent voltage and current sources are utilized to simulate these switches rather than actual power switches. Moreover, the PI controllers of the power converters are learned online by the PSO algorithm based on the entire FCEV system which results that power converters are working specified to meet the FCEV power requirement as well as control the DC-Bus voltage link.
- The designed intelligent EMS ensures that the power sources' mechanisms operate at a high level of efficiency. Under various load power profiles, two EMS strategies have been presented which are fuzzy logic algorithms and artificial neural networks both have been linked with another two strategies (WNN-PI & RWNN-PI) then compared the results.
- The wavelet (Feed-Forward and Recurrent) controller has been designed to ensure that the BAT provides specified energy, the BAT operates in a safe manner, extends the lifetime, as well as not reposed to high load power variations in the DC-Bus link. While the proposed fuzzy logic controller ensures a stable output power of the fuel cell as well as ensures the ultracapacitor has the first response to unexpected load fluctuations. Overall, the system also ensures that the generator of the fuel cell is operating efficiently in its Ohmic region even though low variations in the output voltage of the fuel cell system; also, the output voltage of the battery changes in a very limited range.
- The proposed system meets the SOC requirements for BAT and UC and keeps the charge-discharge as required for FCHEV's acceleration-deceleration periods with a highly efficient response which is led to reduce the H_2 fuel usage that inject to the fuel cell.
- MATLAB-Simulink computer software successfully and accurately simulates the FCHEV by the proposed intelligent EMS as well as the algorithm of the wavelet.
- The PSO technique was successfully used to determine the optimal values for the PI parameters in terms of K_p and K_i, establish the saturation block's limiting valve (low and high limits), and also the WNN variables. Moreover, the PSO Algorithm and fitness function run the simulation and sets the values with the least amount of error. Thus, iteration number is set then resulting in the simulation running 100 times which is enough cycles to get the minimization of a cost function with minimum error.
- In the MATLAB/Simulink software package, The WNN-PI and RWNN-PI controllers have been created and successfully used to regulate the converters which aimed to control the DC-Bus voltage link. This approach improves the hybrid plug-in FCEV system's dynamic behavior and makes it more resistant to load perturbations and parameter changes.

5.2. Future Work

The findings of this work have led to the following suggestions, which are offered in this section as recommendations for additional study:

- The proposed EMS which is based on FLC, and recurrent wavelet linked with PI controller increases the performance and efficiency of the FCEV system, and is determined by a detailed comparison; as a result, the FLC scheme, as well as RWNNPI, should be verified experimentally to confirm the real-world efficiency improvement.
- Test the system with another optimization algorithm such as a genetic algorithm or ant-colony algorithm, in detailed for the optimization system study, then the proposed FCEV with a comparison results of the PSO, ACO, and GA. Moreover, employed the algorithms for optimizing and tuning the rule base of the fuzzy scheme.
- Design and construct a controller that controls the converters power and modifies the voltage of the DC link by using a multiresolution wavelet or complex wavelet. Better outcomes might be obtained with a PI controller based on wavelet theory and multiresolution analysis.

REFERENCES

[1] Wilberforce, Tabbi, Zaki El-Hassan, F. N. Khatib, Ahmed Al Makky, Ahmad Baroutaji, James G. Carton, and Abdul G. Olabi. "Developments of electric cars and fuel cell hydrogen electric cars." International Journal of Hydrogen Energy 42, no. 40 (2017): 25695-25734.

[2] Xin, Xin, and Zhang Chengning. "Optimal Design of Electric Vehicle Power System with the Principle of Minimum Curb Mass." Energy Procedia 105 (2017): 2629-2634.

[3] ZhuangTian. "Optimal design and simulation of Electric vehicle power system" [D].Wuhan University of Technology, 2013.

[4] Huang, Wanyou, Guangcan Wang, and Mingjin Yu. “Analysis of the effect of driving motor on electric vehicle dynamic performance.” International journal of electric and hybrid vehicles 9.4 (2017): 350-360.

[5] Al-Aawar, N, “Optimal Control Strategy for Hybrid Electric Vehicle Powertrain.” IEEE Journal of emerging and selected topics in power electronics., vol3, pp. 362-370, Jun. 2015.

[6] Gao, David Wenzhong, Chris Mi, and Ali Emadi. “Modeling and simulation of electric and hybrid vehicles.” Proceedings of the IEEE 95.4 (2007): 729-745.

[7] Pukrushpan JT, Stefanopoulou AG, Peng H. “Control of fuel cell power systems: principles; modeling; analysis and feedback design.” Springer Inc; 2005.

[8] Un-Noor, Fuad, Sanjeevikumar Padmanaban, Lucian Mihet-Popa, Mohammad Nurunnabi Mollah, and Eklas Hossain. “A comprehensive study of key electric vehicle (EV) components, technologies, challenges, impacts, and future direction of development.” Energies 10, no. 8 (2017): 1217.

[9] Lucia, Umberto. “Overview on fuel cells.” Renewable and Sustainable Energy Reviews 30 (2014): 164-169.

[10] Wikipedia (2020) https://en.wikipedia.org/wiki/Protonexchange_membrane_fuel_cell. Accessed 08 Dec 2021.

[11] Mohr, Malte, et al. “Converter systems for fuel cells in the medium power range—A comparative study.” IEEE Transactions on Industrial Electronics 57.6 (2010): 2024-2032.

[12] Du, W., et al. "Effect of grid-connected solid oxide fuel cell power generation on power systems small-signal stability." IET renewable power generation 6.1 (2012): 24-37.

[13] Inci, Mustafa, and Ömer Türksoy. "Review of fuel cells to grid interface: Configurations, technical challenges and trends." journal of cleaner Production 213 (2019): 1353-1370.

[14] Adamson, K.A. "Stationary Fuel Cells." Elsevier: Amsterdam, The Netherlands, 2007.

[15] Barbir, Frano. "Fuel cell applications." PEM Fuel Cells; Academic Press: Cambridge, MA, USA (2013).

[16] Akinyele, D. O., and R. K. Rayudu. "Review of energy storage technologies for sustainable power networks." Sustainable Energy Technologies and Assessments 8 (2014): 74-91.

[17] Fuel cell & Hydrogen Energy Association (FCHEA) https://www.fchea.org/transportation. Accessed 08 Dec 2021

[18] V.S. Bagotsky, "Phosphoric Acid Fuel Cells, Fuel Cells." John Wiley & Sons, Inc, 2012, pp. 99e106.

[19] Frattini, Domenico, Grazia Accardo, Angelo Moreno, Sung Pil Yoon, Jong Hee Han, and Suk Woo Nam. "A novel nickel-aluminum alloy with titanium for improved anode performance and properties in molten carbonate fuel cells." Journal of Power Sources 352 (2017): 90-98.

[20] Merle, Géraldine, Matthias Wessling, and Kitty Nijmeijer. "Anion exchange membranes for alkaline fuel cells: A review." Journal of Membrane

Science 377.1-2 (2011): 1-35.

[21] Ormerod, R. Mark. “Solid oxide fuel cells.” Chemical Society Reviews 32.1 (2003): 17-28.

[22] Peighambardoust, S. Jamai, Soosan Rowshanzamir, and Mehdi Amjadi. “Review of the proton exchange membranes for fuel cell applications.” International journal of hydrogen energy 35.17 (2010): 93499384.

[23] Bai, Rulin, and Kittisak Jermsittiparsert. “Optimal design of a micro combined CHP system applying PEM fuel cell as initial mover with utilization of Developed Pathfinder Optimizer.” Energy Reports 6 (2020): 3377-3389.

[24] Sulaiman, Nasrin, M. A. Hannan, Azah Mohamed, E. H. Majlan, and WR Wan Daud. “A review on energy management system for fuel cell hybrid electric vehicle: Issues and challenges.” Renewable and Sustainable Energy Reviews 52 (2015): 802-814.

[25] Sulaiman, N., M. A. Hannan, Azah Mohamed, Pin Jern Ker, E. H. Majlan, and WR Wan Daud. “Optimization of energy management system for fuel-cell hybrid electric vehicles: Issues and recommendations.” Applied energy 228 (2018): 2061-2079.

[26] Manoharan, Yogesh, Seyed Ehsan Hosseini, Brayden Butler, Hisham Alzhahrani, Bhi Thi Fou Senior, Turaj Ashuri, and John Krohn. “Hydrogen fuel cell vehicles; current status and future prospect.” Applied Sciences 9, no. 11 (2019): 2296.

[27] Zhou, Bin, Jeffrey B. Burl, and Amir Rezaei. “Equivalent Consumption Minimization Strategy With Consideration of Battery Aging for Parallel Hybrid Electric Vehicles.” IEEE Access 8 (2020): 204770-204781.

[28] Bendjedia, Bachir, Nassim Rizoug, Moussa Boukhnifer, Farid Bouchafaa, and Mohamed Benbouzid. “Influence of secondary source technologies and energy management strategies on Energy Storage System sizing for fuel cell electric vehicles.” International Journal of Hydrogen Energy 43, no. 25 (2018): 1161411628.

[29] Tao, Fazhan, Longlong Zhu, Zhumu Fu, Pengju Si, and Lifan Sun. “Frequency decoupling-based energy management strategy for fuel cell/battery/ultracapacitor hybrid vehicle using fuzzy control method.” IEEE Access 8 (2020): 166491-166502.

[30] Hu, Xiao, Shikun Liu, Ke Song, Yuan Gao, and Tong Zhang. “Novel Fuzzy Control Energy Management Strategy for Fuel Cell Hybrid Electric Vehicles Considering State of Health.” Energies 14, no. 20 (2021): 6481.

[31] Veerendra, Arigela Satya, Mohd Rusllim Mohamed, Pui Ki Leung, and Akeel Abbas Shah. “Hybrid power management for fuel cell/supercapacitor series hybrid electric vehicle.” International Journal of Green Energy 18, no. 2 (2021): 128-143.

[32] Gharibeh, Hamed Farhadi, Ahmad Sadeghi Yazdankhah, Mohammad Reza Azizian, and Meisam Farrokhifar. “Online energy management strategy for fuel cell hybrid electric vehicles with installed PV on roof.” IEEE Transactions on Industry Applications 57, no. 3 (2021): 2859-2869.

[33] Barelli, L., G. Bidini, D. A. Ciupăgeanu, C. Pianese, P. Polverino, and M. Sorrentino. “Stochastic power management approach for a hybrid solid oxide fuel cell/battery auxiliary power unit for heavy duty vehicle applications.” Energy Conversion and Management 221 (2020): 113197.

[34] Zhang, Hongtao, Xianguo Li, Xinzhi Liu, and Jinyue Yan. “Enhancing fuel cell durability for fuel cell plug-in hybrid electric vehicles through strategic power management.” Applied Energy 241 (2019): 483-490.

[35] Masih-Tehrani, Masoud, Mohammad Reza Ha'iri Yazdi, Vahid Esfahanian, Masoud Dahmardeh, and Hassan Nehzati. “Wavelet-based power management for hybrid energy storage system.” Journal of Modern Power Systems and Clean Energy 7, no. 4 (2019): 779-790.

[36] Li, Huan, Yang Zhou, Hamid Gualous, Hicham Chaoui, and Loïc Boulon. “Optimal cost minimization strategy for fuel cell hybrid electric vehicles based on decision-making framework.” IEEE Transactions on Industrial Informatics 17, no. 4 (2020): 2388-2399.

[37] Zhou, Yang, Alexandre Ravey, and Marie-Cecile Péra. “Multi-mode predictive energy management for fuel cell hybrid electric vehicles using Markov driving pattern recognizer.” Applied Energy 258 (2020): 114057.

[38] Sun, Haochen, Zhumu Fu, Fazhan Tao, Longlong Zhu, and Pengju Si. “Datadriven reinforcement-learning-based hierarchical energy management strategy for fuel cell/battery/ultracapacitor hybrid electric vehicles.” Journal of Power

Sources 455 (2020): 227964.

[39] Hoenicke, Pia, Debjani Ghosh, Adel Muhandes, Sumantra Bhattacharya, Christiane Bauer, Josef Kallo, and Caroline Willich. “Power management control and delivery module for a hybrid electric aircraft using fuel cell and battery.” Energy Conversion and Management 244 (2021): 114445.

[40] Sorlei, Ioan-Sorin, Nicu Bizon, Phatiphat Thounthong, Mihai Varlam, Elena Carcadea, Mihai Culcer, Mariana Iliescu, and Mircea Raceanu. "Fuel cell electric vehicles—A brief review of current topologies and energy management strategies." Energies 14, no. 1 (2021): 252.

[41] Lü, Xueqin, Yinbo Wu, Jie Lian, Yangyang Zhang, Chao Chen, Peisong Wang, and Lingzheng Meng. "Energy management of hybrid electric vehicles: A review of energy optimization of fuel cell hybrid power system based on genetic algorithm." Energy Conversion and Management 205 (2020): 112474.

[42] Teng, Teng, Xin Zhang, Han Dong, and Qicheng Xue. "A comprehensive review of energy management optimization strategies for fuel cell passenger vehicle." International Journal of Hydrogen Energy 45, no. 39 (2020): 2029320303.

[43] İnci, Mustafa, Mehmet Büyük, Mehmet Hakan Demir, and Göktürk İlbey. "A review and research on fuel cell electric vehicles: Topologies, power electronic converters, energy management methods, technical challenges, marketing and future aspects." Renewable and Sustainable Energy Reviews 137 (2021): 110648.

[44] Tran, Dai-Duong, Majid Vafaeipour, Mohamed El Baghdadi, Ricardo Barrero, Joeri Van Mierlo, and Omar Hegazy. "Thorough state-of-the-art analysis of electric and hybrid vehicle powertrains: Topologies and integrated energy management strategies." Renewable and Sustainable Energy Reviews 119 (2020): 109596.

[45] Gao, Lijun, Roger A. Dougal, and Shengyi Liu. "Active power sharing in hybrid battery/capacitor power sources." *Eighteenth Annual IEEE Applied*

Power Electronics Conference and Exposition, 2003. APEC'03. Vol. 1. IEEE, 2003.

[46] Chen, Yong-Song, Sheng-Miao Lin, and Boe-Shong Hong. “Experimental study on a passive fuel cell/battery hybrid power system.” Energies 6.12 (2013): 6413-6422.

[47] Ahmed, Oday Ali. “Investigation into high efficiency DC-DC converter topologies for a DC microgrid system.” Diss. University of Leicester, 2012.

[48] Wang, Lei, Zhan Wang, and Hui Li. “Optimized energy storage system design for a fuel cell vehicle using a novel phase shift and duty cycle control.” 2009 IEEE Energy Conversion Congress and Exposition. IEEE, 2009.

[49] Das, Himadry Shekhar, Chee Wei Tan, and A. H. M. Yatim. “Fuel cell hybrid electric vehicles: A review on power conditioning units and topologies.” Renewable and Sustainable Energy Reviews 76 (2017): 268-291.

[50] X. Chen, W. Shen, T. Tu, Z. Cao and A. Kapoor, “An Overview of Lithiumion Batteries for Electric Vehicles”, *IEEE, Conference on Power & Energy IPEC,* pp. 230-235, June, 2013.

[51] Tian, Huixin, et al. “A review of the state of health for lithium-ion batteries: Research status and suggestions.” Journal of Cleaner Production 261 (2020): 120813.

[52] Shuvankar Podder and Md. Ziaur Rahman Khan, “Comparison of Lead Acid and Li-ion Battery in Solar Home System of Bangladesh”, *IEEE, 5th International Conference on Informatics, Electronics and Vision (ICIEV),* pp. 434-438, 2016.

[53] WIND ENERGY STORAGE AND CONVERSION POTENTIAL. Lithium-

ion battery. Website link: http://www.esru.strath.ac.uk/EandE/Web_sites/17-18/windies/lithium-ion-battery-storage.html. Accessed February 2022.

[54] M. Farhadi and M. Abapour, “Three-Switch Three-Phase Inverter With Improved DC Voltage Utilization,” IEEE Transactions on Industrial Electronics, vol. 66, no. 1, pp. 14–24, 2019.

[55] Huggins R. “Energy storage, fundamentals, materials and applications.” New York, NY, USA: Taylor & Springer group; 2016.

[56] W. G. Gerekial, “Galvanic Isolated Bidirectional DC-DC LLC Resonant Converter” M.Sc Thesis, Norwegian University of Science and Technology, June, 2014.

[57] Erickson, Robert W. “DC–DC power converters.” Wiley encyclopedia of electrical and electronics engineering (2001).

[58] Mahdavi, Javad, Ali Agah, Ali Emadi, and Daniel Jeffrey Shortt. “Power Electronic Circuits and Controls.” (2002).

[59] “Du, Changqing, Shiyang Huang, Yuyao Jiang, Dongmei Wu, and Yang Li. "Optimization of energy management strategy for fuel cell hybrid electric vehicles based on dynamic programming.” Energies 15, no. 12 (2022): 4325.

[60] Chen, Jeng-Fung, Shih-Kuei Lo, and Quang Hung Do. “Forecasting shortterm traffic flow by fuzzy wavelet neural network with parameters optimized by biogeography-based optimization algorithm.” Computational intelligence and neuroscience 2018 (2018).

[61] Stanhill, David, and Yehoshua Y. Zeevi. "Two-dimensional orthogonal filter banks and wavelets with linear phase." IEEE transactions on signal processing 46.1 (1998): 183-190.

[62] Cui, Deyu, et al. "A novel intelligent method for the state of charge estimation of lithium-ion batteries using a discrete wavelet transform-based wavelet neural network." Energies 11.4 (2018): 995.

[63] Yavasoglu, Huseyin A., Yusuf E. Tetik, and Huseyin Gunhan Ozcan. "Neural network-based energy management of multi-source (battery/UC/FC) powered electric vehicle." International Journal of Energy Research 44.15 (2020): 12416-12429.

[64] Kalyankar-Narwade, Supriya, Ramesh Kumar Chidambaram, and Sanjay Patil. "Neural Network-and Fuzzy Control-Based Energy Optimization for the Switching in Parallel Hybrid Two-Wheeler." World Electric Vehicle Journal 12.1 (2021): 35.

[65] D. Fewson, "Introduction to Power Electronics", Oxford University Press, Inc., New York, Published by Elsevier Ltd, 1998.

[66] B. Dokic and B. Blanusa, "Power Electronics Converters and Regulators". Springer International Publishing, 3rd edition, 2015.

[67] Reddy M. B., Obulesh Y. P. and Raju S. S., "Particle Swarm Optimization Based Optimal Power Flow For Volt-Var Control." ARPN Journal of Engineering and Applied Sciences, Vol. 7, Jan. 2012, PP. 20-25.

[68] Effatnejad, R., S. Bagheri, M. Farsijani, and R. Talebi. "Economic dispatch with particle swarm optimization and optimal power flow." International

Journal on "Technical and Physical Problems of Engineering" (IJTPE) 5 (2013): 9-16.

[69] Sivanandam, S. N., P. Visalakshi, and A. Bhuvaneswari. "Multiprocessor Scheduling Using Hybrid Particle Swarm Optimization with Dynamically Varying Inertia." Int. J. Comput. Sci. Appl. 4, no. 3 (2007): 95-106.

[70] Soni, Yogendra Kumar, and Rajesh Bhatt. "BF-PSO optimized PID controller design using ISE, IAE, IATE and MSE error criteria." International Journal of Advanced Research in Computer Engineering & Technology (IJARCET) 2, no. 7 (2013): 2333-2336.

[71] Taeib, Adel, Ali Ltaeif, and Abdelkader Chaari. "A PSO Approach for Optimum Design of Multivariable PID Controller for nonlinear systems." arXiv preprint arXiv:1306.6194 (2013).

[72] Wissam H., "Modeling and Control of Nonlinear Systems Using Wavelet Networks", Master Thesis of Engineering, American University of Sharjah School, 2006.

[73] Rajamanickam, Aruna, and Sairabanu Shaik Mohideen. "A Multi-Wavelet Neural Network Particle Swarm Optimization Based MRPID of Interior Permanent Magnet Synchronous Motor Drives." International Journal of Intelligent Engineering and Systems 9, no. 3 (2016): 53-64.

[74] Prasanthi, Achikkulath, Hussain Shareef, Madathodika Asna, Ahmad Asrul Ibrahim, and Rachid Errouissi. "Optimization of hybrid energy systems and adaptive energy management for hybrid electric vehicles." Energy Conversion and Management 243 (2021): 114357.

[75] Billings, Stephen A., and Hua-Liang Wei. “A new class of wavelet networks for nonlinear system identification.” IEEE Transactions on neural networks 16, no. 4 (2005): 862-874.

[76] Dhiraj A. and SUNIL K., “Adaptive Fuzzy Wavelet Network Control Design for Nonlinear Systems”, International Journal of Advanced Technology & Engineering Research (IJATER), Vol. 3, Jan. 2013, PP. 148-157.

[77] Bhowmik, P. S., S. Pradhan, M. Prakash, and S. Roy. “Investigation of wavelets and radial basis function neural network for incipient fault diagnosis in induction motors.” *In 2013 International conference on circuits, controls and communications (CCUBE)*, pp. 1-5. IEEE, 2013.

[78] Mustafa Iysa Hamza, “A Wavelet Network Control Scheme for Path Tracking of Mobile Robot” Master Thesis in Electrical Engineering, University of Basrah, Aug. 2013.

[79] David V., “Wavelet Neural Networks”, Dissertation submitted for the Master Science in Data Analysis, Networks and Nonlinear Dynamics, Department of Mathematics University of York, Aug. 2005.

[80] Lekutai, Gaviphat. “Adaptive self-tuning neuro wavelet network controllers.” PhD diss., Virginia Polytechnic Institute and State University, 1997.

[81] Yoo, S. J., Park, J. B., & Choi, Y. H. “(2005, June). Direct adaptive control using self recurrent wavelet neural network via adaptive learning rates for stable path tracking of mobile robots.” *In Proceedings of the 2005, American Control Conference, 2005. (pp. 288-293).* IEEE.

[82] R. W. Erickson, D. maksimoic, “Fundamentals of Power Electronics”, Kluwer Academic Publishers, 2nd Edition, 2004.

[83] MATLAB Documentation Help, Generic Fuel Cell Model; https://www.mathworks.com/help/physmod/sps/powersys/ref/fuelcellstack.html. 2022.

[84] Jain, Arpit, and Abhinav Sharma. "Membership function formulation methods for fuzzy logic systems: A comprehensive review." J. Crit. Rev 7, no. 19 (2020): 8717-8733.

[85] Kumar, Avanish, and P. R. Thakura. "ADVISOR-based performance analysis of a hybrid electric vehicle and comparison with a conventional vehicle." IETE Journal of Research (2020): 1-9.

[86] BARLOW, Tim J., S. Latham, I. S. McCrae, and P. G. Boulter. "A reference book of driving cycles for use in the measurement of road vehicle emissions." TRL Published Project Report (2009).

[87] Driving Cycle, Available online: https://en.wikipedia.org/wiki/Driving_cycle, Accessed February 2022.

[88] HyPM-HD12 PEMFC Datasheet, Available online: https://silo.tips/download/hypm-fuel-cell-power-modules. Accessed 2022.

[89] U-Charge U1-12XP Lithium-ion Battery Datasheet, Available online: https://www.celltech.se/fileadmin/user_upload/Celltech/Products/Litium_laddningsbara/Valence_Modules/XP_Module_Datasheet.pdf. Accessed 2022.

[90] Maxwell Boostcap®BCAP1200 UC Datasheet, Available online: https://www.datasheetarchive.com/pdf/download.php?id=692d2c8a33a1c020f38f0ee5addb244b9a3475&type=M&term=BCAP1200. Accessed, 2022.

APPENDIX A

(A-1): Fuel Cell Model

There are several categories of fuel cell models, including electro-chemical, empiric or experimental, and electric-circuit based models. Figure A-1 presents the FC model which is the most basic. In this approach, FC was represented as a Thevenin electrical equivalent circuit made up of series resistance (R_{fc}) and a DC voltage source (V_{fc_o}) [47].

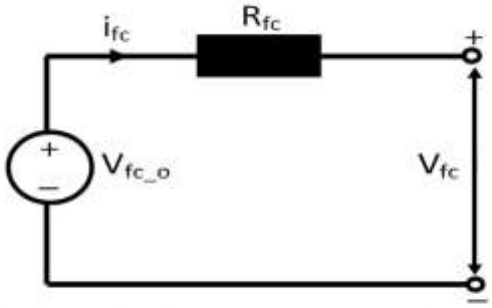

Figure A-0-1 Model for the simplified FC equivalent circuit [47].

The FC membrane's characteristics determine the Ohmic resistance, which is presented as [47]:

$$R_{fc} = \int_0^{L_m} \frac{dx}{Am\, \gamma_T} \qquad (A.1)$$

Where:

L_m: the membrane thickness, A_m: membrane effective area, and γ is the FC membrane conductivity at the operation of temperature.

The voltage fell quickly as shown in Figure I-3. Moreover, the FC's extremely low efficiency in this area, may the FC be damaged. The actual cell voltage, V_{fc}, can be calculated as follows [47]:

$$V_{fc} = E_{oc} - \Delta V_{conc} - \Delta V_{activ} \tag{A.2}$$

Where E_{oc} , ΔV_{conc} , and ΔV_{activ} are the voltage drop caused by Ohmic losses, activation losses and concentration losses respectively.

A thorough mathematical model for the FC generator has been built by using the simpower system toolbox offered by MATLAB/Simulink software as illustrated in Figure A-2 [83]. Based on this model, figure out the possibility of extracting the FC parameters from the actual FC datasheets and applying them in a MATLAB model to be close to the real FC.

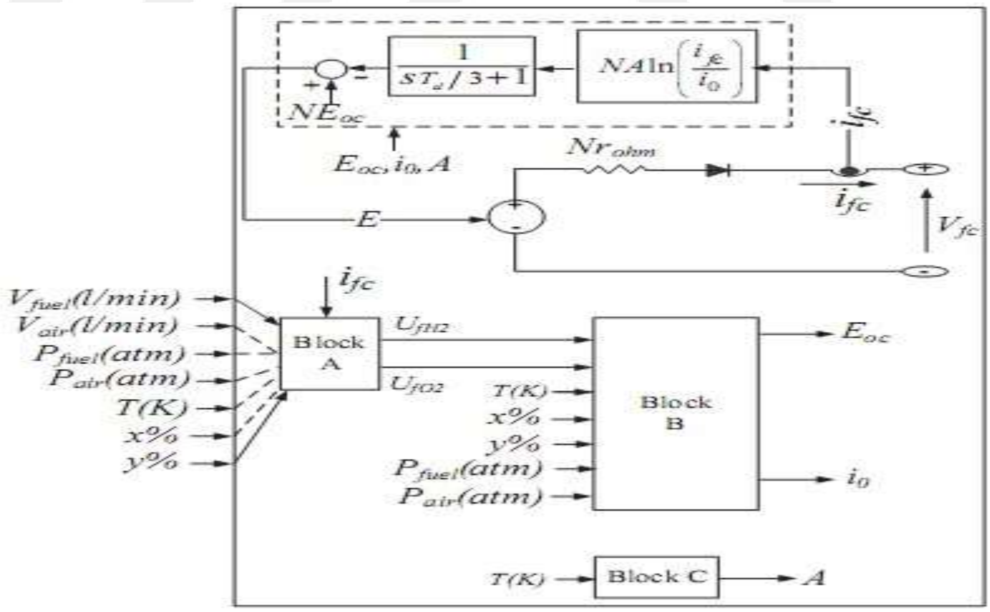

Figure A-0-2 Mathematical model block diagram of the FC generator.

The approach suggested in [7] was modified and results in this proposed FC model. As a result, decoupled characteristics of the electrode from determination the partial pressure of reactants.

The reactant utilizations:

$$U_{fH_2} = \frac{60000RTNi_{fc}}{zFP_{fuel}V_{lpm(fuel)}X\%} \tag{A.3}$$

$$U_{fO_2} = \frac{60000RTNi_{fc}}{2zFP_{air}V_{lpm(air)}y\%} \tag{A.4}$$

The majority of the constants and variables are defined in a set of symbols, where R=8.3145J/(mol K) and F=96485A s/mol. The liter/min (lpm) flow rate employed in the model was converted to m^3/s at a ratio of 1 lpm to 60000 m^3/s, yielding the 60000 constants.

The Ohmic voltage and exchange current are represented by Block B, where Eoc can be expressed as in (A.2) and io is given as:

$$i_0 = \frac{zFK\,(P_{H_2}+P_{O_2})}{Rh}\, exp^{\frac{-\Delta G}{RT}} \tag{A.5}$$

Consequently, all of the parameters in equation (A.5) are defined in a list of symbols, where P_{H2} and P_{O2} represent the partial pressures of oxygen and hydrogen, respectively (atm).

With less oxygen available, the cell's usage climbs over its nominal value, resulting in a change to the Nernst voltage [83]:

$$E_n = 1.229 + (T-298)\frac{-44.43}{zF} + \frac{RT}{zF}\ln(P_{H2}P_{O2}{}^{\frac{1}{2}}) - K_u(U_{fo_2} - U_{fo_2(nom)}$$

(A.6)

In Figure A-2 the Block C represents the Tafel slope which is given by:

$$A = \frac{RT}{z\alpha F} \quad (A.7)$$

Where α is the charge transfer coefficient.

(A-2): Ultracapacitor Model

In order to model the most common types of UC, a mathematical model block provided by MATLAB/Simulink is used to depict the UC characteristics as shown in Figure A-3 [83].

Whereas, the voltage at the output of the UC may be written as follows using the Stern equation:

$$V_{UC} = \frac{N_s Q_T r}{N_p N_e \varepsilon \varepsilon_0 A_i} + \frac{2N_e N_s RT}{F} \operatorname{asinh}^{-1}\left(\frac{Q_T}{N_p N_e{}^2 \sqrt{8RT\varepsilon\varepsilon_o}}\right) - R_{UC} \cdot i_{UC} \quad (A.8)$$

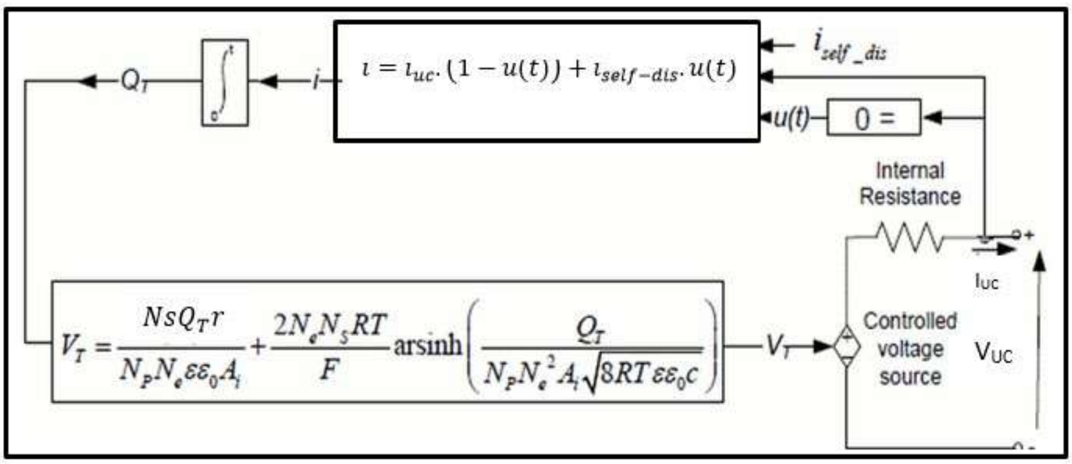

Figure A-0-3 UC equivalent circuit.

Where,

$$Q_T = \int i_{UC}\, dt \tag{A.9}$$

Following are the adjustments made to the electric charge of the UC to mimic the self-discharge phenomenon: (when i_{UC} = 0):

$$Q_T = \int i_{self\_dis}\, dt \tag{A.10}$$

Where:

$$i_{self\_dis} = \begin{cases} \dfrac{C_T\alpha_1}{1 + sR_{UC}C_T} & if\ t - t_{oc} \le t_3 \\ \dfrac{C_T\alpha_2}{1 + sR_{UC}C_T} & if\ t_3 < t - t_{oc} \le t_4 \\ \dfrac{C_T\alpha_3}{1 + sR_{UC}C_T} & if\ t - t_{oc} > t_4 \end{cases} \tag{A.11}$$

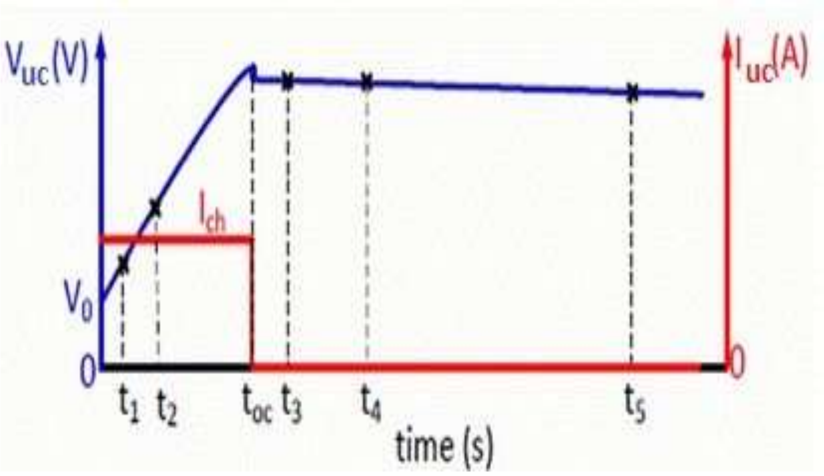

Figure A-0-4 The rates of change of the UC voltage during the time intervals.

Where the definitions of all the parameters in Equations (A.8) and (A.11) are listed in the table of symbols.

(A-3): Battery Model

The batteries taken into consideration for this work are the lithium-ion type, in contrast to other BAT types, the lithium-ion type has been shown more high-energy density and efficiency than others [52]. As a result, EV and FCEV applications find them more attractive. The curve fitting model shown in Figure A-5 [83] serves as the foundation for the BAT model that is provided in Simulink.

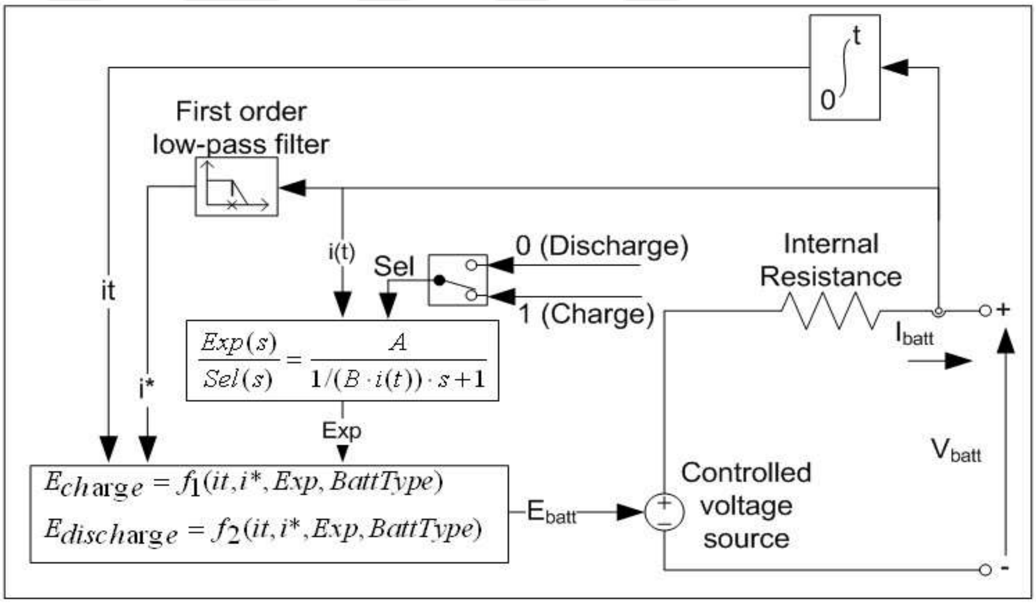

Figure A-0-5 The BAT equivalent circuit.

For Lithium-Ion model, charge state can be expressed (where, i* greater than 0) as:

$$f_1(it, i^*, i) = E_0 - K\,.\frac{Q}{it+0.1\,.\,Q}\,.i^* - K.\frac{Q}{Q-it}\,.it + A.exp(-B.it). \qquad \text{(A.12)}$$

And for discharging state (where, i* less than 0) is expressed as:

$$f2(it, i^*, i) = E_0 - K.\frac{Q}{Q-it} \ .i^* - K.\frac{Q}{Q-it}.it + A.exp(-B.it). \qquad (A.13)$$

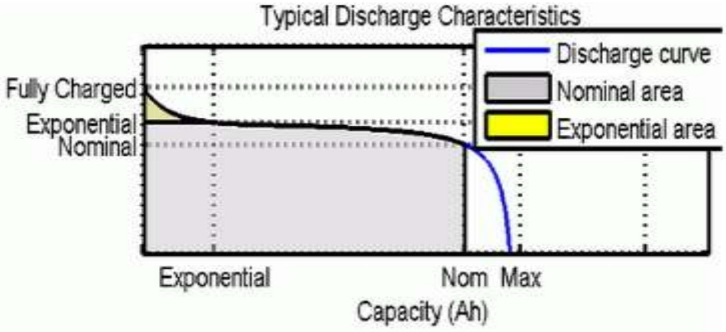

Figure A-0-6 The typical discharge characteristics of the BAT.

The BAT will charge in accordance with a charge characteristic, as depicted in Figure A-7 [83].

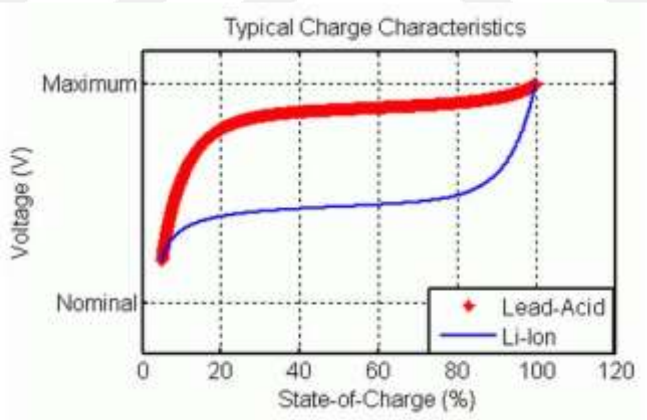

Figure A-0-7 The typical charge characteristics of the BAT.

As observed in Figure A-7, the parameters of the BAT model are determined from the characteristics of discharge and are taken into account to be the same for charging.

APPENDIX B

(B-1): FC parameters

PROPERTY	UNIT	VALUE
PRODUCT INFORMATION		
Model Number		HyPM® HD 12
Part Number		1037312
PHYSICAL		
Dimensions of FCPM (L x W x H)[1]	mm	847 x 446 x 301
Mass[2]	kg	85
Volume of FCPM[3]	L	114
PERFORMANCE		
Rated Electrical Power[4]	kW	12.5
Maximum Electrical Overload		None permitted
Operating Current[4,5]	A_{dc}	0–380
Operating Voltage	V_{dc}	30–60
Peak Efficiency[6]	%	53
Time from Off Mode to Idle[7]	s	≤ 25
Time from Idle to Rated Power[7]	s	≤ 5
FUEL SYSTEM REQUIREMENTS		
Gaseous Hydrogen[8]	%	≥ 99.99
CO	μmol/mol	≤ 0.2
Sulfur (total, ex. H_2S, COS)	μmol/mol	≤ 0.004
Total Hydrocarbons	μmol/mol	≤ 2
Supply Pressure[9]	kPa	515–690
Stack Operating Pressure[9]	kPa	≤ 120
Consumption[10]	L/min	≤ 190
Hydrogen Temperature	°C	2–40
PROPERTY	**UNIT**	**VALUE**
FUEL SYSTEM REQUIREMENTS		
AIR DELIVERY SYSTEM		

Air Delivery System		
Maximum Air Flow Rate[11]	L/min	≤ 1300
Air Filtration[12]		Chemical and Particulate
Composition		Ambient Air
Sulfur	μmol/mol	≤ 0.004
Air Inlet Temperature	°C	2-40
Operating Environment		
Storage Air Temperature[13]	°C	-20–46
Ambient Air Temperature	°C	2–40
Maximum FCPM Interior Temperature[14]	°C	46
Relative Humidity (Operation and Storage)[15]	%	≤ 95
Altitude Range[16]	m	0-400
Orientation	°	±30
Emissions		
Allowable Pressure Drop of Customer Cathode Exhaust	kPa	≤ 3
Water Collected:[17]		
Anode	mL/min	≤ 18
Cathode	mL/min	≤ 24
Noise[18]	dBA	≤ 70

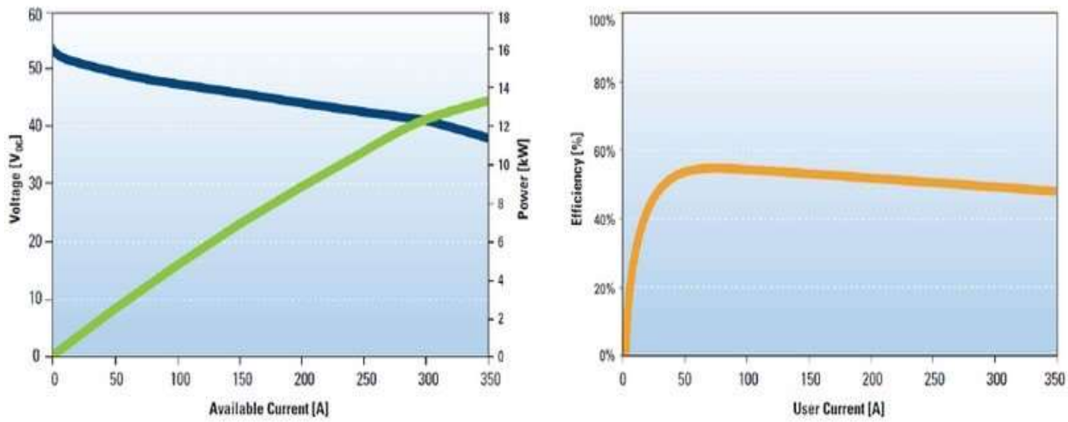

Figure B-0-1 Actual experimental FC characteristics result.

(B-2): BAT parameters

Specifications		U1-12XP	U24-12XP	U27-12XP	UEV-18XP	U27-36 XP
Nominal Module Voltage		12.8 V	12.8 V	12.8 V	19.2 V	38.4 V
Nominal Capacity (C/5, 23°C)		40 Ah	110 Ah	138 Ah	69 Ah	45Ah
Weight (approximate)		6.5 kg	15.8 kg	19.5 kg	14.9 kg	19.6kg
Dimension incl. Terminals LxWxH (mm)		197x131x182	260x172x225	306x172x225	269x148x245	306x172x225
BCI Group Number		U1R	Group 24	Group 27	N/A	Group 27
Terminals, Female-Threaded		M6 x 1.0	M8 x 1.25	M8 x 1.25	M8 x 1.25	M8 x 1.25
Specific Energy		79 Wh/kg	89 Wh/kg	91 Wh/kg	89 Wh/kg	91 Wh/kg
Energy Density		110 Wh/l	139 Wh/l	148 Wh/l	124 Wh/l	148 Wh/l
Standard Discharging @ 25°C	Max. Continuous Load Current	80 A	150 A	150 A	120 A	90 A
	Peak Load Current (30 sec).	120 A	300 A	300 A	200 A	135 A
	Cut-off Voltage	10 V	10 V	10 V	15 V	30 V
Standard Charging	Max. Charge Voltage	14.6 V	14.6 V	14.6 V	21.9 V	43.8 V
	Float Voltage	13.8 V	13.8 V	13.8 V	20.7 V	41.4 V
	Charge Time c/2 *	2.5 hrs	2.5 hrs	2.5 hrs	2.5 hrs	2.5 hrs
DC Internal resistance (max)		15 mΩ	6 mΩ	5 mΩ	10 mΩ	25 mΩ
Equivalent Lithium Content Per Module (g)		48.6	127.98	160.38	121.5	160.38
Part Number		1004434	1004425	1004428	1004431	1005219

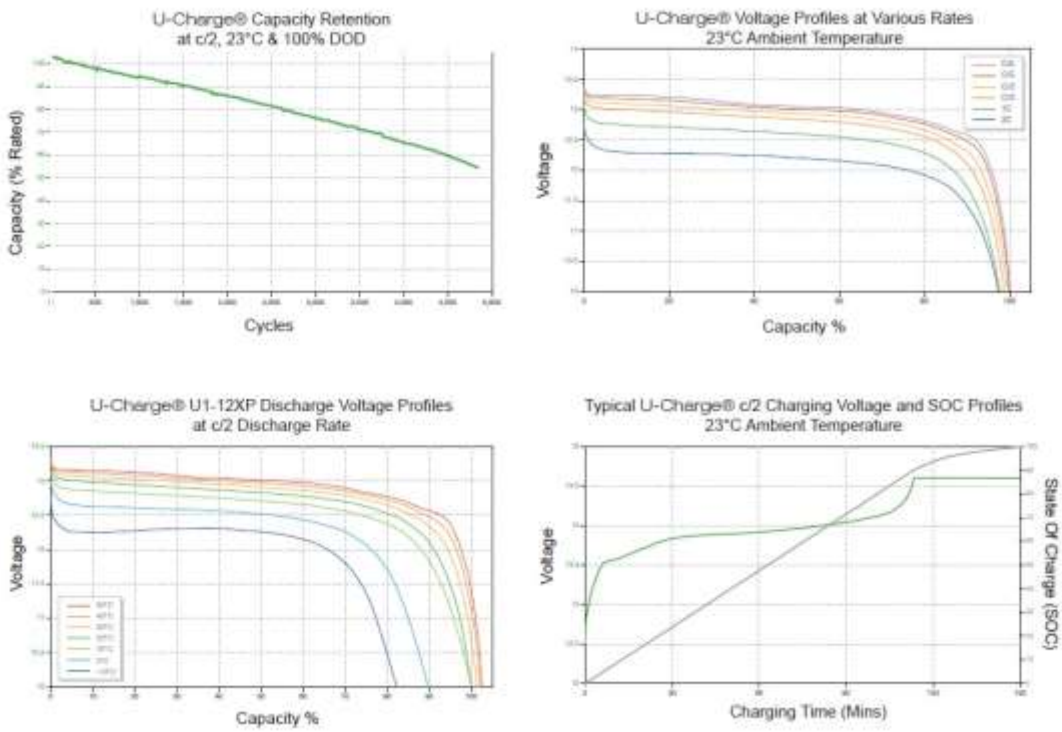

Figure B-0-2 Battery module specifications and characteristics.

(B-3): UC parameters

DATASHEET
K2 SERIES 650 F - 3,000 F ULTRACAPACITORS

Maxwell TECHNOLOGIES

BCAP0650 P270
BCAP1200 P270
BCAP1500 P270
BCAP2000 P270
BCAP3000 P270

FEATURES AND BENEFITS
- Ultra-low internal resistance
- Highest power performance available
- Lowest RC time constant
- 2.7 V operating voltage
- Over 1,000,000 duty cycles
- Proprietary material science and packaging technology
- Threaded terminal or weldable post versions

APPLICATIONS
- Automotive subsystems
- Back-up power
- Grid stabilization
- Hybrid drive trains
- Rail system power
- Transportation
- Utility vehicles

PRODUCT SPECIFICATIONS

CAPACITANCE	BCAP0650	BCAP1200	BCAP1500	BCAP2000	BCAP3000
Nominal capacitance	650 F	1,200 F	1,500 F	2,000 F	3,000 F
Tolerance capacitance	-0% / +20%	-0% / +20%	-0% / +20%	-0% / +20%	-0% / +20%
VOLTAGE					
Rated voltage	2.7 V DC	2.7 V DC	2.7 V DC	2.7 V DC	2.7 V DC
Surge voltage	2.85 V DC	2.85 V DC	2.85 V DC	2.85 V DC	2.85 V DC
Maximum operating voltage			N/A		
RESISTANCE					
ESR, DC Max., room temperature	0.8 mΩ	0.58 mΩ	0.47 mΩ	0.35 mΩ	0.29 mΩ
ESR, 1khz (Max.)	0.6 mΩ	0.44 mΩ	0.35 mΩ	0.26 mΩ	0.24 mΩ
TEMPERATURE					
Operating temperature range Stored uncharged	-40°C to +65°C	-40°C to +65°C	-40°C to +65°C	-40°C to +65°C	-40°C to +65°C
Storage temperature range Cell case temperature	-40°C to +70°C	-40°C to +70°C	-40°C to +70°C	-40°C to +70°C	-40°C to +70°C
POWER					
Pd	6,800 W/kg	5,800 W/kg	6,600 W/kg	6,900 W/kg	5,900 W/kg
Pmax	18,900 W/kg	15,900 W/kg	18,500 W/kg	19,400 W/kg	14,800 W/kg
ENERGY					
Emax	4.11 Wh/kg	4.67 Wh/kg	5.42 Wh/kg	5.63 Wh/kg	5.96 Wh/kg

PRODUCT SPECIFICATIONS (cont.)

DC LIFESPAN	BCAP0650	BCAP1200	BCAP1500	BCAP2000	BCAP3000
Endurance At rated voltage and 65°C.	1,500 hours	1,500 hours	1,500 hours	1,500 hours	1,500 hours
Capacitance change % of rated value	≤20%	≤20%	≤20%	≤20%	≤20%
Internal resistance change % of rated value	≤60%	≤60%	≤60%	≤60%	≤60%
Life test At rated voltage and 25°C.	10 years	10 years	10 years	10 years	10 years
Capacitance change % of rated value	≤20%	≤20%	≤20%	≤20%	≤20%
Internal resistance change % of rated value	≤100%	≤100%	≤100%	≤100%	≤100%
CYCLE LIFE					
Cycles Between specified voltage and half rated voltage under constant current at 25°C.	1 million	1 million	1 million	1 million	1 million
Capacitance change % of rated value	≤20%	≤20%	≤20%	≤20%	≤20%
Internal resistance change % of rated value	≤100%	≤100%	≤100%	≤100%	≤100%
SHELF LIFE					
Shelf Life Uncharged over storage temperature	2 years	2 years	2 years	2 years	2 years
Capacitance change % of rated value	10% decrease	10% decrease	10% decrease	10% decrease	10% decrease
ESR change % of rated value	50% increase	50% increase	50% increase	50% increase	50% increase
CURRENT					
Maximum continuous current	62 A	81 A	97 A	123 A	147 A
Maximum peak current, 1 sec	575 A	955 A	1,185 A	1,585 A	2,165 A
Leakage current, I_{LC} After 72 hours. Initial leakage current can be higher.	1.5 mA	2.7 mA	3.0 mA	4.2 mA	5.2 mA
CONNECTION					
Terminal			Threaded or Weldable		
SIZE					
Dimensions (L x W x H) (mm)			See drawings		
Weight	0.16kg	0.26kg	0.28kg	0.36kg	0.51kg

PRODUCT SPECIFICATIONS (cont.)

RATINGS AND SAFETY					
Vibration resistance	For all: ISO 16750, SAE J2380				
Short circuit current (Isc) **CAUTION:** Current possible with short circuit from rated voltage Do not use as an operating current.	3,350 A	4,650 A	5,700 A	7,700 A	9,300 A

TYPICAL CHARACTERISTICS

THERMAL CHARACTERISTICS					
Thermal resistance (Rth)	6.5°C/W	5.3°C/W	4.5°C/W	3.8°C/W	3.2°C/W

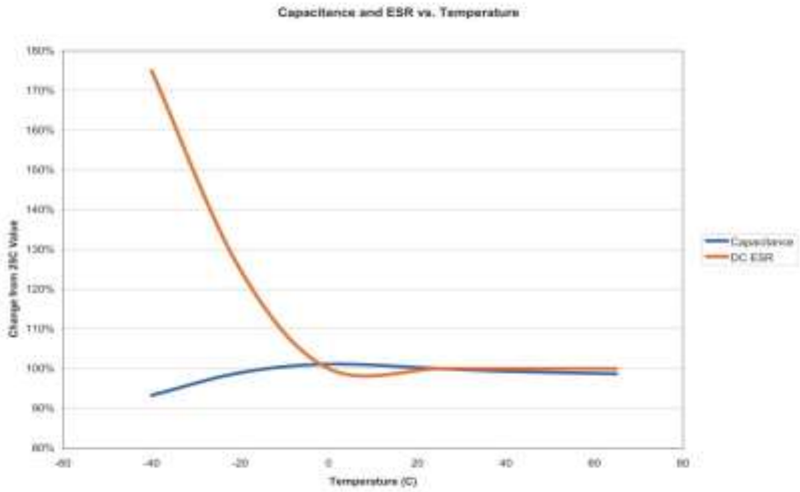

ADDITIONAL TECHNICAL INFORMATION

Capacitance and ESR, DC measured per document no. 1007239, available at www.maxwell.com.

Unless specified, all specifications are at 25°C

I_C = leakage current after 72 hours at 25°C

Isc (short circuit current) = $\frac{V_{RATED}}{ESR}$

R_{th} = thermal resistance

$$Emax = \frac{\frac{1}{2} CV^2}{3{,}600 \times mass}$$

$$Pmax = \frac{\frac{V^2}{4R\,(1khz)}}{mass}$$

$$Pd = \frac{\frac{0.12V^2}{R\,(DC)}}{mass}$$

$$\text{Maximum Peak Current (1 sec)} = \frac{\frac{1}{2} V}{ESR(DC) + \frac{1}{C}}$$

DIMENSIONS

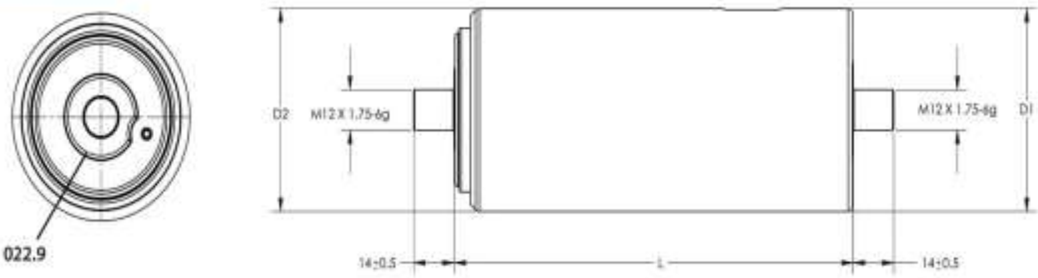

Part Number	Volume	L (±0.3mm)	D_1 (±0.2mm)	D_2 (±0.7mm)
BCAP0650 P270 K04 02	0.211 L	51.5 mm (±0.5mm)	60.4mm	60.7mm
BCAP1200 P270 K04 02	0.294 L	74 mm	60.4mm	60.7mm
BCAP1500 P270 K04 02	0.325 L	85 mm	60.4mm	60.7mm
BCAP2000 P270 K04 02	0.373 L	102 mm	60.4mm	60.7mm
BCAP3000 P270 K04 02	0.475 L	138 mm	60.4mm	60.7mm

DIMENSIONS (cont.)

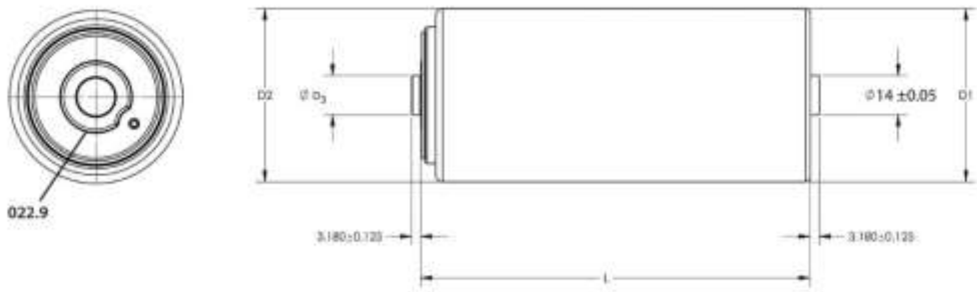

Part Number	Volume	L (±0.3mm)	D_1 (±0.2mm)	D_2 (±0.7mm)	D_3 (±0.05mm)
BCAP0650 P270 K05 02	0.15 L	51.5 mm (±0.5mm)	60.4mm	60.7mm	14mm
BCAP1200 P270 K05 02	0.233 L	74 mm	60.4mm	60.7mm	14mm
BCAP1500 P270 K05 02	0.264 L	85 mm	60.4mm	60.7mm	14mm
BCAP2000 P270 K05 02	0.312 L	102 mm	60.4mm	60.7mm	14mm
BCAP3000 P270 K05 02	0.414 L	138 mm	60.4mm	60.7mm	14mm

Product dimensions are for reference only unless otherwise identified. Product dimensions and specifications may change without notice. Please contact Maxwell Technologies directly for any technical specifications critical to application.

Maxwell Technologies, Inc.
Worldwide Headquarters
9244 Balboa Avenue
San Diego, CA 92123
USA
Tel: +1 858 503 3300
US Free Call: +1 877 511 4324
Fax: +1 858 503 3301

Maxwell Technologies SA
CH-1728 Rossens
Switzerland
Tel: +41 (0)26 411 85 00
Fax: +41 (0)26 411 85 05

Maxwell Technologies, GmbH
Brucker Strasse 21
D-82205 Gilching
Germany
T: +49 (0)8105 24 16 10
F: +49 (0)8105 24 16 19

Maxwell Technologies, Inc.
Shanghai Representative Office
#13, CR Times Square
300 Zhangyang Road, Pudong
Shanghai 200122, P.R. China
Tel: +86 21 5836 5733
Fax: +86 21 5836 5620

Online: www.maxwell.com • Email: info@maxwell.com

APPENDIX C

(C-1): WNN-PI controller parameters set by PSO

POS algorithm to online set the PI controller parameters for Boost and Buck converters. Also, the Feed-Forward wavelet (WNN-PI) controller of BAT current reference:

```
%% Tunning of PI controller and WNN parameters using Particle Swarm
```

```
Optimization

clc close
all

                          %% Initialization %%
n = 10;            % Size of the swarm " no of birds "
bird_setp = 10;  % Maximum number of "birds steps" dim
= 36;          % Dimension of the problem




c2 =1.4;       % PSO parameter C1  c1 =
1.4;      % PSO parameter C2  w =0.8;
% pso momentum or inertia
fitness=0*ones(n,bird_setp);

                %--------------------------%
                %    initialize the parameter %
%----------------------------%
R1 = rand(n,dim); R2 =
rand(n,dim); current_fitness
=0*ones(n,1);

            %-----------------------------------------------%
            % Initializing swarm and velocities and position % %-----------
------------------------------------%

current_position = abs(10*(rand(n,dim)-.5));
velocity = .3*randn(n,dim) ; local_best_position
= current_position ;

                %-------------------------------------------%
                        %     Evaluate initial population          %
                %-------------------------------------------%


for i = 1:n
   % m=9
 %current_fitness =tracklsq(current_position(:,i));


 pi=current_position(i,:);
```

```
    %% the PI controllers of the converters %%
kp1 = pi(1);      ki1 = pi(2);      kp2 = pi(3);      ki2
= pi(4);      kp3 = pi(5);      ki3 = pi(6);      kp4
= pi(7);      ki4 = pi(8);      kp5 = pi(9);      ki5
= pi(10);
    %% the WNN-PI controller of the BAT current reference %%
b1 = pi(11);      b2 = pi(12);      b3 = pi(13);      b4 = pi(14);
b5 = pi(15);      b6 = pi(16);      b7 = pi(17);      b8 = pi(18);
a1 = pi(19);      a2 = pi(20);      a3 = pi(21);      a4 = pi(22);
a5 = pi(23);      a6 = pi(24);
    a7 = pi(25);
a8 = pi(26);
w1 = pi(27);
w2 = pi(28);
w3 = pi(29);
w4 = pi(30);
w5 = pi(31);
w6 = pi(32);
w7 = pi(33);
w8 = pi(34);
ki = pi(35);      kd
= pi(36);



  sprintf('The value of interation Kp= %3.0f, Kd= %3.0f', pi(1),pi(2));

              % Compute function value
 simopt
=simset('solver','ode45','SrcWorkspace','Current','DstWorkspace','Current');

              % Initialize sim options

[tout,xout,yout] = sim('mutatafawnn',[0 1400],simopt);

% "mustafawnn" is the Simulink model and "1400" is the stop time of the
Simulink, because the parameters are set during the UDDS cycle which is
1400 seconds %

              % compute the error
```

```
sys_overshoot=(max(V_Actual)-300)+(max(V_Actual1)-
325)+(max(IL)max(IL1))+(max(VH)-325)+(max(IL2)-max(IL3))+(max(ILb)-max(IL4));

        m=abs(e);
m1=abs(e1);
m2=abs(e2);
m3=abs(e3);
m4=abs(e4);
m5=abs(e5);
        error=sum(m)+sum(m1)+sum(m2)+sum(m3)+sum(m4)+sum(m5);
F=error+sys_overshoot;         current_fitness(i)=F;   end


local_best_fitness  = current_fitness ;
[global_best_fitness,g] = min(local_best_fitness) ;

for i=1:n     globl_best_position(i,:) =
local_best_position(g,:) ; end globl_best_position;

                    %------------------%
                    %  VELOCITY UPDATE  %
                    %------------------%

velocity = w *velocity + c1*(R1.*(local_best_position-current_position)) +
c2*(R2.*(globl_best_position-current_position));

                     %-----------------%
                     %   SWARMUPDATE    %
                     %-----------------%


current_position = current_position + velocity ;

                   %-----------------------%
%  evaluate anew swarm   %
%-----------------------%


                              %% Main Loop
```

```
iter = 0 ;      % Iterations'counter
while  ( iter < bird_setp ) iter = iter
+ 1

for i = 1:n,
pi=current_position(i,:);        kp1
= pi(1);        ki1 = pi(2);        kp2
= pi(3);        ki2 = pi(4);        kp3
= pi(5);        ki3 = pi(6);        kp4
= pi(7);        ki4 = pi(8);        kp5
= pi(9);        ki5 = pi(10);        b1
= pi(11);        b2 = pi(12);
b3 = pi(13);        b4 = pi(14);
b5 = pi(15);        b6 = pi(16);
b7 = pi(17);        b8 = pi(18);
a1 = pi(19);        a2 = pi(20);
a3 = pi(21);        a4 = pi(22);
a5 = pi(23);        a6 = pi(24);
a7 = pi(25);        a8 = pi(26);
w1 = pi(27);        w2 = pi(28);
w3 = pi(29);        w4 = pi(30);
w5 = pi(31);        w6 = pi(32);
w7 = pi(33);        w8 = pi(34);
ki = pi(35);        kd = pi(36);


    sprintf('The value of interation Kp= %3.0f, Kd= %3.0f', pi(1),pi(2));

                % Compute function value
simopt = simset('solver','ode45','SrcWorkspace','Current','DstWorkspace','Current');

                % Initialize sim options

    [tout,xout,yout] = sim('mutatafawnn',[0 1400],simopt);

                % compute the error

sys_overshoot=(max(V_Actual)-300)+(max(V_Actual1)-
325)+(max(IL)max(IL1))+(max(VH)-325)+(max(IL2)-max(IL3))+(max(ILb)-max(IL4));

    m=abs(e);
m1=abs(e1);
```

```
m2=abs(e2);
m3=abs(e3);
m4=abs(e4);
m5=abs(e5);

 error=sum(m)+sum(m1)+sum(m2)+sum(m3)+sum(m4)+sum(m5); % error of all loops%


        F=error+sys_overshoot;
current_fitness(i)=F;   end


for  i  =  1  :  n                    if  current_fitness(i)  <
local_best_fitness(i)                 local_best_fitness(i)  =
current_fitness(i);                 local_best_position(i,:) =
current_position(i,:);         end     end


 [current_global_best_fitness,g] = min(local_best_fitness);


if current_global_best_fitness < global_best_fitness
global_best_fitness = current_global_best_fitness;     for i=1:n
globl_best_position(i,:) = local_best_position(g,:);     end

end


 velocity = w *velocity + c1*(R1.*(local_best_position-current_position)) +
c2*(R2.*(globl_best_position-current_position));  current_position =
current_position + velocity;

 sprintf('The value of interation iter %3.0f ', iter );


end % end of ‘while loop’ it is mean the end of all steps that the birds move
it

                            %xx=fitness(:,10);
                            %[Y,I] = min(xx);
                          %current_position(:,I)
```

```
        Kp1 = globl_best_position(n,1);
        Ki1 = globl_best_position(n,2);
        Kp2 = globl_best_position(n,3);
        Ki2 = globl_best_position(n,4);
        Kp3 = globl_best_position(n,5);
        Ki3 = globl_best_position(n,6);
        Kp4 = globl_best_position(n,7);
        Ki4 = globl_best_position(n,8);
        Kp5 = globl_best_position(n,9);
Ki5 = globl_best_position(n,10);
b1 = globl_best_position(n,11);        b2
= globl_best_position(n,12);        b3 =
globl_best_position(n,13);        b4 =
globl_best_position(n,14);        b5 =
globl_best_position(n,15);        b6 =
globl_best_position(n,16);        b7 =
globl_best_position(n,17);        b8 =
globl_best_position(n,18);        a1 =
globl_best_position(n,19);        a2 =
globl_best_position(n,20);        a3 =
globl_best_position(n,21);        a4 =
globl_best_position(n,22);        a5 =
globl_best_position(n,23);        a6 =
globl_best_position(n,24);        a7 =
globl_best_position(n,25);        a8 =
globl_best_position(n,26);        w1 =
globl_best_position(n,27);        w2
=globl_best_position(n,28);        w3 =
globl_best_position(n,29);        w4 =
globl_best_position(n,30);        w5 =
globl_best_position(n,31);        w6
=globl_best_position(n,32);        w7 =
globl_best_position(n,33);        w8 =
globl_best_position(n,34);        ki=
globl_best_position(n,35);        kd =
globl_best_position(n,36);
```

(C-2): MATLAB Functions Block Codes

1. Boost converter controller

```
function [V,Idc] = Boostfcn(D,Vdc,I,n)
V= Vdc*(1-D);
Idc=I*n*(1-D);
```

2. Buck-Boost converter controller

```
function [Vboost,Iboost,Vbuck,Ibuck] = BuckBoostfcn(D1,D2,Vdc,IL,ILb,n)
Vboost= Vdc*(1-D1);
Iboost=IL*n*(1-D1);
Vbuck= Vdc*D2;
Ibuck=(ILb*D2)/n;
```

(C-3): RWNN-PI controller parameters set by PSO

The same codes used in Appendix C-1 are used for RWNN-PI with a difference that the dim is 14 to find the (a's, b's, w's) and the parameter (K_p & K_i) of the PI controller.

And sys_overshoot is just (sys_overshoot=max(V_Actual)-300;)

C-4): ANNs codes

```
Net=feedforwardnet([30 20 15 10]);
net.divideParam.trainRatio=0.7;
net.divideParam.testRatio=0.15;
net.divideParam.valRatio=0.15;
net.trainParam.lr=0.001;
net.trainParam.min_grad=1e-20;
net.trainParam.goal=1e-30;
net.trainParam.epochs=1000;
net=train(net,inputdata,outpudata)
view(net)%%to view the net architecture%%
gensim(net) %% to export the net to
    the Simulink environment %%
```

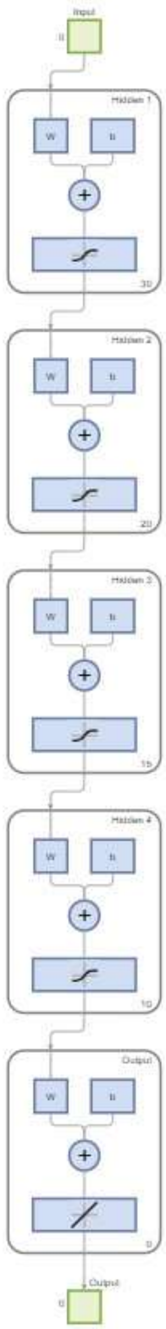

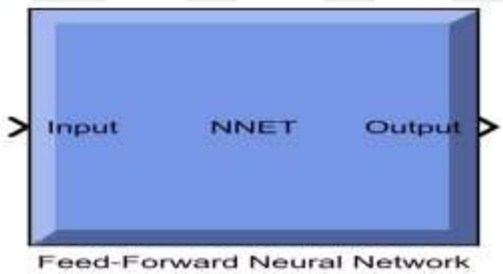

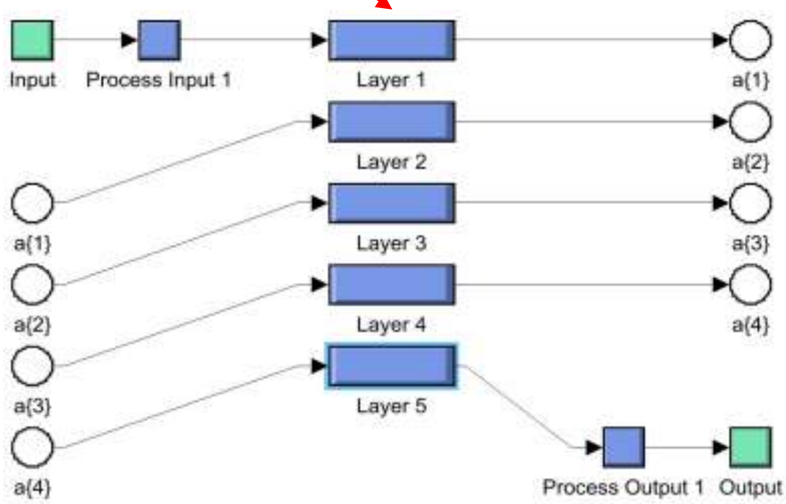

APPENDIX D

Publication:

• Mustafa A. K., Omer Cihan Kivanc and O.A. Ahmed. "Intelligent Energy Management System for Hybrid Electric Vehicle Based on Optimization Wavelet Neural Network by PSO Algorithm." *12th International Conference on Information Systems and Advanced Technologies: Springer ICISAT 2022.*

Presented On 27-Aug.2022


ICISAT'2022

12th International Conference on Information Systems and Advanced Technologies

Certificate of Attendance

Awarded to

Mustafa Kamoona

For attending:

12th International Conference on Information Systems and Advanced Technologies "ICISAT'2022"

and presenting the paper entitled: Intelligent Energy Management System for Hybrid Electric Vehicle Based on Optimization Wavelet Neural Network by PSO Algorithm

Authors: Mustafa Kamoona, Omer Kivanc and Oday Ahmed

ICISAT'2022 General Chair